Centralised yaw and lateral motion control for future electric vehicles

Master's thesis in Automotive Engineering

ISAK ERVALL, ZIAD GEORGE

DEPARTMENT OF MECHANICS AND MARITIME SCIENCES

CHALMERS UNIVERSITY OF TECHNOLOGY
Gothenburg, Sweden 2022
www.chalmers.se

Master's thesis 2022:74

Centralised yaw and lateral motion control for future electric vehicles

ISAK ERVALL, ZIAD GEORGE

CHALMERS
UNIVERSITY OF TECHNOLOGY

Department of Mechanics and Maritime Sciences
Division of Vehicle Engineering and Autonomous Systems
Chalmers University of Technology
Gothenburg, Sweden 2022

Centralised yaw and lateral motion control for future electric vehicles
ISAK ERVALL
ZIAD GEORGE

Supervisor: Derong Yang, Volvo Cars - Gothenburg, Sweden
Examiner: Mats Jonasson, Chalmers - Department of Mechanics and Maritime Sciences - Gothenburg, Sweden

Master's Thesis 2022
Department of Mechanics and Maritime Sciences
Division of Vehicle Engineering and Autonomous Systems
Chalmers University of Technology
SE-412 96 Gothenburg
Telephone +46 31 772 1000

Cover: Vehicle model in IPG CarMaker

Typeset in LaTeX
Printed by Chalmers Reproservice
Gothenburg, Sweden 2022

Centralised yaw and lateral motion control for future electric vehicles
ISAK ERVALL
ZIAD GEORGE
Department of Mechanics and Maritime Sciences
Chalmers University of Technology

Abstract

The disruptive innovation in the ever-growing and developing automotive industry has centralised advanced driver assistance systems (ADAS) and autonomous driving (AD) concepts. The innovations are only enhanced by the rapid electrification of powertrain systems due to strict environmental regulations, allowing for extended functionalities in vehicle motion control.

This master's thesis investigates the possibilities of vehicle motion control systems for future electric vehicles using an over-actuated vehicle with four individual electric motors in both simulations and real-time in a test vehicle. Three different concepts for yaw and lateral motion control are developed. The first concept is geometric path tracking, where two controllers are developed to control the vehicle's lateral motion in an AD scenario. The second concept is a steer by torque vectoring controller where the lateral motion of the vehicle is controlled using only differential torque to act as a backup safety system in case of steering actuator failures. Finally, an energy-efficient torque vectoring controller is developed to evaluate the possibility of reducing the vehicle's energy consumption by optimising the torque allocation.

The controllers were developed in Matlab Simulink and evaluated in a simulation environment consisting of a vehicle model of the test vehicle in IPG CarMaker. The comparison between the two path tracking controllers, i.e. the Pure Pursuit and the Stanley controller, were evaluated based on precision, comfort and robustness. The steer by torque vectoring controller was developed with experimental data from simulations and the test vehicle to design a look-up table for the steering capability. Finally, to develop the energy-efficient torque vectoring controller, an offline optimisation strategy was used to construct a rule-based and a look-up table method for the torque allocation.

The work proved that the Pure Pursuit controller was superior to the Stanley controller and could remain within limits given by regulations, both in the simulations and the test vehicle. Integrated with the steer by torque vectoring controller, the vehicle's lateral motion could be controlled using only differential torques. The possibility of reducing energy consumption by optimising the torque allocation was highly dependent on compromising the precision performance of the path tracking and the torque allocation. With tuning, the controllers could be combined to reduce the vehicle's energy consumption by 1.14 %.

Keywords: Path tracking, Torque vectoring, Pure pursuit controller, Stanley controller, Control allocation, Centralised control, Energy efficiency, Over-actuation

Acknowledgements

First and foremost, we would like to extend our gratitude towards our amazing supervisors, Dr Mats Jonasson and Dr Derong Yang. Not only for your excellent and endless support but also for your vibrant attitude towards the subject. The passion you have shown throughout this project is contagious and is the main reason we were as invested and interested in our work on day one as we were on our last day. A huge thanks to Juliette Torinsson and Anand Ganesan for providing us with valuable ideas and always helping us overcome obstacles. You have been great. Finally, we would like to extend our appreciation to Anna Söderlund for giving us the opportunity to work on this fantastic project and for always making us feel like we are a part of the Lateral Motion Control and Vehicle State team at Volvo Cars. We couldn't ask for a better manager and team.

Also, thank you, Derong, for that one time when you picked us up at night from the test track when the test vehicle broke down, and we were stuck there for several hours in the cold. We still owe you for that one!

Isak Ervall, Ziad George, Gothenburg, June 2022

List of Acronyms

Below is the list of acronyms that have been used throughout this thesis listed in alphabetical order:

AD	Autonomous Driving
ADAS	Advanced Driver Assistance Systems
AVS	Advanced Vehicle Systems
EETVC	Energy Efficient Torque Vectoring Controller
EM	Electric Motor
EPAS	Electronic Power Assistance Steering
EV	Electric Vehicle
PMSM	Permanent Magnet Synchronous Machines
PPC	Pure Pursuit controller
PTC	Path Tracking controller
RMSE	Root Mean Square Error
SbTV	Steer by Torque Vectoring
SC	Stanley controller
TV	Torque Vectoring
TVC	Torque Vectoring Controller

Nomenclature

Below is the nomenclature of indices, sets, parameters, and variables that have been used throughout this thesis.

Indices

i	Index for motor/wheel i
j	Index for iteration j of simulation
a	Index describing left L or right R side of vehicle
b	Index describing front F or rear R axle of vehicle

Parameters

η_{bat}	Battery round-trip efficiency
η_{gb}	Gearbox efficiency
n_t	Transmission ratio
n_{sw}	Steering wheel ratio
$T_{EM,max}$	Max motor torque
$T_{EM,min}$	Min motor torque
m	vehicle mass
c_1,c_2	Longitudinal Force request weighting coefficients
L	Wheelbase
SWA_{thr}	Steering wheel angle threshold
$l_{f,r}$	Distance front/rear axle to CoG
$C_{yf,yr}$	Front/rear cornering stiffness
J_{zz}	Vehicle yaw intertia
r_w	Wheel radius (static)
w	Trackwidth
ω_{max}	Max motor speed

$T_{EM,max}$	Max motor torque
$T_{EM,min}$	Min motor torque
K_u	Understeer gradient
d_{f-r}	Distribution constant

Variables

δ_{req}	Steering wheel angle request
δ_{SW}	Reference steering wheel angle
δ_{K_u}	Understeer gradient extended steering angle
δ_{PPC}	Pure Pursuit Controller steering angle
δ_{PPC,K_u}	Pure Pursuit Controller steering angle with Understeer gradient
δ_{SC}	Stanley Controller steering angle
α	Angle between vehicle heading and target point
$\alpha_{f,r}$	Front/rear tire slip angle
ψ	Yaw angle
$\dot{\psi}$	Yaw rate/yaw velocity
$\ddot{\psi}$	Yaw acceleration
v_x	Longitudinal velocity
$\dot{v}_y$	Lateral acceleration in the body frame
a_y	Lateral acceleration
ϕ_m	Phase margin
ω_c	Crossover angular frequency
τ_{max}	Delay margin
ϕ_e	Heading error
d_f	Lateral error
a_{pedal}	Accelerator pedal position
b_{pedal}	Brake pedal position
ρ_{ref}	Reference curvature
$M_{z,\,ref}$	Reference yaw moment
R	Path radius
l_d	Look-ahead distance
X_{prev}	x-coordinate of preview point
Y_{prev}	y-coordinate of preview point
X_{rear}	x-coordinate of rear axle centre

Y_{rear}	y-coordinate of rear axle centre
T_p	Look-ahead time
$RMSE_{precision}$	Root mean square error of lateral error/deviation
E_{tot}	Total energy consumption
$F_{x,\,ref}$	Reference longitudinal force
F_{yi}	Lateral tire forces at wheel i
$F_{x,right}$	Total right side distributed longitudinal force request
$F_{x,left}$	Total left side distributed longitudinal force request
$F_{x,ab}$	Longitudinal wheel force request on side a and axle b
$T_{i,\,EM,\,req}$	Electric motor torque request for motor/wheel i
$T_{EM,ab}$	Electric motor torque on side a and axle b
T_{FL}	Torque on front left wheel
T_{FR}	Torque on front right wheel
ΔT	Differential torque
$P_{RMSE,precision}$	Quantitation of PTC precision performance
$P_{MAX,precision}$	Quantitation of PTC max lateral error performance
P_{jerk}	Weighted value of RMSE and maximum lateral jerk
$P_{RMSE,jerk}$	Quantitation of PTC comfort performance
$P_{MAX,jerk}$	Quantitation of PTC maximum lateral jerk
P_{tot}	Total Power
P_{bat}	Battery power
$P_{em,i}$	Power consumption of Electric motor i
$P_{em,loss,i}$	Electronic motor losses on wheel i
P_{EPAS}	Power consumption of Electronic Power Assistance Steering
$P_{w,i}$	Power transfer to wheel i
P_{mech}	Mechanical power required for the vehicle's motion
P_{res}	Power losses from resistant factors (friction, drag)
$P_{sx,i}$	Longitudinal slip power losses on wheel i
P_{sy_i}	Lateral slip power losses on wheel i
$P_{rr,i}$	Rolling resistance power losses on wheel i
$P_{precision}$	Weighted value of RMSE and maximum lateral error
a_1,a_2	Weighting coefficients of of $P_{precision}$

Contents

List of Figures

List of Tables

1
Introduction

The automotive industry is constantly evolving when automakers develop safer, more comfortable and more efficient vehicles to meet customer demands and stay competitive. In recent years the transition from conventional combustion engines to electric powertrains has increased as regulations and automakers strive to lower emissions. Climate change has been acting as a basis for the recent electrification. However, in recent years, customer demands and disruptive innovations have also made Advanced Driver Assistance Systems (ADAS) and Autonomous Driving (AD) development central in the automotive sector. The advancement of these demands, together with rapid electrification, has extended functionalities and presented new possibilities for vehicle motion control systems [1]. In parallel with the public demand for highly advanced vehicle systems, the demand for better range and charging infrastructures makes it essential to keep developing new vehicle motion control systems to continuously improve energy efficiency and AD/ADAS systems for future electric vehicles.

Active vehicle motion control systems are an important development area as it concerns the enhancement of safety, comfort and efficiency during driving and involves the application of several sensors concerning environment perception and vehicle motion sensing. Autonomous vehicles are becoming customary, which means that all their subsystems are being developed and optimised at a fast rate. A Path Tracking controller (PTC) constitutes one of these subsystems and is required to ensure safe traffic behaviour. The initial focus of path tracking studies was on steering actuation, which was primarily developed with the purpose of driver modelling. However, with the upcoming demand on Advanced Vehicle Systems (AVS) in conventional vehicles, the research focus switched from driver modelling to autonomous driving applications [2]. Autonomous driving requires a thorough understanding of vehicle motion control. More specifically, as associated with this thesis, lateral motion control. Lateral vehicle control refers to the steering of the vehicle. [3] describes the design of steering controllers as either an imitation of the human driver or as dynamic models of a vehicle and control methods based on linear control theory in the same manner as [2]. More specifically, designing an autonomous four-wheel drive Electric Vehicle (EV) is concerned with the modelling of a control law to manoeuvre the car accurately and smoothly along a reference path [4].

As far as the propulsion systems of EV's go, a wide range of topologies can be implemented. A single Electric Motor (EM) propelling the front or rear axle or even individual motors on each wheel are two possible configurations of propulsion archi-

tectures [5]. According to [6], the layout with four-wheel hub motors appears to be the most attractive configuration due to the simple and efficient torque distribution to each wheel. The distribution of individual wheel torques is often referred to as Torque Vectoring (TV) in the literature. TV can generate a yaw moment on the chassis and therefore controls the yaw motion of the vehicle to increase lateral stability and improve vehicle handling. As the numbers of actuators increase, the level of functional integration can be increased because each wheel provides tractive and braking forces independent of each other, allowing for the control of yaw motion to improve the vehicle's directional stability. However, [1] states that an increase in vehicle behaviour flexibility indicates an increased number of possible failure modes that can transpire during the appliance of these systems. Therefore in the current development stage, it is of a compromising nature.

The configuration and design of the actuator and sensor architecture included in AD/ADAS and AVS are constrained by environmental aspects. All of the actuator and sensor energy consumption should be balanced and optimised with the driving dynamics. To some extent, this is applied to the sensors and electronic devices but, more importantly, to the electric actuators converting electrical energy to kinetic energy. It is described in [7] that a configuration of four EM's can enhance the energy efficiency using wheel torque control allocation algorithms. The motor power losses, tyre slip power losses or even a combination of these are used as examples. An efficient understeer characteristic design, i.e. energy-efficient reference yaw rate, can be implemented in any control allocation algorithm. According to [8], the understeer characteristic design alone can reduce the vehicle's energy consumption as much as the energy-efficient control allocation algorithms.

1.1 Background

Lateral motion control in terms of path tracking is not a new concept in the automotive industry and is well-researched in the literature. In a self-driving scenario, the vehicle has to be equipped with some algorithm to guide the vehicle without the steering inputs from a human driver. To accomplish such a task, one can implement a PTC. The purpose of a PTC is to apply appropriate steering motion to a vehicle executing a geometrically defined path and thereby guide the vehicle along that path. The goal is to minimise the difference in the vehicle's heading angle and the heading angle of the predefined path, or minimise the lateral error between the vehicle and the path while maintaining stability, depending on the PTC [9].

There are various types of path tracking methods; some are simpler, and others are more complex. Either can be sufficient, however, depending on the scenarios. What method to choose or how they can be combined will affect the performance of the path following. It can lead to instability or a loss of precision if the surrounding circumstances changes, i.e. the vehicle velocity. It is, therefore, essential to have a good understanding of what type of path tracking controller to use or how they can be combined to improve the path tracking performance. As mentioned previously, one of the initial purposes of developing path tracking for steering control was to

model a human driver, as the human driver can be seen as an advanced adaptive path tracking controller [2], which is described in more detail in [10]. However, path tracking has evolved to become one key factor in developing successful autonomous vehicles [11]. Today, different path tracking techniques can be divided into controllers based on simple geometric relationships that make use of either a kinematic or a dynamic vehicle model. The well-known linear single-track model or kinematic bicycle model is often used. These controllers could obtain the characteristics of a conventional feedback controller or even be modelled with more optimal control formulations such as the linear quadratic regulators with or without feedforward contributions [9], [12]. Using these relatively simple control laws for path tracking has already been proven successful in some well-known autonomous vehicle projects. In 2004-2005, the vehicles that finished in the top positions in the DARPA Grand Challenge, a competition where teams compete with autonomous robots/vehicles across an unrehearsed off-road terrain, utilised simple geometric controllers based on simple kinematic vehicle models. However, as the design objectives changes, new development challenges are presented when the precision and vehicle dynamics in other operating windows, i.e. higher speeds, must be considered. As an example, the autonomous vehicle that won the DARPA Urban Challenge, which has other challenges to consider compared to the previous competition, used a much more advanced model predictive control strategy. The comparison between different PTC's has been well documented in the literature. Both [2] and [9] give a detailed comparison of the performance and when different methods can be successful.

In an AD scenario, the steering wheel actuator commonly controls the lateral motion, which receives actuation inputs from the PTC. The lateral motion control is possible due to the power-assisted steering, which can apply torque to the steering system and thereby control the steering wheel angle. However, the steering capability would be affected if a failure occurred in the power steering system. Therefore, power-assisted steering is one of the vehicle's critical safety systems. A failure could mean that the vehicle drives off the road. Hence, to prevent catastrophic outcomes, it is required to have a backup system that can be activated if a failure occurs in the primary system. The backup systems are often designed based on redundancy, which means that the safety-critical system is duplicated to minimise the risk of both systems failing simultaneously. The secondary system can therefore take over if the primary system fails. However, previous research has also investigated the possibility of designing a backup system that can control the vehicle's lateral motion completely separated from the conventional steering system.

In [13], the possibility of utilising differential friction braking to control the vehicle's lateral motion to provide a fail-operational ability for self-driving vehicles is investigated. The report presents the capability and the suspension's effect on the steering capability. The results showcase that differential friction braking can be used to steer the vehicle but that there are limitations on how large curvature is achievable. Another research by [14] also develops a backup system using selective braking. However, this research focuses on mitigating errors in a steer-by-wire system. In [15], differential braking-assisted steering is also investigated to reduce the

effort from the human if the power steering system fails. Common in the previous research is that the friction brakes are utilised as a backup system. However, new electric powertrains enable new possibilities to use electric motors to control the vehicle's lateral motion instead of friction brakes. Finally, in [15], it is also stated that the advantage of a backup system for steering that uses differential braking, either by friction brakes or regenerative braking with the electric motors, is that it only requires software implementation but no hardware modifications.

Another use case when having multiple electric motors is to distribute the torque between them to improve, for example, the vehicle's handling. A control system that distributes the individual motor torque is called a torque vectoring controller. TV as a general concept is relatively intuitive with regard to a basic understanding of lateral dynamics. With a vehicle drivetrain layout of four individual onboard EM's, one could describe turning manoeuvres as nothing more than torque differences on each side. However, this general explanation of TV does not regard precision and excludes the different possibilities associated with TV. The most common use case with TV is to control the vehicle's yaw motion to improve, for example, the cornering ability and the vehicle's stability. The main blocks constituting a TV control framework according to [16] are the reference generator, a high-level controller and a low-level controller. The reference generator defines a target yaw rate and a sideslip angle. The high-level controller calculates the required total torque and yaw moment in a complete vehicle sense, and the low-level controller calculates the required force and yaw moment to individual torque demands for the wheels. However, TV control algorithms can be modelled with regard to specific performance requirements. Safety, stability, optimised energy efficiency or a combination of these and other properties could be used as a basis for the TV control algorithm. [16] states that most reference yaw rate generators focus on tuning the understeer coefficient. However, as stated, TV control algorithms can be modelled based on specific performance properties. For example, [6] proposes two different control strategies for TV. The first logic is based on optimal control theory, and the second control strategy is on the understeer/oversteer behaviour of the vehicle using a dynamical yaw index associated with measured dynamical vehicle properties. In the first logic, vehicle sideslip and yaw rate are estimated using lateral acceleration measurements and roll stiffness distribution of the vehicle. The second control strategy uses a proportional regulator for the purpose of keeping the vehicle in steady state cornering conditions, which leads to a prevention of excessive increase of sideslip angle. This method is advantageous in the way that it does not estimate the friction coefficients since that is only required to avoid excessive longitudinal force demands and also avoid the estimation of the sideslip angle since the regulated quantity is a yaw index being proportional to the lateral acceleration and inversely proportional to the yaw rate and vehicle speed.

TV can also be combined with the PTC. However, the combination of a PTC and a Torque Vectoring Controller (TVC) is not a well-documented system which [2] emphasises. There have been some appropriate investigations with gainful results. [2] compares the integration of TV with different steering-based PTC's during obstacle

avoidance tests. Single point PTC's without a look-ahead point and multiple-point preview PTC's are implemented as both independent of the TVC, where the TVC receive the steering angle output of the PTC to generate a reference yaw rate and also as a merged system with integrated steering and direct yaw moment control. The performance indications of the different configurations were evaluated concerning several quantities, including the entry speed of the vehicle into the different reference paths and the root mean square values for two different quantities, namely the position error relative to the reference path and the yaw angle error between vehicle trajectory relative to the reference path. The yielded results are partly evaluated with the entry speed of the vehicle. The path tracking controllers with preview had the highest entry speeds for the basic reference path. However, when the reference path obtained a further smoothed-out shape, the controllers without preview achieved the highest entry speeds. The implementation of torque vectoring, both integrated and separate multi-layer concepts, improved the entry speed by 1 to 3 km/h. Another study diving into the combination of path tracking and TV is described in [17], which proposes a control scheme consisting of three parts. The different parts are a non-linear model predictive PTC to generate the steering angle and the desired longitudinal force of the EV, a lateral stability controller to provide an extra yaw moment to balance stability and mobility with the use of a lateral stability criterion to judge vehicle stability and a TVC. This integrated model predictive and torque vectoring control was tested for different scenarios and improved lateral stability by maintaining control in a combined steer and brake process in a sharp turning manoeuvre on high friction roads. The path tracking precision was enhanced for the lane change test and the turning test with low friction road due to improved vehicle mobility at relatively bad road conditions, which reduced the vehicle side slip.

Even though the efficiency of EM's is superior to internal combustion engines and is more environmentally friendly due to the exclusion of fossil fuels, there is still room for improvement. Utilising four onboard independent EM's allows the implementation of optimal force allocation algorithms to reduce the energy consumption further while cornering. The engineering of energy-efficient systems is a continuous development area, and even with a transition to environmentally friendly energy sources, i.e. electric powertrains, and a significant increase in propulsion system efficiency, there is still room for improvement in terms of energy optimisation. This idea stems from the fact that electric vehicles have a relatively low mileage per charge [18]. An attempt to improve the efficiency was made in [19], where it is explained that a configuration of four individual EM's results in an over-actuated system, i.e. a mathematically under-determined problem [1], leading to an infinite amount of torque distribution combinations to achieve the requested output. This property allows for optimisation opportunities. [19] improves the efficiency of a TVC by distributing the tractive/braking forces and the yaw moment requests according to an energy-efficient control allocation strategy which was based on drivetrain power loss measurements. The results showed a 4 % reduction in energy consumption during cornering conditions.

Finally, it is evident that there has been a lot of research and development previously regarding the topic of yaw and lateral vehicle motion control. The ever so advancing development of the different path tracking methods for autonomous vehicles with various success in different applications have played a key role in developing safer and smother autonomous vehicles. However, the development and comparison of different PTC's are often conducted independently of other motion control systems focusing on front-steered vehicles. More research can still be conducted comparing different methods of path tracking and how to combine them with other vehicle motion control systems.

Furthermore, it is also evident that with the growing number of electric vehicles and the possibilities in yaw control that the electric powertrain enables, rapid research and development are ongoing on the topic of torque vectoring. The purpose of this development has mainly been on driving dynamics, such as controlling understeering for better cornering performance. Another focus area when developing TVC is its potential to improve energy efficiency. New electric powertrains also enable new backup systems for lateral motion control to be developed and the capability of such systems is not very well researched in the literature. Even though there has been research on combining PTC with TVC, which has been presented earlier in this report, merging these two vehicle motion control functions into one is still a new research area which requires more attention in the development of new autonomous electric vehicles. In the research presented in this section, the focus area in merging these functions has also previously been focusing on improving the handling qualities of the vehicle with regards to, for example, stability, comfort or safety in specific manoeuvres rather than improving energy efficiency.

Consequently, from the research presented in this section, it is evident that there exists a potential for vehicle dynamics enhancement when further developing path tracking and torque vectoring. The handling qualities can be improved beyond the conventional stability control systems of today's vehicles. Moreover, when considering the possibility of improving energy efficiency with TV, combining the two yaw and lateral vehicle motion control functions into one centralised framework for controlling different actuators enables improvements in both driving dynamics and energy efficiency. Therefore, this is an important research area in developing safe, comfortable and energy-efficient electric vehicles of the future.

1.2 Research problem

In future EV's, the number of active vehicle control functions, as well as sensors for vehicle motion sensing and environment perception, are expected to increase. Combining this with different actuator configurations concerning EM's that are possible with EV's enables various numbers of different active vehicle motion control functions. These functions could be used to enhance the level of safety, comfort and energy efficiency. However, even though there has been much independent research on PTC's and TVC's, with some presented in the previous section, there is still room to develop new PTC's and TVC's to improve the path following and energy

efficiency of future EV's. Furthermore, how different motion control functions can be combined and how new electric powertrain configurations can be used as backup systems need more research. There should also be a balance between the energy consumption of all these sensors and actuators with the driving dynamics in both manual and autonomous driving scenarios. The energy efficiency in these driving scenarios can be optimised by combining different actuators. The redundant sensors and actuators also enable the design of a safer and smoother fall-back system if an actuator or a sensor stops working.

This thesis project focuses on these problems, specifically concerning how yaw and lateral motion control in terms of PTC and TVC can improve the primary and backup path following and the vehicles' energy efficiency in a centralised framework in the car. Both as separate controllers or in a combination. Moreover, the theoretical research is also extended to include a practical implementation in a test vehicle. The research problems can be summarised in the following questions:

- Which of the evaluated geometric path tracking algorithms are superior for path following concerning precision comfort and robustness?
- Can torque vectoring be used as a safety backup steering system to ensure fail-operational ability if the steering system fails?
- Can an optimised torque vectoring controller reduce the vehicle's energy consumption?
- Can path tracking control be combined with torque vectoring control in a centralised control system for optimal path following and energy consumption?

The project is divided into different topics, each aiming to address the research questions. Technical content included in the first research problem is evaluating and implementing different PTC's utilising only front-wheel steering. The performance of the PTC's are evaluated concerning precision, comfort and robustness, which will be examined in both mild and dynamic driving conditions to appraise the robustness of the PTC's. The second research problem includes the development of an integrated path tracking controller and a torque allocator with the purpose to steer the vehicle as a backup system using differential torques only. Considering that this is a backup safety system, the requirement of this integrated controller is to keep the vehicle within an arbitrary distance on a reference path and not focus on energy efficiency, comfort or robustness. The third and fourth research problems can be summarised as structuring and formulating the energy optimisation problem to design a torque vectoring controller for both optimal path following and energy consumption.

1.3 Aim

The main work expected here is to design and implement a centralised controller for vehicle yaw and lateral motion control in manual driving, as well as a handful of AD/ADAS scenarios. Centralised means that all the motion requests are calculated centrally at the vehicle motion control layer, where one specific actuator request,

e.g. target steering angle, will be generated and sent to the steering actuator control module. The goal is to fulfil the manual and AD driver-requested trajectory in an energy-efficient and safe way when deploying different actuators.

1.4 Limitations

The PTC's that are to be evaluated are the Pure Pursuit controller (PPC) and the Stanley controller (SC). However, several other PTC's could provide useful knowledge and reinforce the expected results based on the purpose of this thesis. Nevertheless, the time frame in which this thesis will be conducted will not allow for a thorough investigation of more path tracking concepts. Consequently, it will not fulfil the purpose of this thesis if more than the two PTC's in question are studied and evaluated. Suppose some fundamental functional changes that are characteristics of the controllers mentioned above are to be made to acquire a slightly altered but different PTC. In that case, that one will be evaluated in the same manner.

Implementing optimal torque allocation algorithms to reduce the vehicle's energy consumption is comprehensive and open for development. The algorithm can be based on several variables to optimise, and multiple methods can be applied. Therefore, a unique energy-efficient torque allocation algorithm will not be derived in this project due to the time constraints and a small precision compromise of studying and evaluating existing methods concerning the actuators and the system in general of the test vehicle. For example, if a torque allocation algorithm is based on the measurement of road friction coefficient using optical sensors to measure light absorption [20], then that method would be excluded since this equipment is unavailable in the test vehicle.

1.5 Societal, ethical and ecological aspects

The electric vehicles of the future play an important role in making the vehicle fleet more environmentally friendly. As new regulations for car manufacturers get more strict and when countries plan to implement a ban on selling combustion cars [21], the requirement to develop new electric vehicles increases. Meanwhile, automakers also develop new technologies in active safety and autonomous driving, which strive to improve the safety standards for road and traffic occupants. Consequently, the importance of safe and sustainable vehicles also requires a discussion on how a concept may comply with apparent environmental and ethical issues that can affect the society it is operated in.

This thesis project focuses on the development of yaw and lateral motion control systems for electric road vehicles. It is important that the societal, ethical and ecological aspects of these systems are not overlooked. When developing a control system that acts on different actuators to control the vehicle's motion, it is crucial to ensure that it is safe. In 2016 approximately 1.3 million people died as a result of road traffic accidents [22], and one big incentive for developing new ADAS and AD

systems is to reduce this number. AD has the potential to make driving safer for both vehicle and traffic occupants, and level 5 autonomous vehicles will eventually be available for a broader market. However, more development is still required to ensure its safety and path tracking algorithms are one part of this development. Developing path tracking algorithms can, therefore, contribute to a better society with reduced road traffic accidents and deaths in the long term.

Another aspect of electric vehicles is their ecological impact on the environment. Some research shows that, on average, the life-cycle emissions from electric vehicles are lower than newer petrol cars, and even inefficient electric vehicles are less emission-intensive than the most energy-efficient new petrol car [23]. However, the environmental aspects of electric cars still require attention. Especially as previously mentioned, the vehicle's energy efficiency can be improved by optimising the torque allocation. The ecological aspects of this thesis are, therefore, also of importance.

Finally, to conclude this discussion, it is evident that this thesis has both an ethical and an ecological aspect. It is crucial to ensure a safe and robust control system, as errors could endanger human life. The design for energy optimisation will also contribute to addressing the so apparent environmental issues as well. Developing a centralised yaw and lateral motion control system for torque vectoring and path tracking will likely contribute to safer and more energy-efficient vehicles in the future.

2
Control Allocation

An essential part of this project is the fact that the vehicle used in this study is over-actuated. With increasing electrification and higher demands on safety, the number of actuators and how they are used in the vehicle have changed. Previously, the actuators were used for only one task, for example, friction brakes to brake the vehicle. Now, friction brakes are also used in safety functions related to stability functions, such as rollover protection. When adding an electric motor, the braking task can be performed by either the electric motor or the friction brakes. This redundancy of actuators leads to control-related challenges. Which actuators should be used, and how should the requests be allocated between them to achieve the desired vehicle motion? In this chapter, the control architecture to solve this problem is introduced, which is control allocation.

2.1 Definition of over-actuation

An easy-to-understand definition of over-actuation is based on the understanding that with an over-actuated system, one has the possibility to choose how a specific task is to be performed. From a theoretical point of view, if a task has less degrees of freedom to control than there are actuators that could perform the task, then the system is over-actuated. For example, suppose a vehicle is equipped with friction brakes and electric motors. In that case, it is over-actuated regarding the deceleration task since it could be performed by either the friction brakes or the electric motors [24]. The degree of freedom when braking a vehicle is 1 (longitudinal motion), but 2 actuators can perform the task. Therefore, the vehicle is over-actuated. Similarly, the vehicle can be over-actuated regarding the lateral motion. Ground vehicles can be modelled as a rigid body with three degrees of freedom when the steering is considered, which are characterised by three dynamic states: longitudinal, lateral, and yaw motion [25]. A vehicle equipped with four independently actuated electric motors for each wheel provides the freedom to allocate the wheel forces individually. Each actuator, i.e. electric motor, can give rise to each one of the states and therefore, the vehicle is over-actuated concerning the longitudinal, lateral and yaw motion. Adding the friction brakes and the steering wheel, there can be a total of nine actuators to control the vehicle's planar motion. Consequently, there are many options to achieve the same vehicle motion.

2.2 Definition of control allocation

Control allocation goes hand to hand with over-actuation as it refers to the different methods to allocate a given control variable to solve the over-actuation problem. Control allocation distributes the total control demand between the different actuators. There are different control allocation methods, for example, pseudo-inverse, daisy-chaining, and direct control allocation [24]. Other examples of control allocation worth mentioning include online solvers using active-set algorithms or offline optimisation using look-up tables. Control allocation can be described as actuation selection of the control effort in the sense that the control effort is primarily decided, which is then allocated to the different actuators with consideration to an arbitrary characteristic of the system [24]. The control variable could be allocated concerning comfort, performance and/or energy efficiency. This project's primary interest is to allocate the torque request to the different EM's to increase the vehicle's energy efficiency, which is enabled by the fact that there are an infinite number of torque allocation combinations available. Utilising an optimised control allocation method can reduce the vehicle's energy losses. Worth to note is that this will be done online, where the allocation will be decided instantaneously, not prematurely.

2.3 A Centralised Control Architecture

Historically, vehicles have had decentralised control architectures, meaning that each actuator has one specific purpose and control module, which receives requests and allocates them to the actuator to achieve the desired motion. However, this is unsuitable for an over-actuated system [24], and therefore, this is changed to a more appropriate control architecture which centralises the allocation of the actuators.

As the name would suggest, the centralised control architecture centralises the coordination and allocation of the different actuators in one place in the vehicle, i.e. the selection and allocation of the steering wheel angle, the motor torques, and the friction brakes are centralised in the control allocation. One advantage with control allocation is that it separates the actuator selection and regulation tasks in the control design, which implies that the regulation tasks are done prior to the actuator selection [24]. Consequently, the centralised controller consists of two main parts: the reference generator and the control allocation. The reference generator interprets the driver inputs and sensor data and regulates/computes reference signals, which are the inputs to the control allocation. The control allocation then coordinates and allocates the outputs to the different actuators based on the reference signals and sensor data to achieve the desired vehicle motion.

Another benefit of this architecture is the arbitration of different requests from different control algorithms, which means how they are prioritised and coordinated between the actuators. Furthermore, the individual control modules in the decentralised control structure are often manufactured by suppliers, making it more complicated to develop new control algorithms. The centralised control architecture

enables the integration and development of new vehicle motion control systems with existing software, which is essential in this project.

3
Methodology

This chapter introduces the methodology for the project. The chosen simulation environment where the controllers are developed is presented in section 3.1, which includes the driver and vehicle model and the chosen control architecture structure. The test vehicle utilised to evaluate the controllers in the project is presented in section 3.2. Finally, a simplified vehicle model for the test vehicle, which is used in the initial development stages, is derived in section 3.3.

3.1 Simulation Environment

The simulation environment is developed in IPG CarMaker and Matlab Simulink, which is illustrated by the block chart in Figure 3.1. IPG CarMaker contains the driver model, the surrounding environment and most of the vehicle model. The control architecture is developed in Matlab Simulink, which consists of a reference generator and a control allocator. The actuator control block consists of the powertrain model and the steering wheel angle control and is also developed in Matlab Simulink to complete the vehicle model.

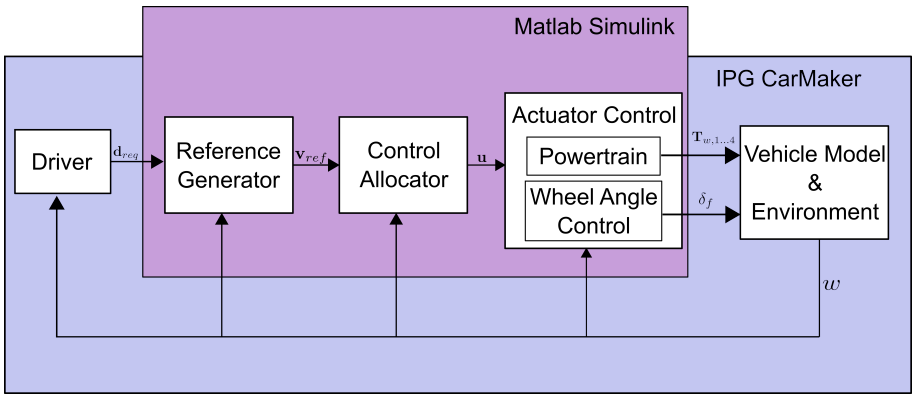

Figure 3.1: Block chart illustration of the simulation environment and control architecture

The IPG CarMaker driver model can control the vehicle's planar motion by the steering wheel angle δ_{req}, accelerator pedal a_{pedal}, and brake pedal b_{pedal} requests. The driver request signals are bundled in a vector $\mathbf{d}_{req}$ as displayed in Figure 3.1. The use cases include a driver-in-the-loop, which means that the IPG CarMaker

driver model follows a predefined path and velocity profile. Therefore, the driver acts as the feedback control, which closes the control loop by, for example, increasing the accelerator pedal position if the desired vehicle motion is not met.

$$\mathbf{d}_{req} = \begin{bmatrix} \delta_{req} \\ a_{pedal} \\ b_{pedal} \end{bmatrix} \tag{3.1}$$

The reference generator processes the requested signals from the driver, $\mathbf{d}_{req}$, to interpret the desired vehicle motion and generate reference signals to the control allocator. The driver always controls the longitudinal motion throughout this study with the accelerator and brake pedal. In the reference generator, the requested pedal positions are translated into a reference longitudinal force request, $F_{x,ref}$ by the driver interpreter using a simple linear model given by

$$F_{x,\,req}(a_{pedal}, b_{pedal}) = \begin{cases} c_1 \cdot a_{pedal}, & \text{if } a_{pedal} > 0 \\ 0, & \text{if } v = 0 \\ c_2 \cdot b_{pedal}, & \text{otherwise} \end{cases} \tag{3.2}$$

$$0 \leq a_{pedal} \leq 1, \quad 0 \leq b_{pedal} \leq 1 \tag{3.3}$$

where c_1 and c_2 are constants. The reference generator also computes a reference curvature ρ_{ref} describing the curvature of the reference vehicle trajectory. The reference curvature is computed by the geometric path tracking controller, which will be described in more detail in chapter 4. The final reference signal is the reference yaw moment, $M_{z,ref}$, which will be described in chapter 6. The reference signals are bundled in the vector $\mathbf{v}_{ref}$.

$$\mathbf{v}_{ref} = \begin{bmatrix} \rho_{ref} \\ F_{x,\,ref} \\ M_{z,\,ref} \end{bmatrix} \tag{3.4}$$

Once the reference signals are acquired, the control allocator computes the torque distribution between the different EM's, $T_{EM,1...4}$ and the steering wheel angle, δ_{SW}, based on the reference signals. Note that the control allocation will allocate the request signals differently depending on the configuration. In this project, three different controllers are developed, a path tracking controller, a steer by torque vectoring controller and an energy efficient torque vectoring controller. Consequently, the utilised controller will determine the output of the control allocation. If, for example, the torque vectoring controller is not utilised, the control allocation will

allocate an equal torque request to each motor based on the reference longitudinal force request, $F_{x,ref}$. The vector $\mathbf{u}$ contains all the requested control signals from the control allocator. The architecture for each controller and how the reference signals and the control allocation is computed is described in more detail for each respective controller in chapter 4, 5 and 6.

$$\mathbf{u} = \begin{bmatrix} \delta_{SW} \\ T_{1,\,EM,\,req} \\ T_{2,\,EM,\,req} \\ T_{3,\,EM,\,req} \\ T_{4,\,EM,\,req} \end{bmatrix} \tag{3.5}$$

The request signals in $\mathbf{u}$ are then processed in the final Matlab and Simulink model, i.e. the actuator controller. The actuation control block models the actuator hardware, which means that it calculates all the power losses throughout and confines the control signals within their respective actuator limits. The EM and inverter losses, transmission losses and battery efficiency are modelled. The losses are described in detail in chapter 6.

The actuator controller outputs are then sent to the vehicle model in IPG CarMaker, which will feed the vehicle and environment data back to all the blocks in the system. These signals are compiled in the vector $\mathbf{w}$.

$$\mathbf{w} = \begin{bmatrix} v_x \\ \psi \\ X_{pos} \\ Y_{pos} \\ \dots \end{bmatrix} \tag{3.6}$$

The first four elements of $\mathbf{w}$ are the most significant signals that will be included in calculations and discussions. v_x is the vehicle's longitudinal velocity, ψ is the vehicle's yaw rate, X_{pos} and Y_{pos} is the vehicle's position. However, several other variables are also used throughout the model that utilises other feedback signals from the vehicle model and the environment, hence the ellipsis points at the end of $\mathbf{w}$. These signals are, however, not discussed in the report.

3.2 Test Vehicle

The test vehicle used in this study is a modified Polestar 1 where the originally mounted front axle combustion engine has been replaced with two Permanent Magnet Synchronous Machines (PMSM). Therefore the test vehicle is equipped with four

identical PMSM's connected to each wheel respectively, with a fixed transmission ratio and a half-shaft. Each EM can be controlled independently by allocating the torque requests. The test vehicle is modelled both in IPG CarMaker and in Matlab Simulink. However, the process of developing the vehicle model is not covered in this report as it was not included in this project. The relevant vehicle parameters are presented in Table 3.1.

Description	Symbol	Value	Unit
Vehicle mass	m	2159	$[Kg]$
Distance rear axle to CoG	l_r	1.22	$[m]$
Distance front axle to CoG	l_f	1.523	$[m]$
Rear cornering stiffness	C_{yr}	173390	$[N/rad]$
Front cornering stiffness	C_{yf}	126950	$[N/rad]$
Vehicle yaw intertia	J_{zz}	4860	$[kgm^2]$
Wheel radius (static)	r_w	0.33	$[m]$
Transmission ratio	n_t	10	[1]
Steering wheel ratio	n_{sw}	16	[1]
Trackwidth	w	1.645	$[m]$
Max motor speed	ω_{max}	12000	$[rpm]$
Max motor torque	$T_{EM,max}$	270	$[Nm]$
Min motor torque	$T_{EM,min}$	-270	$[Nm]$

Table 3.1: Vehicle and actuator parameters

The test vehicle is equipped with a GPS sensor to obtain the necessary real-time variables. Figure 3.2 is a schematic view of the vehicle drivetrain and GPS sensor. The test vehicle is also equipped with a MicroAutoBox from dSpace, which enables testing of the developed controllers in real-time in the test vehicle. The MicroAutoBox is suitable when testing new functions in a rapid prototyping scenario where it acts as an interface that bypasses and sets different signals on the CAN bus in the vehicle.

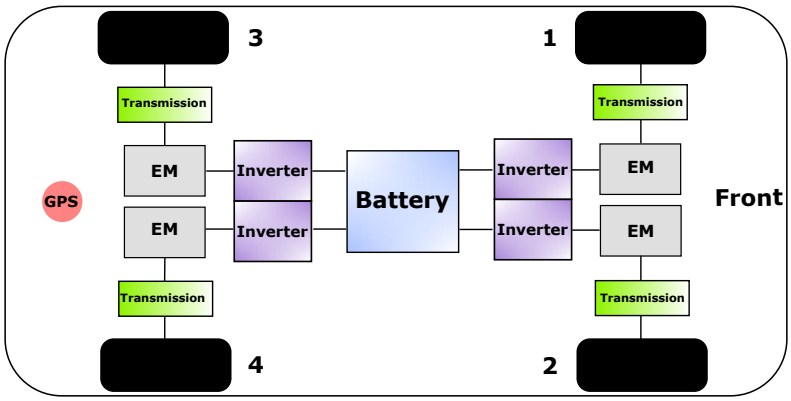

Figure 3.2: Schematic view of the test vehicle drivetrain and GPS sensor

3.3 System Modelling

As mentioned previously, the process of developing the IPG CarMaker vehicle model is not described in this report. However, the process of developing the controller concepts in this study and integrating them for real-time applications consists of several steps. A good approach can, therefore, be to use a simplified vehicle model and simulation environment in the initial development stages before utilising the IPG CarMaker simulation environment and then evaluating the controllers in the test vehicle. Therefore, a simplified vehicle model is developed and used to develop the PTC, which is described in the following sections.

3.3.1 Kinematic bicycle model

A regularly exploited vehicle model in the development of geometric PTC's is the kinematic bicycle model, which is a simplification of the Ackermann kinematic vehicle model in the way that the wheels on each axis are combined to form a two-wheeled model [9]. The kinematic bicycle model is visualised in Figure 3.3.

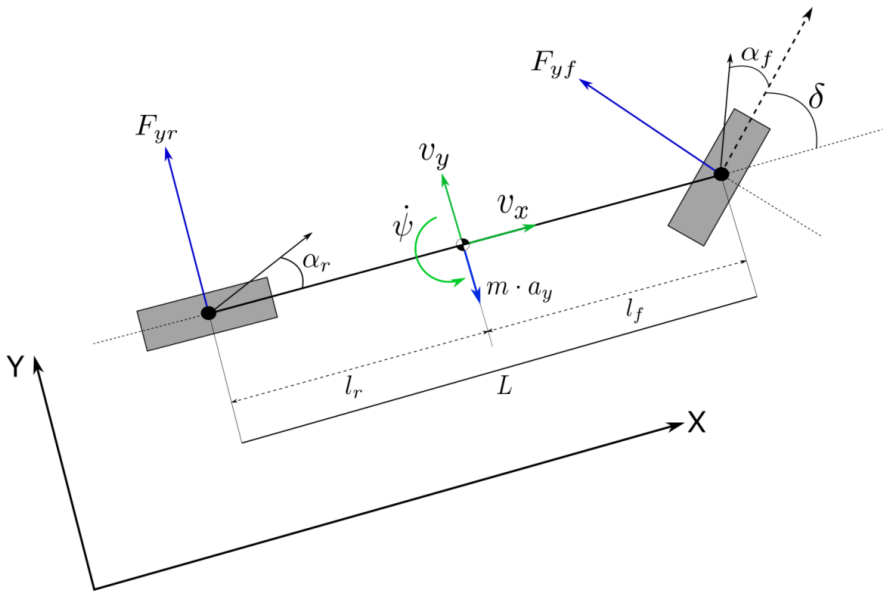

Figure 3.3: Kinematic bicycle model

Note that in Figure 3.3, the local reference frame is positioned at the vehicle's centre of mass, which would allow for simple application of the laws of motion. Also, assuming small steering angles, the following simplifications can be made:

$$\sin(\delta) \approx \delta, \qquad \cos(\delta) \approx 1, \qquad \tan(\delta) \approx \delta. \tag{3.7}$$

As illustrated in Figure 3.3, free-body diagrams are used to describe the physical models. The deriving equations of the free-body diagram are presented in equations 3.8 - 3.14. Equations 3.8 and 3.9 make up the equilibrium equations of the model

$$m \cdot a_y = F_{yf} \cdot \cos(\delta) + F_{yr} \approx F_{yf} + F_{yr} \tag{3.8}$$

$$J_{zz} \cdot \ddot{\psi} = l_f \cdot \cos(\delta) \cdot F_{yf} - l_r \cdot F_{yr} \approx l_f \cdot F_{yf} - l_r \cdot F_{yr} \tag{3.9}$$

where

$$a_y = \dot{v}_y + \dot{\psi} \cdot v_x. \tag{3.10}$$

Equation 3.8 describes the lateral force dynamic equilibrium and is obtained by applying Newton's second law of motion. Note that the term describing the lateral force produced by the front tires utilises the small steering angle simplification. The lateral acceleration as derived in equation 3.10 is a sum of the lateral acceleration $\dot{v}_y$ in the body frame and the centripetal acceleration of the vehicle. Since all the forces in the X-Y plane rotate around the centre of gravity of the vehicle, the moments produced by the tire forces act in opposite directions and equation 3.9 demonstrates that the difference of these moments is equal to the moment produced by the inertia J_{zz}.

The constitutional equations describe the relations between forces, moments and motions, which in this case refers to the tire model described by equations 3.11 and 3.12, which defines the lateral tire forces as the product of the tire cornering stiffness and the tire slip angle. The tire model falls under the type of constitutional cases describing dry friction contact.

$$F_{yf} = -C_f \cdot \alpha_f \tag{3.11}$$

$$F_{yr} = -C_r \cdot \alpha_r \tag{3.12}$$

The compatibility equations describe the relations between motions, such as positions, velocities and accelerations. Equations 3.13 and 3.14 apply the simplifications of small steering angles to define the tire slip angles as a function of the motion-related variables.

$$\alpha_f = \arctan\left(\frac{l_f \cdot \dot{\psi} + v_y}{v_x}\right) - \delta \approx \frac{l_f \cdot \dot{\psi} + v_y}{v_x} - \delta \tag{3.13}$$

$$\alpha_r = \arctan\left(\frac{-l_r \cdot \dot{\psi} + v_y}{v_x}\right) \approx \frac{-l_r \cdot \dot{\psi} + v_y}{v_x} \tag{3.14}$$

The mathematical model of the physical system as presented in equations 3.8 - 3.14 act as a basis for the derivation of the state-space form of the specific derived continuous linear time-invariant system, which is a linear representation of the dynamic system. Expressing the system in state-space form is a basis for dynamics processing. Equations 3.15 and 3.16 displays the state space form

$$\dot{x} = A \cdot x + B \cdot u \tag{3.15}$$

$$y = C \cdot x + D \cdot u \tag{3.16}$$

Where x is the state vector with states $x \in \mathbb{R}^n$ and state derivatives $\dot{x} = \frac{dx}{T_p} \in \mathbb{R}^n$. The output vector is denoted by $y \in \mathbb{R}^j$ and the input vector $u \in \mathbb{R}^m$. The dimensions of the matrices A, B, C and D are presented below

$$A \in \mathbb{R}^{n\,x\,n}, \quad B \in \mathbb{R}^{n\,x\,m}, \quad C \in \mathbb{R}^{j\,x\,n}, \quad D \in \mathbb{R}^{j\,x\,m} \tag{3.17}$$

with n being the number of states, m the number of inputs and j number of outputs.

The state variables are the local lateral vehicle velocity v_y, the vehicle yaw rate $\dot{\psi}$, the vehicle yaw angle ψ, and the global lateral position Y. Note that the state variables could be any arbitrary variable, provided that the variable can describe the state of the system. The state vector is defined as

$$x = (v_y \; \dot{\psi} \; \psi \; Y)^T \in \mathbb{R}^4 \tag{3.18}$$

and the state derivative variables are defined according to equations 3.19 - 3.20 respectively.

$$\dot{v}_y = \frac{v_y(-C_{yr} - C_{yf}) + \dot{\psi}(C_{yr} \cdot l_r - C_{yf} \cdot l_f - m \cdot v_x^2)}{m \cdot v_x} + \frac{C_{yf} \cdot \delta}{m} \tag{3.19}$$

$$\ddot{\psi} = \frac{v_y(l_r \cdot C_{yr} - l_f \cdot C_{yf}) + \dot{\psi}(-C_{yr} \cdot l_r^2 - C_{yf} \cdot l_f^2)}{J_{zz} \cdot v_x} + \frac{C_{yf} \cdot l_f \cdot \delta}{J_{zz}} \tag{3.20}$$

The expressions for $\dot{v}_y$ and $\ddot{\psi}$ are derived by factoring them out and substituting the appropriate variables in equations 3.8 - 3.14.

The input and output variables are chosen with regard to the objective of the system. Since the vehicle model is the plant model, which is more commonly known as the process of the control system, the output variables, i.e. the control variables, are chosen to be identical to the state variables, namely the local lateral vehicle velocity v_y and the vehicle yaw rate $\dot{\psi}$. Having numerous outputs provides the freedom to use several methods to find the optimal controller with respect to precision and comfort, amongst other measurable qualities. Also, the outputs should be a representation of the vehicle motion. The actuating variable, which is the input variable to the vehicle model, is chosen as the steering angle δ as it is frequently used as the output of the PTC [11], [2], [9], and the input to the kinematic bicycle model [26], [27]. The input vector u and output y are therefore defined as

$$u = \delta \in \mathbb{R}^1 \tag{3.21}$$

$$y = (v_y \ \dot{\psi})^T \in \mathbb{R}^2 \tag{3.22}$$

and using the general state space form as presented in equations 3.15 and 3.16 and the expressions for the state derivative variables defined by equations 3.19 and 3.20, the matrices A, B, C and D are derived and presented below.

$$A = \begin{pmatrix} -\frac{C_{yr}+C_{yf}}{m \cdot v_x} & \frac{C_{yr} \cdot l_r - C_{yf} \cdot l_f - m \cdot v_x^2}{m \cdot v_x} \\ \frac{C_{yr} \cdot l_r - C_{yf} \cdot l_f}{J_{zz} \cdot v_x} & -\frac{C_{yr} \cdot l_r^2 + C_{yf} \cdot l_f^2}{J_{zz} \cdot v_x} \end{pmatrix} \in \mathbb{R}^{2\ x\ 2} \tag{3.23}$$

$$B = \begin{pmatrix} \frac{C_{yf}}{m} \\ \frac{l_f \cdot C_{yf}}{J_{zz}} \end{pmatrix} \in \mathbb{R}^{2\ x\ 1} \tag{3.24}$$

$$C = \begin{pmatrix} 1 & 0 \\ 0 & 1 \end{pmatrix} \in \mathbb{R}^{2\ x\ 2} \tag{3.25}$$

$$D = \begin{pmatrix} 0 \\ 0 \end{pmatrix} \in \mathbb{R}^{2\ x\ 1} \tag{3.26}$$

All the terms in equations 3.15 and 3.16 are now defined, and the state space model of the physical system is presented in equations 3.27 and 3.28.

$$\begin{pmatrix} \dot{v}_y \\ \ddot{\psi} \end{pmatrix} = \begin{pmatrix} -\frac{C_{yr}+C_{yf}}{m \cdot v_x} & \frac{C_{yr} \cdot l_r - C_{yf} \cdot l_f - m \cdot v_x^2}{m \cdot v_x} \\ \frac{C_{yr} \cdot l_r - C_{yf} \cdot l_f}{J_{zz} \cdot v_x} & -\frac{C_{yr} \cdot l_r^2 + C_{yf} \cdot l_f^2}{J_{zz} \cdot v_x} \end{pmatrix} \cdot \begin{pmatrix} v_y \\ \dot{\psi} \end{pmatrix} + \begin{pmatrix} \frac{C_{yf}}{m} \\ \frac{l_f \cdot C_{yf}}{J_{zz}} \end{pmatrix} \cdot \delta \tag{3.27}$$

$$\begin{pmatrix} \dot{v_y} \\ \ddot{\psi} \\ \dot{\psi} \\ Y \end{pmatrix} = \begin{pmatrix} 1 & 0 \\ 0 & 1 \end{pmatrix} \cdot \begin{pmatrix} v_y \\ \dot{\psi} \end{pmatrix} + \begin{pmatrix} 0 \\ 0 \end{pmatrix} \cdot \delta \tag{3.28}$$

The relationship between the output signal of a control system and the input signal is represented by a transfer function. Since transfer functions represent linear time-invariant systems in the frequency domain, the transfer function is acquired by dividing the numerator polynomial, i.e. the output variable in the frequency domain, by the denominator polynomial, which is the input variable in the frequency domain. The transfer functions from steering angle to local lateral vehicle velocity v_y and the vehicle yaw rate $\dot{\psi}$ are defined by equations 3.29 and 3.30, respectively. The parameters used in the matrices A and B given by equations 3.23 and 3.24 are presented in Table 3.2.

Parameter	Value	Unit
m	2159	$[Kg]$
l_r	1.22	$[m]$
l_f	1.523	$[m]$
C_{yr}	173390	$[N/rad]$
C_{yf}	126950	$[N/rad]$
v_x	60	$[km/h]$
J_{zz}	4860	$[kgm^2]$

Table 3.2: Parameter values used for kinematic bicycle model

$$G_{\delta \to v_y}(s) = \frac{v_y(s)}{\delta(s)} = \frac{58.8s - 241.8}{s^2 + 15.17s + 60.57} \tag{3.29}$$

$$G_{\delta \to \dot{\psi}}(s) = \frac{\dot{\psi}(s)}{\delta(s)} = \frac{39.78s + 345.3}{s^2 + 15.17s + 60.57} \tag{3.30}$$

The yaw angle ψ is another variable that could be used to handle the position and state of the vehicle. Luckily it is easily derived since the transfer function of the yaw rate $\dot{\psi}$ is already defined. The time derivative of the yaw rate is equal to the yaw angle, and in the frequency domain, an integration is represented by the factor $1/s$. Therefore the yaw angle is defined as

$$\psi = \dot{\psi} \cdot \frac{1}{s} \to G_{\delta \to \psi} = \frac{\psi(s)}{\delta(s)} = \frac{39.78s + 345.3}{s^3 + 15.17s^2 + 60.57s} \tag{3.31}$$

3.3.2 Frequency response analysis

The bode plots for the transfer functions from steering angle to lateral velocity, yaw rate and yaw angle are shown in Figures 3.4 - 3.6 respectively.

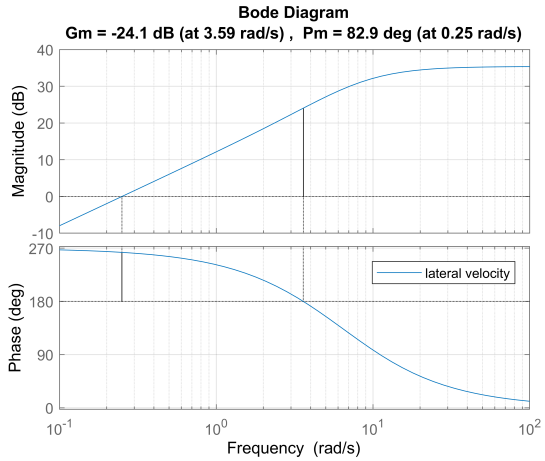

Figure 3.4: Bode plot for transfer function from steering angle to lateral velocity

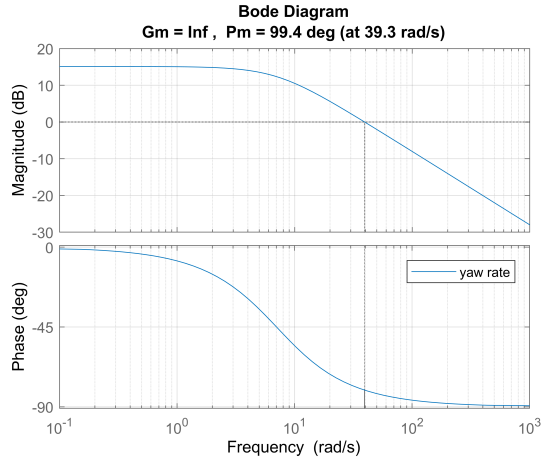

Figure 3.5: Bode plot for transfer function from steering angle to yawrate

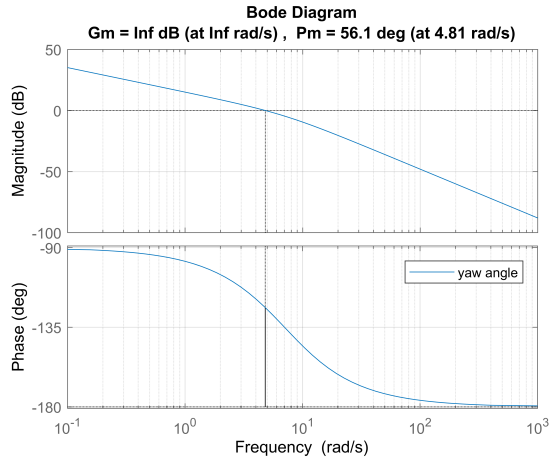

Figure 3.6: Bode plot for transfer function from steering angle to yaw angle

The phase margin is positive for each system, and the gain margin of $G_{\delta \to \dot{\psi}}$ and $G_{\delta \to \psi}$ are infinite, meaning that these systems are stable. However, the gain margin of the transfer function $G_{\delta \to v_y}$ is negative, which does not necessarily mean that the system is unstable. There is much more to stability analysis than observing the sign of the gain margin because unstable systems are undefined for this method. For a LTI system to be stable, the transfer function of that system must have all poles on the left-hand side of the complex plane. Poles at 0 mean that the system is marginally stable. Positive zeros of the transfer function do not directly insinuate instability, only a negative phase shift, which could eventually lead to instability. The poles and zeros of the transfer function $G_{\delta \to v_y}$ are shown in Figure 3.7.

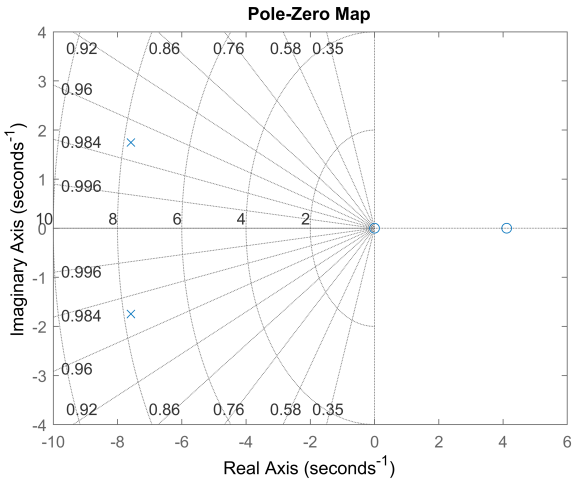

Figure 3.7: Pole-Zero plot for $G_{\delta \to v_y}$

As can be seen from Figure 3.7, there is a zero with a real value of approximately 4.1. With two already stable transfer functions, i.e. $G_{\delta \to \dot{\psi}}$ and $G_{\delta \to \psi}$, the use of the transfer function $G_{\delta \to v_y}$ will be excluded from the development of the controllers.

The robustness of a system can partly be characterised by its delay margin. The delay margin is the critical value where a closed-loop system transitions from stable to unstable conditions. In [28], it is explained that this critical value is acquired by using a first-order Padé approximation, with the final formula given by

$$\tau_{max} = \frac{\phi_m}{\omega_c} \; [s] \tag{3.32}$$

where ϕ_m is the phase margin at the crossover angular frequency ω_c, i.e. the angular frequency where the transfer function gain is 0 dB. For the transfer function $G_{\delta \to \psi}$, which will be widely utilised throughout this project, the delay margin is

$$\tau_{max} = \frac{\phi_m}{\omega_c} = \frac{56.1 \cdot \frac{\pi}{180}}{4.81} = 0.203\ [s] \tag{3.33}$$

A high delay margin is synonymous with high robustness, and it is desired that the control plant of the system is robust in order to be able to handle delays that are introduced as the complexity of the systems increase.

4

Geometric Path Tracking

In this chapter, two concepts for geometric path tracking are described and evaluated both in the simulation environment and in the test vehicle that was presented in the previous chapter. The concepts evaluated in this study are the Pure Pursuit and the Stanley controller. The path tracking controllers' task is to control the vehicle's lateral motion in an AD scenario by allocating the steering wheel angle to follow a specific reference path. There are three essential attributes of the controllers that are evaluated in this study: the controller's precision, comfort and robustness.

4.1 Geometric Path Tracking Controllers

There are various methods to formulate a geometric path tracking control law. The different PTC's could differ in how the reference point on the vehicle is placed on the front or rear axle or any arbitrary point on the vehicle. Another characteristic of a PTC is how the target point is defined. The target point can be defined somewhere along the path, or there is no target point. The used control and tuning parameters could also vary for different PTC's. In this section, all characteristics of the PPC and the SC will be presented and described.

4.1.1 Geometric Vehicle Model

One essential variable for the PTC's that will be used throughout this project is the curvature ρ and its relation to the front tire steering angle δ. The curvature is the vehicle's rear axle trajectory for a certain steering angle. The geometric relationship between the front tire steering angle and the curvature can be formulated by simplifying the vehicle to the bicycle model according to Figure 4.1.

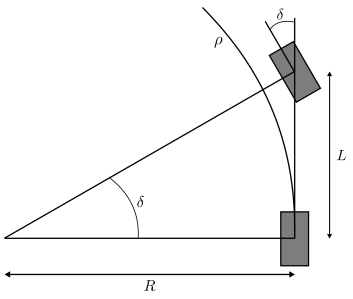

Figure 4.1: Geometric vehicle model

As displayed in Figure 4.1, the front tire steering angle can be formulated as

$$tan(\delta) = \frac{L}{R} \tag{4.1}$$

and the curvature is inversely proportional to the radius of the vehicle's trajectory R, according to

$$\rho = \frac{1}{R}. \tag{4.2}$$

Consequently, the relationship between the curvature and the front tire steering angle can be formulated as

$$tan(\delta) = L \cdot \rho \rightarrow \rho = \frac{\tan(\delta)}{L}. \tag{4.3}$$

4.1.2 Pure Pursuit Controller

The PPC is a common geometric PTC [11] describing how a human driver would turn to a point in front of the vehicle. This point is referred to as the look-ahead point, and its distance depends on the vehicle velocity since this is consistent with the look-ahead point of an actual driver as a driver looks further ahead at higher speeds. Geometrically, this can be drawn as displayed in Figure 4.2.

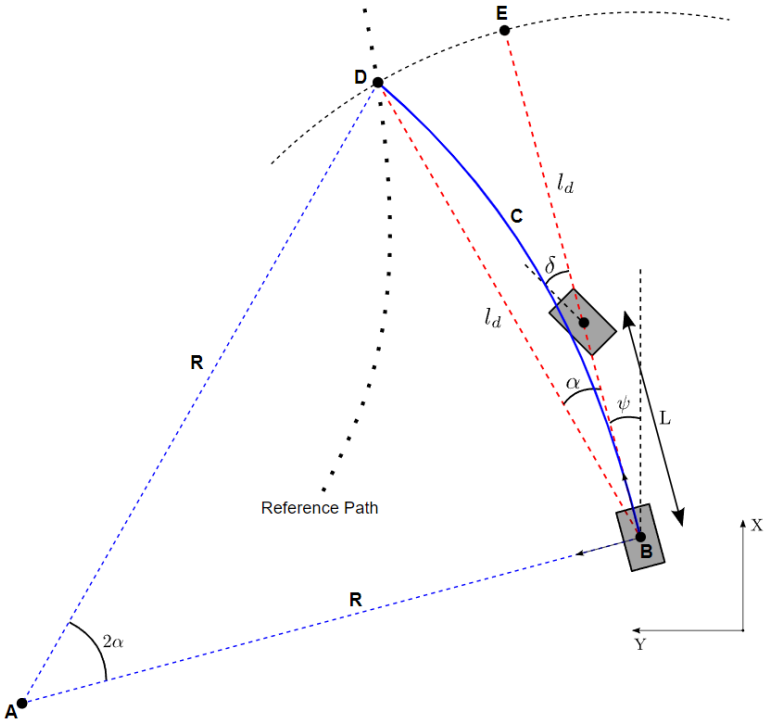

Figure 4.2: Geometric visualisation of the Pure Pursuit Controller

Deriving the equations for the PPC is introduced by recognising that the law of sines can be applied to find a relation between the radius R and the angle α according to equation 4.4.

$$\begin{aligned} \frac{l_d}{\sin(2 \cdot \alpha)} &= \frac{R}{\sin(\frac{\pi}{2} - \alpha)} \rightarrow \\ \frac{l_d}{2 \cdot \sin(\alpha) \cdot \cos(\alpha)} &= \frac{R}{\cos(\alpha)} \rightarrow \\ 2 \cdot R &= \frac{l_d}{\sin(\alpha)} \approx \frac{l_d}{\alpha} \end{aligned} \tag{4.4}$$

The radius R is the distance from the instantaneous centre of rotation denoted as A and the rear axis of the vehicle B, describing the arc C in which the vehicle travels in an arbitrary instance. The angle α is the angle between the vehicle heading, i.e. the line from B to the look-ahead point E, and the line from B to the target point on the path D. δ is the front tire steering angle, and L is the wheelbase. l_d is the look-ahead distance, which is the distance from B to E and is defined as

$$l_d = T_p \cdot v \tag{4.5}$$

where T_p is the look-ahead time, and v is the vehicle speed along its longitudinal axis. Consequently, the look-ahead distance changes with the velocity and the length of this distance can be tuned by the look-ahead time parameter. The expression for the radius can now be inserted in equation 4.2 to obtain an expression for the required curvature according to

$$\rho_{ref} = \frac{2 \cdot sin(\alpha)}{l_d} \approx \frac{2 \cdot \alpha}{l_d}. \tag{4.6}$$

The curvature ρ_{ref} is the reference from the controller, hence the notation ρ_{ref}. The curvature can then be transformed into a steering angle according to the relation in equation 4.3. The steering angle formulation for the PPC can therefore be defined according to

$$\delta_{PPC} = arctan(\frac{2 \cdot sin(\alpha) \cdot L}{l_d}) \approx \frac{2 \cdot \alpha \cdot L}{l_d}. \tag{4.7}$$

However, an extended version of the steering angle defined in equation 4.7 can be derived by adding the understeer gradient term to the reference steering angle. The understeer gradient K_u is defined as the additionally needed steering angle input per increase of lateral force units [29]. Practically it could be understood as the additional steering angle input needed to keep the same curve radius as the

operating velocity is increased due to the increased slip at the front tires. Intuitively, the understeer gradient formulation should be dependent on the vehicle velocity. In a mathematical context, the added term is described as the additional steering angle needed for a certain curvature R^{-1} at low speed, and consequently, K_u is interpreted as a measure of how much the additional term R^{-1} is changed with an increase of vehicle velocity. The extended reference steering angle δ_{K_u} is defined as

$$\delta_{K_u} = arctan(\frac{L}{R} + \frac{K_u \cdot v^2}{R}) \approx \frac{L}{R} + \frac{K_u \cdot v^2}{R} \tag{4.8}$$

with the understeer gradient defined as

$$K_u = m \cdot \frac{C_r \cdot l_r - C_f \cdot l_f}{C_f \cdot C_r \cdot (l_f + l_r)}. \tag{4.9}$$

Substituting R in equation 4.8 with R derived in equation 4.4 yields the steering angle formulation for the PPC with the understeer gradient term according to

$$\delta_{PPC,K_u} = \frac{2 \cdot \alpha \cdot (K_u \cdot v^2 + L)}{l_d}. \tag{4.10}$$

In the later stages of development, the PPC is used in the IPG CarMaker simulation environment. That entails replacing the kinematic bicycle model with the fully non-linear vehicle model used in IPG, which takes moving masses, aerodynamics, scrub radius effect and several other psychical phenomenons into account. A more comprehensive vehicle model such as this enables the use of large steering angles. Therefore the small angle approximation is disregarded, and the resulting steering angle formulation for the PPC is

$$\delta_{PPC} = \arctan(\frac{2 \cdot sin(\alpha) \cdot L}{l_d}) \tag{4.11}$$

or with the understeer gradient K_u,

$$\delta_{PPC,K_u} = \arctan(\frac{2 \cdot sin(\alpha) \cdot (K_u \cdot v^2 + L)}{l_d}). \tag{4.12}$$

Now that the steering angle formulation for the PPC is derived, the actual construction of the controller is commenced. The closed-loop control system consists of the primary development stages of the lateral controller and the kinematic bicycle model presented in section 3.3.1. The development of the PPC is initialised with the path

definition, which is externally pre-defined outside of the actual lateral controller block. A reference path is initially represented by a set of vectors representing the longitudinal and lateral coordinates of the reference path. A straight road would therefore consist of a linearly spaced vector with an arbitrary amount of elements in the longitudinal direction, i.e. the x-axis and the vector representing the lateral position of the elements is simply a vector of zeros.

The angle α is the only unknown variable in the steering angle formulation given by equation 4.11 and 4.12, and therefore the main objective of the PPC is to calculate α. Studying Figure 4.2, it is evident that α is the angle between the line from B to E and the line from B to E, defined as $\angle DBE$. The look-ahead point is defined as the point in which the vehicle will find itself in the next iteration, given that the yaw angle is constant, making the line from the rear axle to the look-ahead point instantaneously perpendicular to the longitudinal axis of the vehicle. The look-ahead point is calculated as

$$X_{prev} = X_{rear} + v \cdot T_p \cdot \cos(\psi) \ \ [m] \tag{4.13}$$

$$Y_{prev} = Y_{rear} + v \cdot T_p \cdot \sin(\psi) \ \ [m] \tag{4.14}$$

with X_{rear} and Y_{rear} being the coordinates of the rear axle. Recall that the product $v \cdot T_p$ describes the look-ahead distance l_d. Therefore, higher operating velocities will increase the distance from the rear axle to the calculated look-ahead point. The look-ahead time T_p could be seen as a tuning parameter. The target point is the second unknown coordinate required to calculate α. Two methods were used to acquire the target point.

1. A vector of length $||l_d||$ with one end fixed on the rear axle of the vehicle is rotated iteratively with an arbitrarily small angle, starting from the look-ahead point. When the end of the vector is as close as it could be to a point on the reference path, the target point is found.
2. The Pythagorean theorem is used to calculate the distances between the look-ahead point and the points of the reference path. The target point is therefore acquired by choosing the point on the reference path closest to the look-ahead point.

Method 1 requires more computational power than Method 2 since it requires a nested loop but provides a theoretically more accurate approximation of the target point. The two methods are illustrated in Figure 4.3 and 4.4, respectively.

As the reference path is a set of discrete points, i.e. not continuous, the target point found from Method 1 as described above will never coincide with the exact point of the reference path. The discrete set of points will also affect the target point found using Method 2 since the target point on the path with a theoretical minimum distance will create a line orthogonal from the target point to the look-ahead point, which will not be with a discrete set of points. The issues experienced

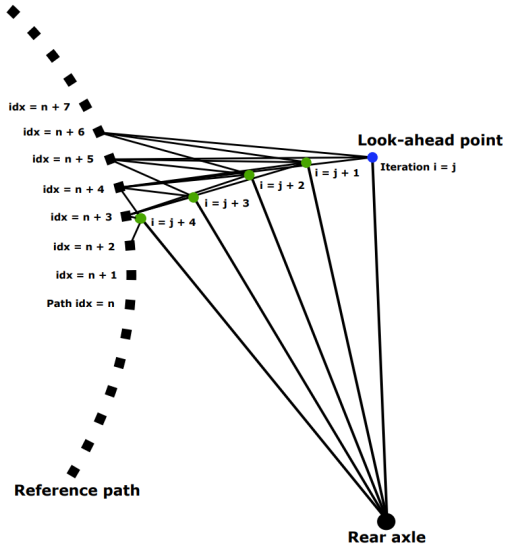

Figure 4.3: Method 1: Iterating both angle and distance in nested loop to find minimal distance

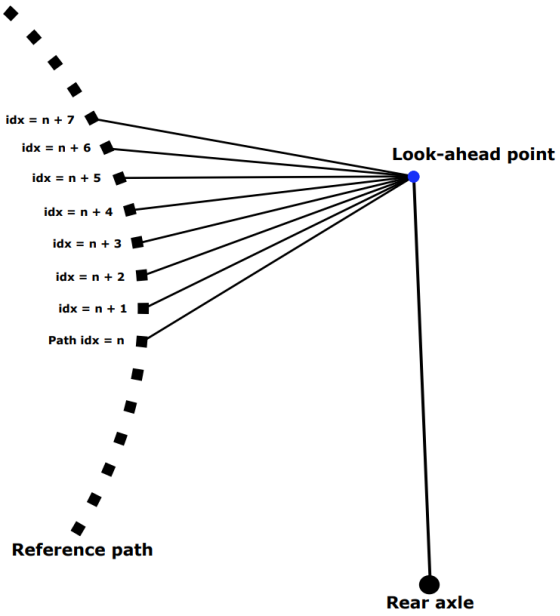

Figure 4.4: Method 2: Iterating distance in simple loop to find minimal distance

in these methods are solved using interpolation to extract the theoretically accurate target point. However, the difference in precision between the different methods is close to zero, and Method 2 was therefore implemented in the controller.

The first vector from the vehicle's rear axle to the look-ahead point and the second vector from the vehicle's rear axle to the target point is now defined, and consequently, α is obtained. Note that the reference orientation recognises a left turn as a positive steering angle. Therefore the controller needs to recognise the position of the vehicle. Either it is on the left or the right side of the reference path. The method utilised to identify the vehicle position relative to the path is presented in Appendix A.

4.1.3 Stanley Controller

The SC is based on two operating terms to be adjusted in parallel [11] as opposed to the PPC, which only adjusts the relative angle between a target point and a look-ahead point. The first term refers to an error in heading ψ_e, and the second term handles the lateral error d_f of the vehicle relative to the reference path. Figure 4.5 interprets the SC geometrically.

The first control variable is the heading error ψ_e, which describes the error in the vehicle heading relative to the heading of the line tangent to the point closest to the front axle of the vehicle. Using the notations in Figure 4.5, It can be described as the angle $\angle DAE$. This term has a different characteristic since it aims to correct the relative angle between the vehicle and the direction of the path itself. Consequently,

the vehicle will not be steered towards the actual path, only the direction of the tangent line, i.e. the line from B to C (or A to D).

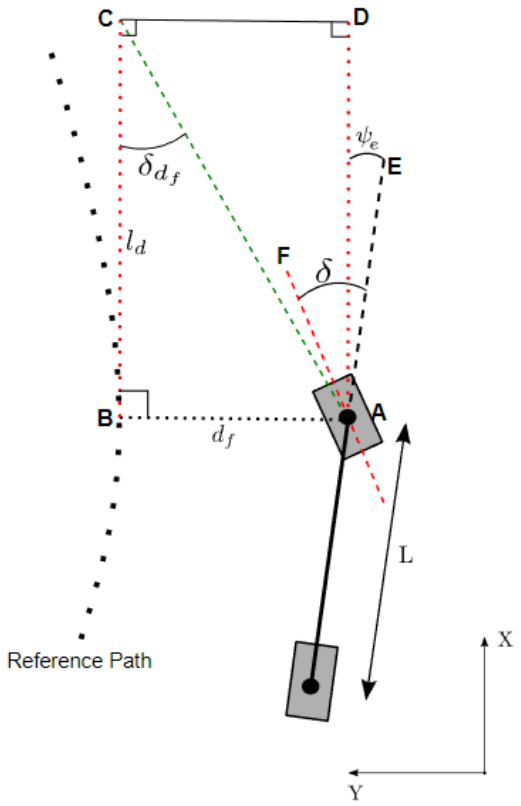

Figure 4.5: Geometric visualisation of the Stanley Controller

The second control variable is the lateral error d_f. The lateral error deals with the adjustment of a pure lateral displacement between the vehicle's front axle and the reference path. In contrast to the PPC, the SC does not steer towards any target point as it does not include a target point. However, the steering angle formulation for the lateral error d_f depends on the same variable that the PPC used to define its look-ahead point l_d, as can be seen by equation 4.5. The added steering following the lateral error d_f is represented as δ_{d_f} as seen in Figure 4.5. Note that the angle δ_{d_f} is given by $\angle ACB$ in the right-angled triangle ABC. The part of the steering angle formulation that is represented by the lateral error d_f is therefore given by

$$\delta_{d_f} = \arctan(\frac{d_f}{l_d}) = \arctan(\frac{d_f}{v \cdot T_p}). \tag{4.15}$$

The steering angle formulation for the SC is the sum of the steering angle additions as a result of the heading error ψ_e and the lateral error d_f.

$$\delta_{SC} = \psi_e + \delta_{d_f} \tag{4.16}$$

Note, however, from equation 4.16 that in order to obtain δ_{d_f}, the lateral error d_f needs to be calculated. So correctly speaking, δ_{SC} is a function of ψ_e and $\delta_{d_f}(d_f)$ as

$$\delta_{SC} = f(\psi_e, \delta_{d_f}(d_f)). \tag{4.17}$$

The reference curvature can then be obtained by the relation in equation 4.3 according to

$$\rho_{ref} = \frac{tan(\delta_{SC})}{L}. \tag{4.18}$$

Adding the understeer gradient K_u to the steering angle formulation for the SC requires more steps or, more specifically, conversions than the derivation for the PPC steering angle formulation with K_u did. By replacing the radius R in equation 4.8 with the curvature and then substituting the curvature with the expression in equation 4.18, the final steering angle formulation for the SC with the understeer gradient K_u is given by

$$\delta_{SC,K_u} = \arctan(\frac{\tan(\delta_{SC}) \cdot (L + \cdot K_u \cdot v^2)}{L}). \tag{4.19}$$

The lateral error d_f is the first unknown entity and is acquired by utilising Method 2 given by Figure 4.4. The method is consistent, but the visual difference is that the vehicle's front axle is used to find the closest point to the path, not the look-ahead point as visualised in Figure 4.4. Remember that the reference path is a set of discrete points; therefore, the point found using Method 2 is interpolated between the neighbouring points on the path to find the actual minimum distance between points A and B.

The heading error ψ_e, being the second unknown, is a simple angle between two lines in its core aspect; therefore, these lines must be defined. The first line starts at point A and ends at point E, i.e. the vehicle heading. Note that the heading error ψ_e is independent of the length of the line AE. Therefore, the only requirement on this line is its direction. For the sake of simplicity, point E is defined by equations 4.13 and 4.14.

The second line is the line tangent to point B, i.e. the line from point B to point C. Calculating the line tangent to the point on the reference path requires finding the slope of that line with high precision since sudden changes in the slope due to relatively large inaccuracies results in undesirable oscillating steering behaviour. Since the reference path is defined in a global coordinate system, the slope would be equal to infinity when driving in parallel with the vertical axis of the global coordinate system. That issue is resolved using a rotational matrix to rotate the

fragment of the curve around the point of interest on the path to operating with small values where no complications occur. The process of obtaining the relative angle between the tangent line and the vehicle's heading using the transformation matrix is thoroughly described in Appendix B. The vehicle's position relative to the path is obtained using the derivation conducted in Appendix A, as used in the PPC.

4.2 Control architecture - Lateral Motion Control

Illustrated in Figure 4.6 is the control architecture for the PTC's. The PTC generates the reference curvature ρ_{ref} in the Reference Generator block, which is defined by equation 4.6 and 4.18 for the PPC and SC, respectively. The curvature reference is then converted into a requested steering angle δ_{SW} in the Control Allocator according to

$$\delta_{SW} = arctan((L + K_u \cdot v^2) \cdot \rho_{ref}) \tag{4.20}$$

which is obtained by replacing R in equation 4.8 with the curvature.

The longitudinal motion is controlled by the driver. The accelerator and brake pedal positions a_{pedal} and b_{pedal} are translated into a longitudinal force request $F_{x,ref}$ in the Reference Generator, which is then processed to a torque distribution to achieve the desired speed in the Control Allocation block.

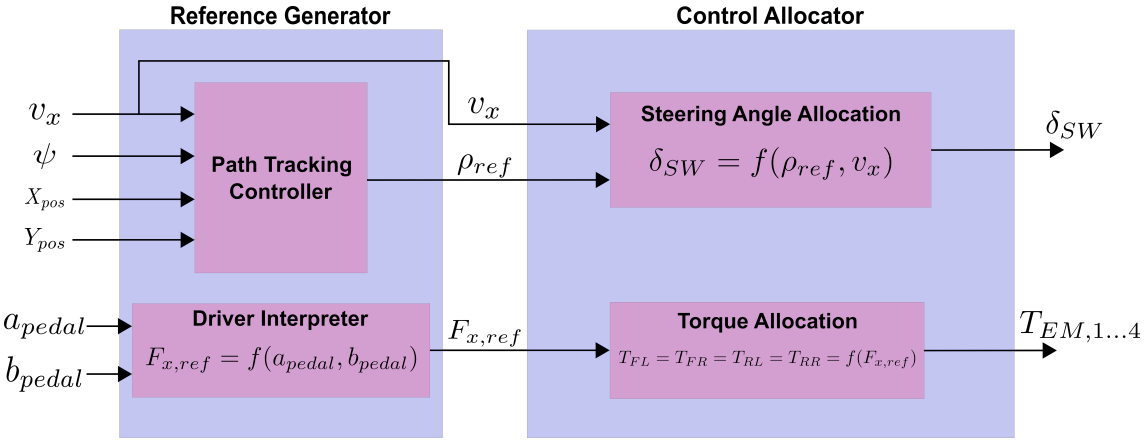

Figure 4.6: Control architecture of path tracking controller

Finally, the controllers can be tuned in two ways. As mentioned previously, the controllers can be tuned with the look-ahead time, T_p. The other method is to add the understeer gradient term, K_u, in equation 4.20.

4.3 Path Tracking Evaluation

The method of evaluating the different PTC's is presented in this section.

4.3.1 Quantifying attributes of evaluation

To evaluate the two geometric PTC's that have been presented in the previous section, i.e. the PPC and the SC, a set of different test cases are utilised. They are defined to be able to compare the performance of the controllers according to different attributes. These attributes and the evaluation methods are presented in this section.

Attribute 1: Precision
The first attribute that is evaluated is the controller's precision, which is evaluated by comparing the lateral distance between the vehicle and the reference path for the two controllers. The precision, therefore, displays how good the controller can follow the reference path. The lateral distance between the vehicle and the reference path is called the lateral deviation, which is defined as the shortest distance between the reference path and a reference point on the vehicle. The middle point on the vehicle's rear axle is used as the reference point when calculating the lateral deviation to compare the controllers. This attribute is essential since the vehicle has to stay within the road markings and not deviate from the road either by corner cutting or applying steering too late. UN regulations for wheeled vehicles [30] state that the acceptable lateral deviation when using an automated lane keeping system should be within 0.375 m of the centre of the driving lane. Therefore, this limit is used as a threshold for maximum lateral deviation. The lateral deviation for the test cases is displayed both as the maximum lateral deviation achieved during the manoeuvre and the Root Mean Square Error (RMSE) for the lateral deviation according to equation 4.21.

$$RMSE_{precision} = \sqrt{\sum_{j=1}^{n} \frac{d_{f_j}^2}{j}} \tag{4.21}$$

where n is the number of iterations, and d_f is the lateral deviation. Both the RMSE of the lateral deviation and the maximum lateral deviation $MAX_{precision}$ of a drive cycle will be used to grade the precision of the PTC's as shown in equation 4.22

$$P_{precision} = a_1 \cdot P_{RMSE,precision} + a_2 \cdot P_{MAX,precision} \tag{4.22}$$

where $P_{precision}$ is a weighted value of the RMSE and maximum lateral deviation. a_1 and a_2 are weighting coefficients set to 0.8 and 0.2, respectively, as it is decided that the **grade** of the precision $P_{RMSE,precision}$ has a greater effect on the evaluated attributes than the **grade** of the instantaneous maximum lateral deviation $P_{MAX,precision}$ during the test cycle. The thresholds for $P_{RMSE,precision}$ and $P_{MAX,precision}$ are listed in Appendix C.

Attribute 2: Comfort
The second attribute that is evaluated is related to passenger ride comfort. Comfort in this context is normally associated with a lateral jerk, amongst other variables, which is the rate of change of the vehicle's lateral acceleration. For a given test case, the RMSE of the lateral jerk and the maximum lateral jerk will be measured. UN regulations [31] states that the moving average over half a second of the lateral jerk generated by the vehicle should not exceed 5 m/s^3 instantaneously. Considering that the test cases to be conducted are modelled with the intention of handling dynamic manoeuvres, this threshold is well suited as an extreme limit. According to [32], the threshold for comfort is around 0.5 m/s^3. However, mild driving conditions were considered when defining that threshold. A fair evaluation should increase the comfort threshold as a result of all dynamic test cases. The lower limit for the RMSE is therefore set to 0.8 m/s^3. Equation 4.23 shows the relation that will be used to grade the comfort concerning lateral jerk.

$$P_{jerk} = a_1 \cdot P_{RMSE,jerk} + a_2 \cdot P_{MAX,jerk} \tag{4.23}$$

where P_{jerk} is a weighted value of the **grade** of the lateral jerk RMSE $P_{RMSE,jerk}$ and maximum lateral jerk $P_{MAX,jerk}$. This method, however, cannot differentiate between low-frequency and high-frequency components of the signal (drive cycle). According to [33], frequencies of 0.2 Hz and above of the lateral acceleration are considered uncomfortable. Therefore, the area under the Fourier Transform signal (energy spectral density) of the lateral acceleration above 0.2 Hz will be used as a measure of comfort and the lateral jerk. The Fourier Transform provides the amplitude and the frequency of all lateral acceleration components and is, therefore, an indication of how uncomfortable the PTC's are for a given test case. This quantity will be graded similarly to the lateral jerk, i.e. with thresholds. The lateral jerk and energy spectral density thresholds are listed in Appendix C.

Attribute 3: Robustness
The final attribute which is evaluated is robustness. Robustness, in this case, refers to how much the performance of the previously mentioned attributes changes with different circumstances. If the PTC is robust, then the performance should stay the same if the velocity is increased or if a time delay to the control signals is introduced. For example, if the controller can handle more extensive delays for input signals (for example, GPS position) and still maintain its performance compared to another PTC, it means that the PTC has a higher robustness.

Finally, to summarise the evaluation, three attributes are evaluated when comparing the PPC and the SC: precision, comfort, and robustness.

4.3.2 Test cases

Three types of test cases are utilised to evaluate the PTC's, which are presented in this subsection.

Test case 1: Step response with 1 m lateral offset

The first test case is a step response in the reference path of 1 m. This test case is used to evaluate the different characteristics of the two controllers when they are introduced to a step input, i.e. how they turn into the reference path when it suddenly changes. The comparison in performance is evaluated concerning the robustness and turn-in behaviour. The reference path definition is presented in Figure 4.7 and 4.8. The reference path consists of x-y-coordinates with a 1 m spacing between each coordinate. Note that a step of 1 m is not a very realistic scenario for the controllers. They are expected to have a lower lateral deviation and not experience this type of discrete step in the reference path.

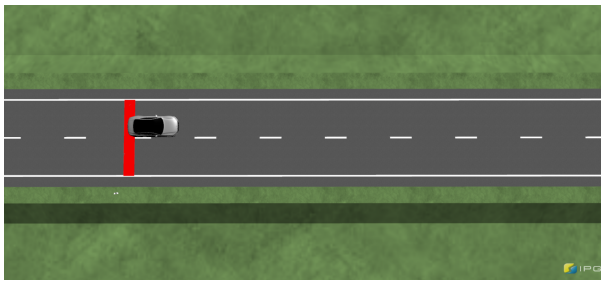

Figure 4.7: Test case 1: Step response with 1 m lateral offset in IPG CarMaker

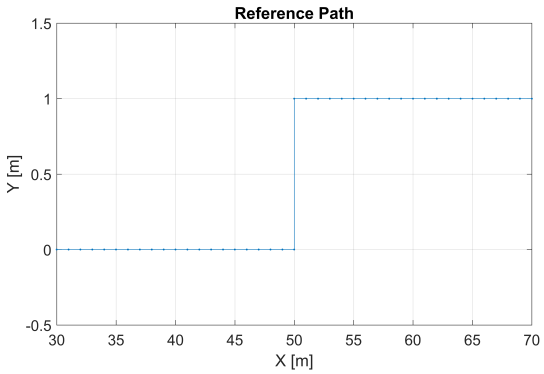

Figure 4.8: Test case 1: Step response with 1 m lateral offset, reference path

Test case 2: 90° turn

The 90° turn evaluates the effect of look-ahead time T_p on the steady-state error. Important to note also is the fact that there is a threshold lateral acceleration associated with ride comfort. According to [34], a study on lateral acceleration thresholds for ride comfort, the average limit of comfort is 1.8 m/s^2. The limit used in this study will therefore be set to 2 m/s^2 for simplicity. To evaluate the robustness of the controllers in more dynamic manoeuvres, a lateral acceleration a_y of 4 m/s^2 will also be used. Using the formula for centripetal acceleration a_y given by

$$a_y = \frac{v^2}{R} \tag{4.24}$$

the radius of the 90° turn can be calculated by choosing an arbitrary velocity. Two 90° turns are chosen for this test case. The first has a radius of 50 m, and the second one has a radius of 312.5 m. The reference path for the 50 m radius turn is displayed in Figure 4.9 and 4.10.

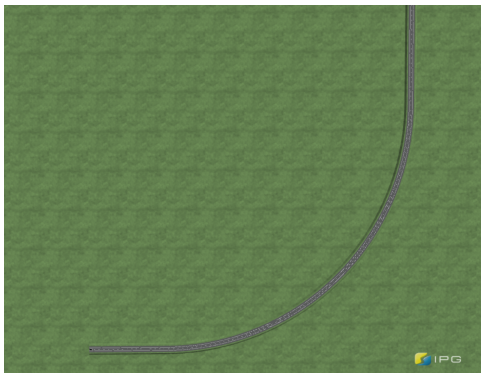

Figure 4.9: Test case 2: 90° turn, radius = 50 m in IPG CarMaker

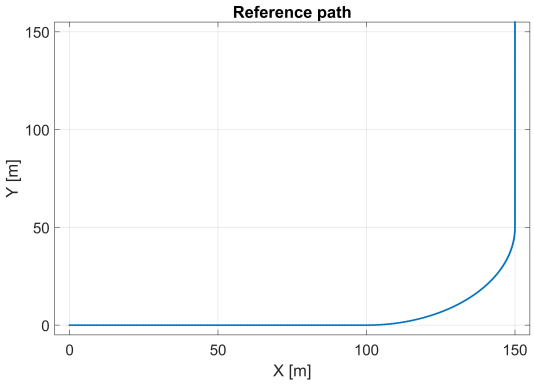

Figure 4.10: Test case 2: 90° turn, radius = 50 m reference path

Test case 3: Hällered Proving Ground - Handling Track 1

The handling track course is used to test the PTC's when the road curvature is changing. This specific road course corresponds to the handling track located at Hällered Proving Ground and is used to evaluate the PTC's in the test vehicle. The simulation results can, therefore, be compared to those obtained from driving with the test vehicle.

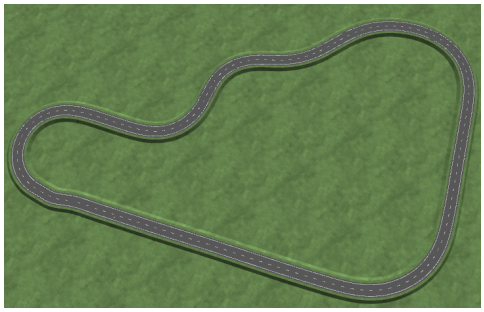

Figure 4.11: Test case 3: Hällered Proving Ground - Handling Track 1 in IPG CarMaker

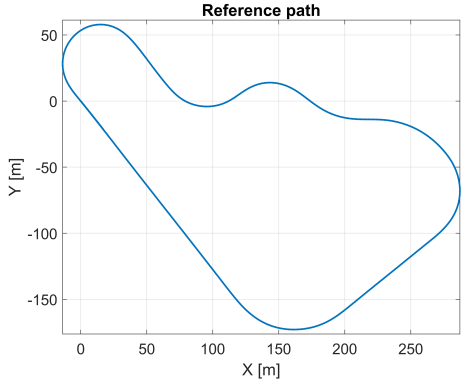

Figure 4.12: Test case 3: Hällered Proving Ground - Handling Track 1 reference path

Figure 4.13: Test case 3: Hällered Proving Ground - Handling Track 1

4.3.3 Test matrices

Since the PTC's are evaluated in three different environments, i.e. Matlab Simulink, IPG CarMaker and the actual test vehicle, only some test cases will be used for all environments. Below are the specific test cases with relevant parameters for each test matrix.

Environment 1: Matlab Simulink
The test case that will be conducted in the Matlab Simulink simulation environment is the step response with a 1 m lateral offset, i.e. test case 1. Table 4.1 presents the test case settings and tuning.

Test case	Tuning	Velocity
1: Step response	$T_p \in [0.6, 0.8, 1.0]$ [s]	v = 90 $[km/h]$

Table 4.1: Test cases to be simulated in Matlab Simulink

Environment 2: IPG CarMaker:
The test cases to be conducted in the IPG Carmaker/Matlab Simulink simulation environment are presented in Table 4.2. Note that the notation "w K_u" means that the understeer gradient term is included in equation 4.20 when the reference curvature is converted into the requested steering angle.

Test case	Tuning	Velocity
1: Step response	$T_p \in [0.6$ w $K_u, 0.6, 0.8, 1.0]$ [s]	v $\in [36, 90]$ $[km/h]$
2: 90° turn - R=50 m	$T_p \in [0.6$ w $K_u, 0.6, 0.8, 1.0]$ [s]	v = $[36, 51]$ $[km/h]$
2: 90° turn - R=312.5 m	$T_p \in [0.6$ w $K_u, 0.6, 0.8, 1.0]$ [s]	v = $[90, 128]$ $[km/h]$
3: Handling Track 1	$T_p \in [0.6$ w $K_u, 0.6, 0.8, 1.0]$ [s]	v = 50 $[km/h]$

Table 4.2: Test cases to be simulated in IPG Carmaker

Environment 3: Test vehicle
In the test vehicle, the PTC's will be evaluated at Handling Track 1. This test case is presented in Table 4.3.

Test case	Tuning	Velocity
3: Handling Track 1	$T_p \in [0.6$ w $K_u, 0.8$ w $K_u, 1.0$ w $K_u]$ [s]	v = 50 $[km/h]$

Table 4.3: Test cases to be simulated in the test vehicle

4.4 Path tracking results

The results for the different PTC's are presented in this section. The results are obtained by performing the different test cases presented in the previous section in all environments, i.e. Simulink, IPG CarMaker and the test vehicle.

4.4.1 Simulink - kinematic bicycle model

The kinematic bicycle model of Figure 3.3 is used as a vehicle model, specifically the transfer function $G_{\delta \to \psi}$, along with the steering angle formulations for the PPC and the SC, given by equations 4.11 and 4.16 respectively. The resulting manoeuvres for the step response with 1 m lateral offset at the look-ahead time of $T_p = 0.6$, 0.8 and 1.0 is visualised in Figure 4.14. The behaviour of the PTC's are consistent since the PPC overshoots regardless of the look-ahead time, and the exact opposite for the SC, as it never overshoots. The precision of the SC is insignificantly superior to the PPC, and both PTC's exhibit robust, smooth and stable behaviour due to the absence of oscillations and rapid turning manoeuvres.

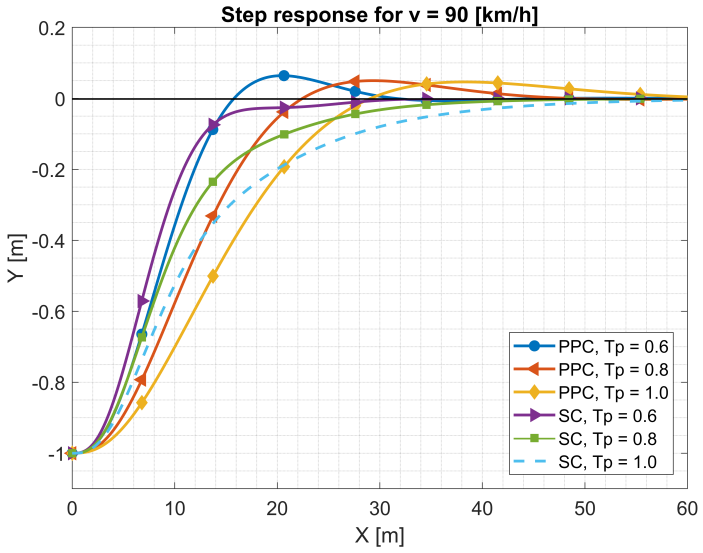

Figure 4.14: Step response of PTC's when v = 90 km/h, $T_p = [0.6, 0.8, 1.0]$

4.4.2 IPG CarMaker - Simulation Results

This subsection presents the simulation results from the IPG CarMaker environment. The results are divided into the different test cases with their corresponding test matrices defined in section 4.3.3.

Test Case 1: Step response with 1 m lateral offset
The first test case displays the step response for the two controllers when they are presented with a step error of 1 m in lateral deviation. The simulation results are presented in Figure 4.15 and 4.16 for one lower velocity of 36 km/h and a higher

velocity of 90 km/h. Note that the figures display different results for both the PPC and the SC with the available tuning of changing the look-ahead time and adding the understeer gradient term. Not all results from the test matrix are displayed. Only the best and worst results to showcase the differences between the controllers. In Figure 4.15, where the velocity is low, the results showcase that the SC experienced an overshoot of 0.37 and 0.16 m for $T_p = 0.6$ and 1.0 s, compared to the PPC, which experienced an overshoot of 0.05 and 0.06 m for $T_p = 0.6$ and 1.0 s. Comparing this with the results in Figure 4.16 at 90 km/h, the SC does not have any overshoot anymore, but it is still present for the PPC. Looking at both figures, it is evident that the PPC performs similarly in both low and high velocities, meaning that the SC is sensitive to velocity changes and is, therefore, not as robust as the PPC for this particular case. For the PPC, the overshoot and the time it takes to converge with the step in the reference path increase when the look-ahead time is increased. Furthermore, the results also showcase the different behaviour between the two controllers. The PPC starts to turn before the step, which means it will have corner cutting in contrast to the SC, which starts to turn later than the PPC. Note that the behaviour of the controllers, as illustrated in Figure 4.16, is consistent with the behaviour displayed in Figure 4.14 for the same speed even though the simulation environments differ.

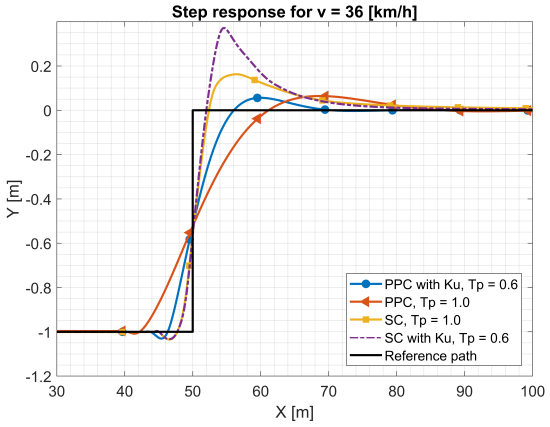

Figure 4.15: Step response for v = 36 $[km/h]$

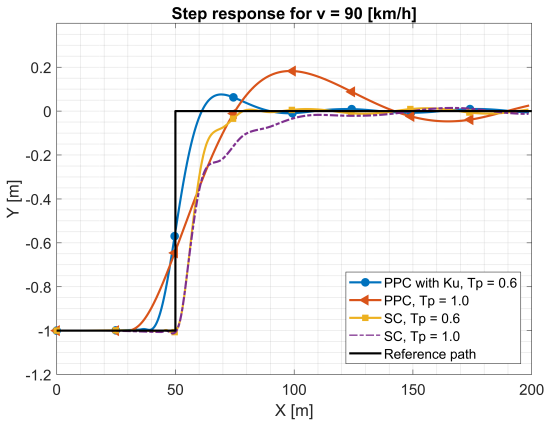

Figure 4.16: Step response for v = 90 $[km/h]$

Test Case 2: 90° turn with 50 m radius

The lateral deviation simulation results for the 90° turn with a radius of 50 m are presented in Table 4.4 and 4.5. For this scenario, the velocity is 36 km/h and 51 km/h, respectively, meaning that the lateral acceleration is 2 m/s^2 for the lower velocity and 4 m/s^2 for the scenario with a higher velocity. When comparing the lateral deviation, it is evident that the SC has a lower lateral deviation than the PPC in terms of RMSE and maximum deviation for both the lower and the higher velocity. However, the difference in lateral deviation between the controllers is reduced when the look-ahead time, T_p, is reduced. When adding the understeer gradient, K_u, the PPC improves even further, consequently reducing the difference between the

RMSE [m]			Max error [m]		
$\mathbf{T_p}$	**PPC**	**SC**	$\mathbf{T_p}$	**PPC**	**SC**
1.0	0.079	0.029	**1.0**	0.246	0.069
0.8	0.054	0.018	**0.8**	0.161	0.047
0.6	0.035	0.007	**0.6**	0.095	0.026
0.6 ($\mathbf{K_u}$)	0.014	0.015	**0.6 ($\mathbf{K_u}$)**	0.060	0.028

Table 4.4: Test Case 2: 90° turn, $R = 50\ m$, $v = 36\ km/h$, $ay = 2\ m/s^2$, lateral deviation simulation results

RMSE [m]			Max error [m]		
$\mathbf{T_p}$	**PPC**	**SC**	$\mathbf{T_p}$	**PPC**	**SC**
1.0	0.221	0.137	**1.0**	0.591	0.298
0.8	0.156	0.109	**0.8**	0.403	0.236
0.6	0.104	0.080	**0.6**	0.248	0.173
0.6 ($\mathbf{K_u}$)	0.029	0.032	**0.6 ($\mathbf{K_u}$)**	0.111	0.077

Table 4.5: Test Case 2: 90° turn, $R = 50\ m$, $v = 51\ km/h$, $ay = 4\ m/s^2$, lateral deviation simulation results

controllers. The reduction in lateral deviation with an added K_u term implies that the best RMSE for the PPC is 0.1 cm higher than the SC at 36 km/h and 0.3 cm higher than the SC at 51 km/h. Another observation is that the understeer gradient term worsens the performance of the SC at lower velocities. The smallest difference in the maximum lateral deviation between the PPC and the SC is that the PPC is 3.2 cm higher than the SC at 36 km/h and 3.4 cm higher than the SC at 51 km/h. Consequently, the difference in lateral deviation when the controllers are tuned is insignificant. However, when the controllers are not tuned, the SC is more precise. The lateral deviation of the drive cycle is shown in Figure 4.17 and 4.18.

The difference in comfort for the two PTC's can be distinguished by the results presented in Table 4.6 and 4.7. The jerk RMSE and the maximum jerk are lower for all cases with the PPC. The PPC also experiences less high-frequency lateral acceleration changes as the area under the Fourier Transform is significantly lower. For visualisation, the jerk and Fourier Transform signals for driving at 36 km/h in the 90° turn with a 50 m radius are included in Appendix D.

RMSE Jerk [m/s³]			Max Jerk [m/s³]			Area [m/s²]		
T_p	PPC	SC	T_p	PPC	SC	T_p	PPC	SC
1	0.436	0.854	**1**	1.450	3.916	**1**	0.021	0.061
0.8	0.497	0.865	**0.8**	1.864	3.960	**0.8**	0.029	0.062
0.6	0.595	0.882	**0.6**	2.556	4.026	**0.6**	0.040	0.063
0.6 (K_u)	0.600	0.924	**0.6 (K_u)**	2.632	4.142	**0.6 (K_u)**	0.041	0.065

Table 4.6: Test Case 2: 90° turn, $R = 50\ m$, $v = 36\ km/h$, $ay = 2\ m/s^2$, comfort simulation results

RMSE Jerk [m/s³]			Max Jerk [m/s³]			Area [m/s²]		
T_p	PPC	SC	T_p	PPC	SC	T_p	PPC	SC
1	0.976	2.068	**1**	2.944	8.811	**1**	0.054	0.168
0.8	1.125	2.104	**0.8**	3.823	8.954	**0.8**	0.074	0.171
0.6	1.348	2.161	**0.6**	5.200	9.163	**0.6**	0.102	0.176
0.6 (K_u)	1.358	2.330	**0.6 (K_u)**	5.485	9.453	**0.6 (K_u)**	0.106	0.184

Table 4.7: Test Case 2: 90° turn, $R = 50\ m$, $v = 51\ km/h$, $ay = 4\ m/s^2$, comfort simulation results

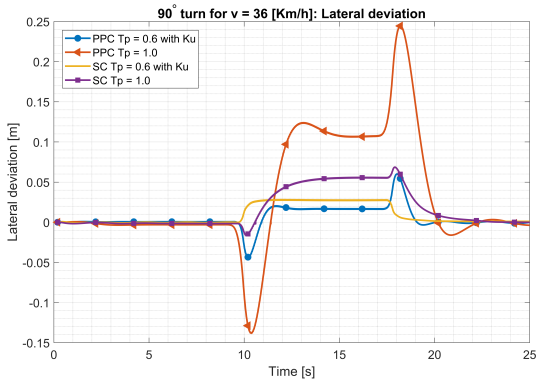

Figure 4.17: Radius 50 m, lateral deviation at 36 km/h

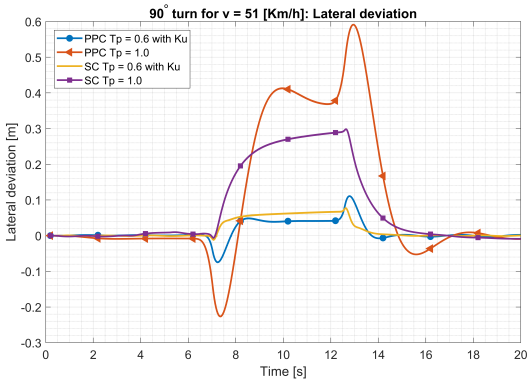

Figure 4.18: Radius 50 m, lateral deviation at 51 km/h

Test Case 2: 90° turn with 312.5 m radius

The two velocities used in the 90° turn with a radius of 312.5 m are 90 km/h and 128 km/h, corresponding to a lateral acceleration of 2 m/s^2 and 4 m/s^2 respectively. The simulation results for the lateral deviation in these scenarios are presented in Table 4.8 for 90 km/h and in Table 4.9 for 128 km/h. The results show that the lateral deviation is generally higher than in the test case with a 50 m radius with lower velocities. Similarly to before, the lateral deviation is also improved when the look-ahead time T_p is reduced. It is also evident that the SC is better

RMSE [m]			Max error [m]		
$\mathbf{T_p}$	**PPC**	**SC**	$\mathbf{T_p}$	**PPC**	**SC**
1.0	0.359	0.229	**1.0**	0.547	0.315
0.8	0.255	0.185	**0.8**	0.399	0.254
0.6	0.167	0.142	**0.6**	0.274	0.193
0.6 ($\mathbf{K_u}$)	0.016	0.104	**0.6 ($\mathbf{K_u}$)**	0.049	0.146

Table 4.8: Test Case 2: 90° turn, $R = 312.5m$, $v = 90\ km/h$, $ay = 2\ m/s^2$, lateral deviation simulation results

RMSE [m]			Max error [m]		
$\mathbf{T_p}$	**PPC**	**SC**	$\mathbf{T_p}$	**PPC**	**SC**
1.0	1.263	0.685	**1.0**	2.046	0.958
0.8	0.882	0.557	**0.8**	1.465	0.774
0.6	0.568	0.526	**0.6**	0.985	0.724
0.6 ($\mathbf{K_u}$)	0.055	0.299	**0.6 ($\mathbf{K_u}$)**	0.122	0.415

Table 4.9: Test Case 2: 90° turn, $R = 312.5m$, $v = 128\ km/h$, $ay = 4m/s^2$, lateral deviation simulation results

than the PPC concerning precision. However, when the understeer gradient term is added, the PPC improves drastically and performs better than the SC in terms of both maximum lateral deviation and RMSE. When the understeer gradient term is added, the RMSE for the SC is 7.8 cm higher than the PPC at 90 km/h and 23 cm higher than the PPC at 128 km/h. With an increased lateral acceleration, it is clear that both the absolute value and the difference for the lateral deviation have increased. At 90 km/h, the maximum lateral deviation is 9.7 cm higher, and at 128 km/h, it is 29.2 cm higher for the SC compared with the PPC.

For both 90 km/h and 128 km/h with $T_p = 0.6$ and with the understeer gradient K_u, the SC tends to oscillate. Also, the oscillations are more significant at 90 km/h than at 128 km/h. With the PPC, this is not present in any configuration. The comfort evaluation results are shown in Table 4.10 and 4.11, where the PPC is superior.

In Figure 4.19 and 4.20 the lateral deviation is presented for the entire test case. Comparing these results with what was presented in Figure 4.17 and 4.18, it is clear that the understeer gradient term has a much higher effect on the performance at higher velocities where the PPC performs much better than the SC. The figures also showcase that the SC oscillates more than the PPC when the look-ahead time is 0.6 s and the understeer gradient is added.

RMSE Jerk [m/s³]			Max Jerk [m/s³]			Area [m/s²]		
T_p	PPC	SC	T_p	PPC	SC	T_p	PPC	SC
1	0.384	0.864	**1**	1.438	6.471	**1**	0.014	0.058
0.8	0.446	0.875	**0.8**	1.951	6.411	**0.8**	0.023	0.061
0.6	0.560	0.924	**0.6**	2.973	6.856	**0.6**	0.034	0.064
0.6 (K_u)	0.532	1.396	**0.6 (K_u)**	3.156	8.001	**0.6 (K_u)**	0.035	0.101

Table 4.10: Test Case 2: 90° turn, $R = 312.5\ m$, $v = 90\ km/h$, $ay = 2\ m/s^2$, comfort simulation results

RMSE Jerk [m/s³]			Max Jerk [m/s³]			Area [m/s²]		
T_p	PPC	SC	T_p	PPC	SC	T_p	PPC	SC
1	0.924	2.004	**1**	2.845	9.443	**1**	0.036	0.143
0.8	1.064	2.081	**0.8**	3.672	9.716	**0.8**	0.053	0.150
0.6	1.309	2.068	**0.6**	5.057	9.513	**0.6**	0.081	0.151
0.6 (K_u)	1.271	3.637	**0.6 (K_u)**	5.814	9.381	**0.6 (K_u)**	0.087	0.170

Table 4.11: Test Case 2: 90° turn, $R = 312.5\ m$, $v = 128\ km/h$, $ay = 4\ m/s^2$, comfort simulation results

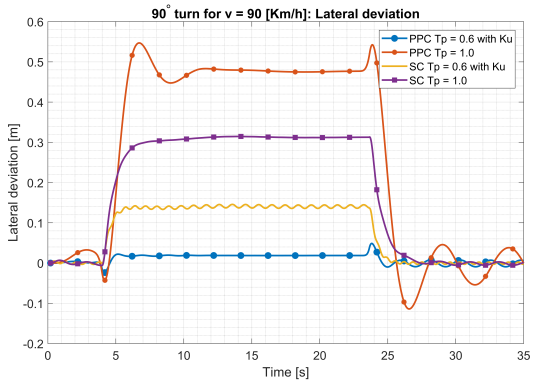

Figure 4.19: Radius 312.5 m, lateral deviation at 90 km/h

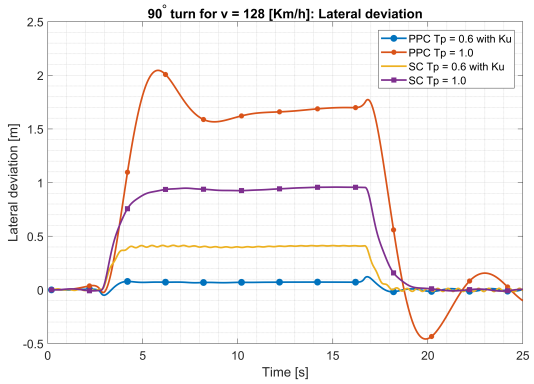

Figure 4.20: Radius 312.5 m, lateral deviation at 128 km/h

Test Case 3: Hällered Proving Ground - Handling Track 1
In Table 4.12, the simulation results for the lateral deviation are presented when driving at a constant velocity of 50 km/h on Handling Track 1 from Hällered Proving Ground. Comparing the PPC and the SC results shows that the difference in lateral deviation is reduced when the look-ahead time, T_p, is reduced similarly to the results presented before. For $T_p = 0.6$ s, the difference in RMSE is 3.2 cm, and the difference in maximum deviation is 5.5 cm. Tuning the controllers with the understeer gradient reduces the difference even further to 0.6 cm and 0.4 cm for the RMSE and the maximum lateral deviation, respectively. The SC, however, consistently have a lower lateral deviation than the PPC. Furthermore, the SC does not change in performance as much as the PPC with different look-ahead times, i.e. the look-ahead time has a larger impact on the performance of the PPC than the SC. The difference in lateral deviation between the controllers is also illustrated in Figure 4.21 and 4.22, where the PPC is visually more affected by the look-ahead time. However, when tuned, it performs similarly to the SC regarding the lateral deviation.

RMSE [m]			**Max error [m]**		
$\mathbf{T_p}$	**PPC**	**SC**	$\mathbf{T_p}$	**PPC**	**SC**
1.0	0.345	0.265	**1.0**	0.811	0.625
0.8	0.241	0.216	**0.8**	0.567	0.506
0.6	0.163	0.131	**0.6**	0.385	0.330
0.6 ($\mathbf{K_u}$)	0.083	0.077	**0.6 ($\mathbf{K_u}$)**	0.200	0.196

Table 4.12: Test case 3: Lateral deviation simulation results from Handling Track 1 at 50 km/h

Table 4.13 presents the comfort evaluation results. Similarly to test case 2, the PPC is still more comfortable with less jerk and high-frequency lateral acceleration components than the SC.

RMSE Jerk [m/s^3]			**Max Jerk [m/s^3]**			**Area [m/s^2]**		
$\mathbf{T_p}$	**PPC**	**SC**	$\mathbf{T_p}$	**PPC**	**SC**	$\mathbf{T_p}$	**PPC**	**SC**
1	1.663	1.829	**1**	5.298	6.127	**1**	0.062	0.071
0.8	1.704	1.834	**0.8**	5.569	6.107	**0.8**	0.062	0.071
0.6	1.743	1.819	**0.8**	5.723	5.777	**0.8**	0.065	0.068
0.6 ($\mathbf{K_u}$)	1.740	1.867	**0.6 ($\mathbf{K_u}$)**	5.843	5.984	**0.6 ($\mathbf{K_u}$)**	0.065	0.068

Table 4.13: Test case 3: comfort simulation results from Handling Track 1 at 50 km/h

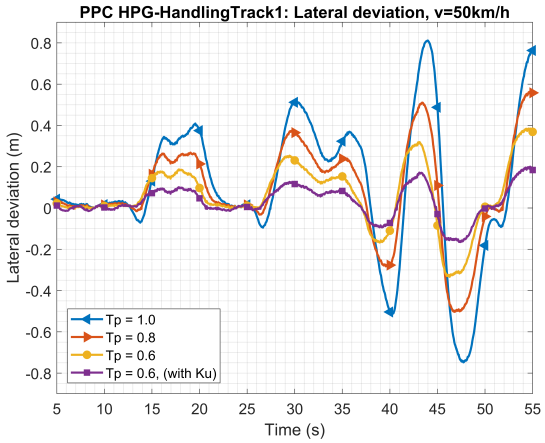

Figure 4.21: HPG: Handling Track 1 PPC, Lateral Deviation, IPG

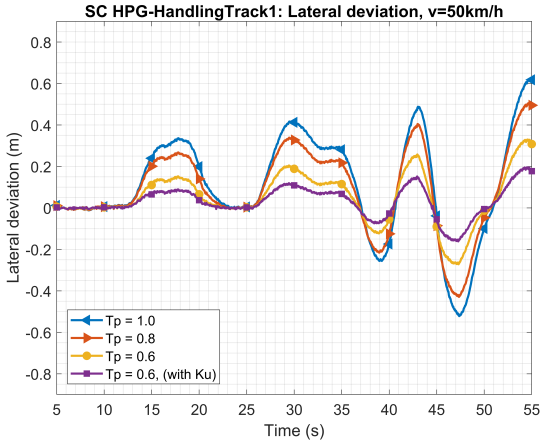

Figure 4.22: HPG: Handling Track 1 SC, Lateral Deviation, IPG

4.4.3 Test Vehicle Results

The test vehicle results are presented in Table 4.14. Comparing the results from the test vehicle in real-time, which are presented in Figure 4.23 and 4.24, with the simulation results, the results are consistent concerning tuning as lower values of the look-ahead time T_p improves the precision. In comparison, higher values of T_p allow for more comfortable manoeuvres, as can be seen in Table 4.15, which shows the quantification of the comfort for this test case. Figure 4.27 - 4.29 illustrates the lateral acceleration, lateral jerk and Fourier transform of the lateral acceleration, respectively, which clearly demonstrates the superiority of the PPC. The lateral acceleration in the body frame oscillates at a relatively high frequency with high amplitudes as well, leading to a worsened experienced comfort. In Appendix D, similar figures are listed for a configuration in the 90° turn.

The velocity profiles of the test runs are shown in Figure 4.25 and 4.26. The desired speed is 50 km/h for the test cases conducted at Handling Track 1, which is mentioned in Table 4.3, but this was manually controlled by the driver in real-time, and therefore, a constant speed could not be withheld.

RMSE [m]			**Max error [m]**		
$\mathbf{T_p}$	**PPC**	**SC**	$\mathbf{T_p}$	**PPC**	**SC**
1.0 ($\mathbf{K_u}$)	0.205	0.588	**1.0 ($\mathbf{K_u}$)**	0.499	1.129
0.8 ($\mathbf{K_u}$)	0.181	0.525	**0.8 ($\mathbf{K_u}$)**	0.466	1.100
0.6 ($\mathbf{K_u}$)	0.147	0.411	**0.6 ($\mathbf{K_u}$)**	0.356	0.852

Table 4.14: Test case 3: Lateral deviation test vehicle results from Handling track 1 at 50 km/h

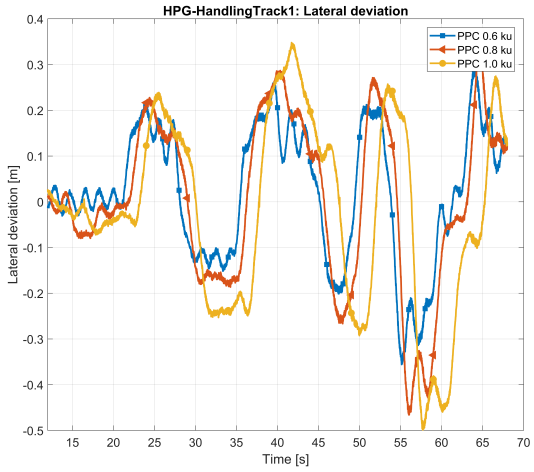

Figure 4.23: HPG: Handling Track PPC, Lateral Deviation, Test vehicle

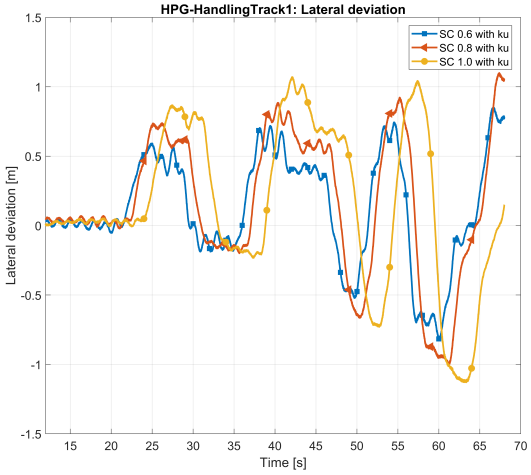

Figure 4.24: HPG: Handling Track SC, Lateral Deviation, Test vehicle

RMSE Jerk [m/s³]			**Max Jerk [m/s³]**			**Area [m/s²]**		
T_p	**PPC**	**SC**	**T_p**	**PPC**	**SC**	**T_p**	**PPC**	**SC**
1 (K_u)	1.309	1.857	**1 (K_u)**	4.158	5.325	**1 (K_u)**	0.039	0.044
0.8 (K_u)	1.475	2.322	**0.8 (K_u)**	4.870	5.771	**0.8 (K_u)**	0.040	0.086
0.6 (K_u)	1.668	3.256	**0.6 (K_u)**	5.273	7.352	**0.6 (K_u)**	0.048	0.101

Table 4.15: Test case 3: comfort test vehicle results from Handling track 1 at 50 km/h

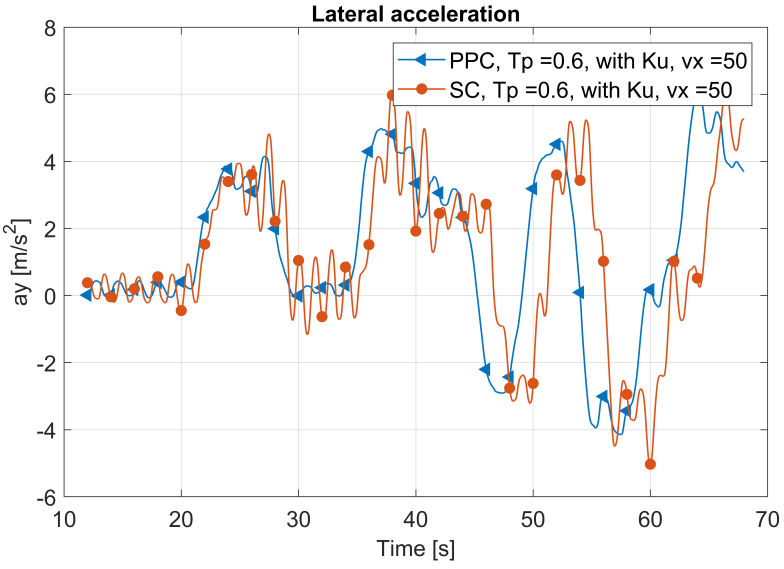

Figure 4.27: HPG: Handling Track, Lateral acceleration, Test vehicle

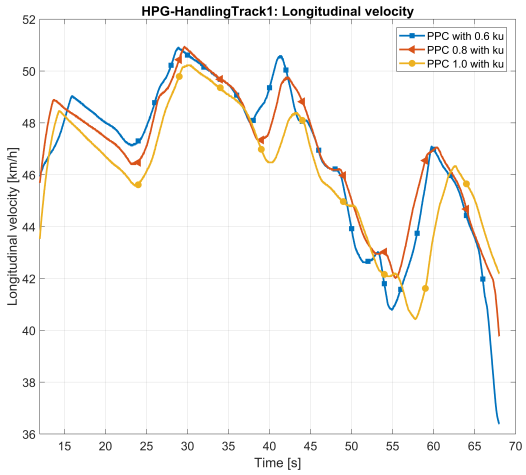

Figure 4.25: HPG: Handling Track PPC, Longitudinal velocity, Test vehicle

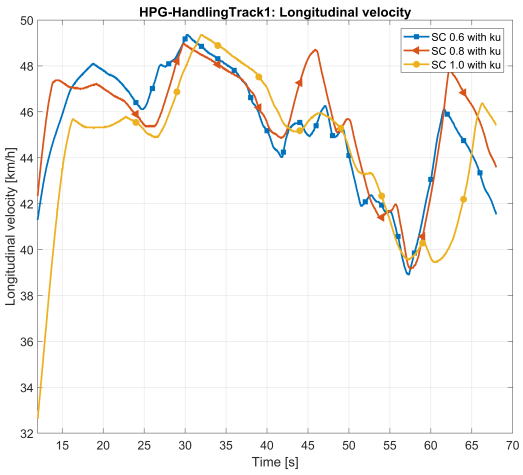

Figure 4.26: HPG: Handling Track SC, Longitudinal velocity, Test vehicle

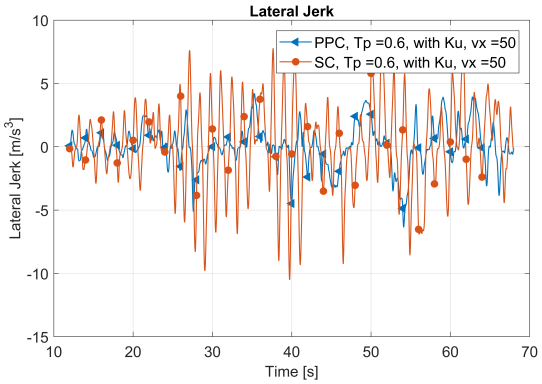

Figure 4.28: HPG: Handling Track, Lateral Jerk, Test vehicle

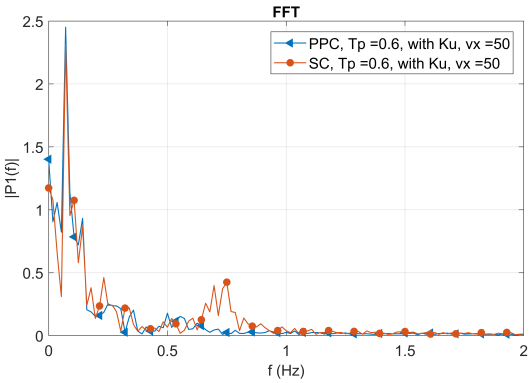

Figure 4.29: HPG: Handling Track, Fourier transform, Test vehicle

4.5 Influence of delay

Controller applications use digital implementation, meaning that Analog/Digital (AD) converters are used for sensors, and Digital/Analog (DA) converters are used for the actuators. Both of these converters introduce time delays. In a simulation environment, these time delays are often neglected. Therefore, an extra test case is performed where the delays are included in the model. Conclusions can then be drawn regarding the robustness of the controllers, and also as an attempt to confirm the behaviour of the controllers as seen from the results in section 4.4.3. The critical value where the closed loop system transitions from stable to unstable are called delay margin as specified in section 3.3.1. The delay is added in IPG CarMaker by applying a transport delay to the input signals of the PTC's. The tests were conducted by introducing a 1 m lateral error step input. The test cases are presented in Table 4.16, where both the PPC and the SC will be evaluated.

Test case	Tuning	Velocity
1: Step input	$T_p \in [0.6, 1.0]$ [s]	v $\in [36, 90]$ $[km/h]$

Table 4.16: Delay margin test cases

Figure 4.30 and 4.31 display the behaviour of the different controllers in X-Y plots for the test cases explained before. At low velocities, the SC has the slight edge independently of the look-ahead time as it becomes unstable at a delay of 650 and 795 ms, respectively, with a look-ahead time of 0.6 and 1.0 s as opposed to the PPC, which becomes unstable at 500 and 780 ms for each respective look-ahead time. For high velocities, however, the delay margin of the SC is reduced drastically to 32 and 37 ms for each look-ahead time, whereas the PPC is only reduced to 158 and 350 ms for a look-ahead time of 0.6 and 1.0 s. The robustness of the PPC is superior to the SC concerning handling delays to a broader range of speeds. However, the performance of the PPC is affected more than the SC at different look-ahead times T_p. The results are summarised in Table 4.17.

Delay margin [ms] (36 km/h)			**Delay margin [ms] (90 km/h)**		
$\mathbf{T_p}$	**PPC**	**SC**	$\mathbf{T_p}$	**PPC**	**SC**
1.0	780	795	**1.0**	350	37
0.6	500	650	**0.6**	158	32

Table 4.17: Delay margins of PPC and SC in the case of a 1 step input

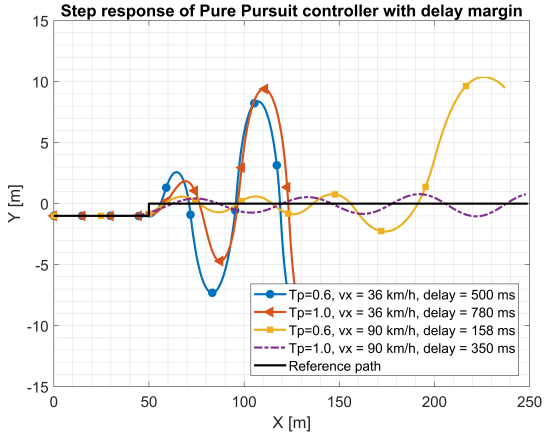

Figure 4.30: PPC - Step response for different T_p and velocities v_x

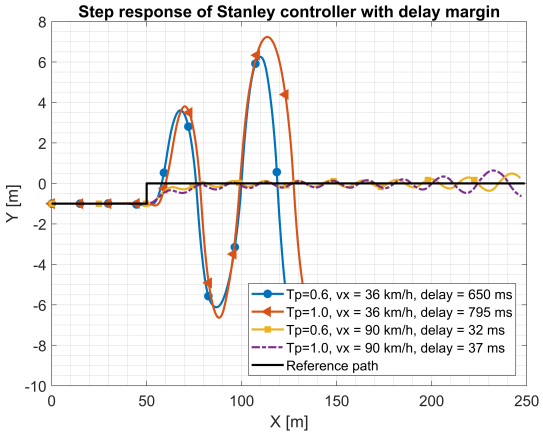

Figure 4.31: SC - Step response for different T_p and velocities v_x

4.6 Chapter Conclusion

The results display that the difference in precision between the PPC and the SC is insignificant at lower velocities, even though the SC performs marginally better. However, at higher velocities, the PPC has a superior performance compared to the SC. Relating the precision results to the initial threshold for maximum lateral deviation of 37.5 *cm* listed on the requirements of an automated lane keeping system stated in the UN regulations, there are several instances where this limit is not exceeded. The SC maintains within the threshold in more cases than the PPC, but as mentioned, the PPC becomes superior at higher velocities.

The comfort evaluation is consistent in how the PPC is always more comfortable. The lateral jerk is always less severe, and the oscillations within the uncomfortable regions are always higher for the SC. The characteristics of the controllers and their effect on comfort are independent of the velocity. However, an increase in the look-ahead time seems to smoothen the vehicle's trajectory. Therefore, the trade-off between comfort and precision is apparent as an increase in look-ahead time seemed to worsen the controllers' precision.

When evaluating the controllers' robustness, the results showcase that at low velocities, both controllers have a high delay margin. However, at high velocities, the delay margin for the SC is drastically reduced compared to the PPC. Consequently, the PPC is more robust to signal delays than the SC.

Table 4.18 and 4.19 shows a simplification of the evaluation of the different attributes at low and high velocities, respectively. These tables summarise all the results using simple descriptive words and originate from Appendix C, where all results have been quantified with a "grade" from 1-5, whereas 5 is excellent and 1 is inadequate. Note that only the best tuning configuration for each test case is considered when summarising the results. The scaling goes from **very bad** to **very good**, where

very bad is close to grade 1, and **very good** is close to grade 5. Table 4.20 presents the controllers' robustness evaluations. The scaling is simply **Passed** or **Failed**.

	Precision	**Comfort**
Pure Pursuit Controller	Very Good	Good
Stanley Controller	Very Good	Bad

Table 4.18: Low velocities, final comparison

	Precision	**Comfort**
Pure Pursuit Controller	Very Good	Very Good
Stanley Controller	Good	Bad

Table 4.19: High velocities, final comparison

	Robustness
Pure Pursuit Controller	Passed
Stanley Controller	Failed

Table 4.20: Robustness final comparison

The final conclusion from this evaluation is that the difference between the controllers at low velocities is negligible concerning precision. However, the SC does have a marginally better precision due to the corner cutting present for the PPC. At higher velocities and more dynamic driving with changing road curvature, the difference between the controllers is more noticeable. In this scenario, the PPC performs better than the SC concerning all attributes, as displayed in Table 4.19. The PPC can maintain good ride comfort and precision in higher velocities and is more robust to signal delays. The SC have good precision but drops its ride comfort and will be more affected by signal delays. Because of the controller design, the PPC and SC have different characteristics. The PPC can have corner cutting depending on the look-ahead time, which will affect the precision compared to the SC, which does not have the same corner cutting behaviour. However, the ride comfort for the SC is affected since it turns later and can have more oscillations. When tuning the controllers, the trade-off between precision and ride comfort must be considered; it can be good to have less precision in favour of ride comfort.

Finally, at low velocities, one can choose either the SC or the PPC since there is no significant difference in performance. However, since the PPC is more robust

to signal delays at higher velocities, the PPC can be applied at a broader range of driving scenarios where it maintains its ride comfort and stability compared to the SC. The evaluation of robustness refers to a maintained performance at a variety of velocities at different magnitudes of signal delays. Consequently, the PPC is the superior PTC in this study. Therefore, when path tracking is used in the centralised controller in the remainder of the project, it implies using the PPC.

5

Steer By Torque Vectoring

The PTC's presented in the previous chapter utilise the steering wheel actuator to control the lateral motion of the vehicle in an AD scenario. As a human driver does not steer the vehicle in this case, it is crucial to ensure a fail-operational ability in the control design to account for potential risks. This chapter presents a new method of controlling the vehicle's lateral motion, which is Steer by Torque Vectoring. This system aims to steer the vehicle by applying differential torque, ΔT, to the EM's instead of using the steering wheel and thereby serve as a backup system to ensure fail-operational ability in case of steering actuator failures.

5.1 Safety Critical Systems

A modern vehicle has many safety-critical systems, for example, the power steering and the brake system. It is required that these safety-critical systems have a backup function that can be activated if the primary system fails to prevent catastrophic failures. Often these backup systems are based on redundancy, meaning that if the primary system fails, the redundant system is not affected and can take over. For example, in a hydraulic brake system, the redundant backup system can be designed with a dual-circuit brake system with separated brake lines to different wheels. In conventional power-steered vehicles, the mechanical connection between the steering rack and the steering wheel is the secondary redundant mechanical link that enables the driver to still be able to steer the vehicle without power-assisted steering.

In an autonomous vehicle, the human driver is not in control of the steering wheel, and as the autonomous systems get increasingly sophisticated, the human driver can be less alert to take over the steering if the autonomous system fails. With an increased level of autonomy in the future, a driver may not even be present in the driver's seat. Furthermore, with the development and potential implementation of a steer-by-wire system in future vehicles, the mechanical link (steering column) between the steering wheel and the steering rack is removed since this is the goal of such a system. Therefore, the fail-operational ability with this kind of steering system must rely on other redundant systems. The potential risk with autonomous vehicles and steer-by-wire systems is, therefore, failures leading to a loss of steering capacity. The failures can be caused by, for example, steering actuator faults, communication errors and power blackouts. Consequently, if a fault occurs, the vehicle should have a backup system that can take over the control of the steering actuation and control the vehicle to a safe state.

The redundancy to enable a fail-operational system has previously mainly focused on duplicating components on all levels, a method used extensively in aircraft. However, this solution adds cost and significant complexity to the systems and may not even remove all possible failure modes [35]. An alternative solution is to use existing actuators and control systems to have an independent backup steering system instead of duplicating components. As mentioned before, previous research utilises selective braking or propulsion wheel torque to steer the vehicle as a backup system, which can be done by using friction brakes and/or EM's. In modern vehicles, there are already available control systems for selective braking with electronic stability systems, for example, ABS, which utilises sensors and actuators that also can be used by the backup systems. These stability systems are, however, only used to avoid a loss of control by keeping the vehicle within limits regarding body slip and roll. They help to stabilise the vehicle in an oversteer or understeer situation. However, they do not take over the steering actuation, which is the task of the backup system presented in this research.

Since the vehicle in this project is equipped with four EM's, each connected to an individual wheel, this enables steering by applying differential torque to the motors. The car is also equipped with friction brakes that can be utilised in combination or independently with the EM's to control the lateral motion. Therefore, the backup system's task is to utilise the EM's and/or the friction brakes to steer the vehicle to bring it to a safe state after a steering actuator failure. As mentioned previously, the name for this backup system is Steer by Torque Vectoring (SbTV) since the EM can allocate both regenerative braking and/or propulsion torque when controlling the lateral motion. TV refers to the controller allocating the total torque request between the four motors and the friction brakes to achieve the requested lateral motion. The following sections present the design and capability of this backup system.

5.2 Steering Failure Characteristics

The test vehicle in this project has a mechanical steering system that is assisted electronically with a motor, referred to as Electronic Power Assistance Steering (EPAS). This system adds an extra steering torque in addition to the driver input to the steering wheel. The added torque from the EPAS reduces the steering torque that the human driver has to apply. A failure in this system can have different characteristics. Too much or too little steering torque will affect the vehicle's trajectory. Furthermore, a more severe scenario would be if the steering torque from the steering actuator is lost completely. If this occurs when the vehicle is driving autonomously, the driver may not intervene and take control of the vehicle, meaning there will be no steering wheel torque applied. In this project, the only steering failure characteristic considered is when no steering wheel torque can be applied, i.e. neither the EPAS nor the human driver applies any steering wheel torque.

The severity of a failure will depend on the vehicle's initial motion, which are states regarding velocity, position and heading relative to the road. Additionally, the road

curvature, boundaries and obstacles ahead will also affect the outcome of the potential failure. Another aspect of the failure is the detection time and its correctness. The delay between detecting and categorising the failure to actuator action will also affect the severity of the failure itself. There can also be environmental disturbances that affect the ability to manage a failure, such as wind gusts, rutted roads and varying road friction. In general, the vehicle's ability to manage a steering failure depends on the following characteristics; the character of steering failure, the initial motion of the vehicle, road boundaries ahead, vehicle characteristics, failure detection, control algorithms and disturbances. However, in this thesis, failure detection and environmental disturbances are not included in the design of the SbTV controller.

5.3 Steering Capability

The steering capability is defined as the cornering curvature that can be achieved when a certain difference in longitudinal force is applied to the wheels. The difference in longitudinal wheel force can be obtained by applying different amounts of friction braking and/or applying different amounts of motor torque at the wheels. When doing one or both of these things at the different wheels of the vehicle, some contributing aspects will determine the resulting cornering curvature for the vehicle. These factors and how to determine the capability will be described in more detail in the following subsections.

5.3.1 Contributing factors

When applying differential torque to the wheels, the vehicle's steering capability has two contributing factors. The first factor is called the scrub radius effect, and it is determined by the front axle suspension geometry. When a torque is applied to the wheel, the longitudinal tire force will induce a yawing moment around the vertical axis of the tire because of the moment arm, which is called the scrub radius. This yawing moment around the vertical axis will affect the steering angle and, therefore, the cornering curvature. The scrub radius is a suspension parameter defined as the lateral distance between the centerline of the tire and the tire's centre of rotation. The scrub radius is negative if the centre of rotation is outside the tire's centerline relative to the vehicle, which is determined by where the kingpin axis intersects with the road plane. An illustration of the scrub radius and the suspension geometry for a left front tire is displayed in Figure 5.1.

In addition to the yawing moment induced by the longitudinal tire force and the scrub radius effect, the lateral tire force will also create a yawing moment around the tire's vertical axis. Due to the lateral shear stress in the contact patch of the tire, the lateral force acts behind the tire's centerline, and this distance is called the pneumatic trail, which is illustrated in Figure 5.1. The resulting yawing moment from the lateral tire force and the pneumatic trail is often called aligning moment because it usually aligns the tire in the direction of zero side slip. Furthermore, since the tire is on a steered axle, another moment arm exists for the lateral force due to

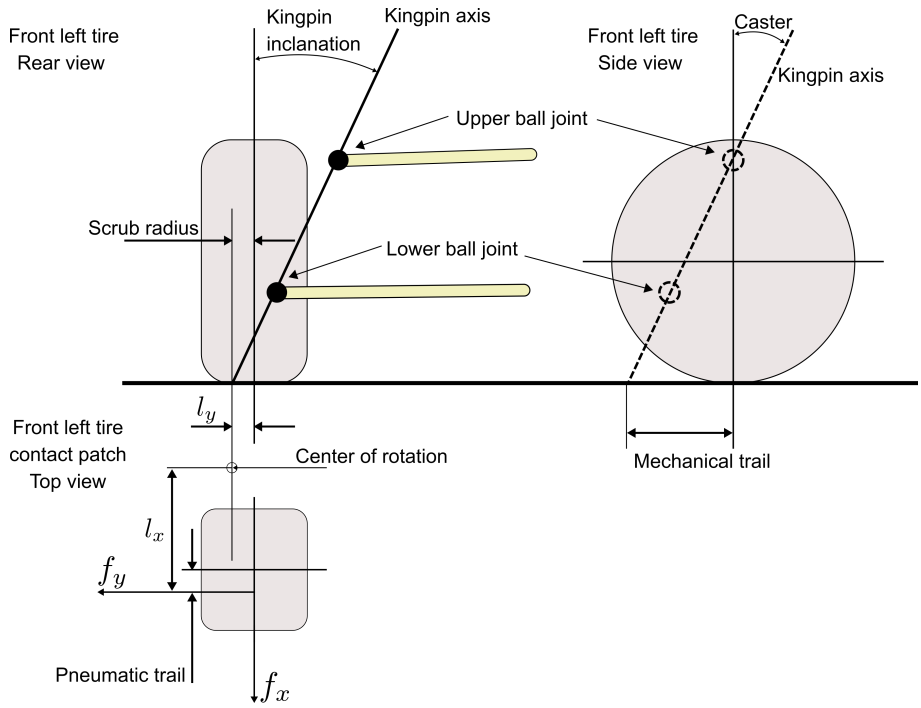

Figure 5.1: Left front tire suspension geometry, illustration with a negative scrub radius and a positive mechanical trail

the suspension linkage design. This moment arm exists because of the longitudinal distance between the tire's centerline and its centre of rotation in a side view, see Figure 5.1, which is called the mechanical trail. The lateral tire force, therefore, has a moment arm comprised by adding the pneumatic trail and the mechanical trail, which will induce a moment around the tire's vertical axis, called the steering moment. The mechanical trail is often designed to be positive, making the steering and aligning moments act in the same direction. When manoeuvring in a curve, the steering and aligning moment tend to make the steering wheel align itself in the direction of the vehicle's motion if the driver removes the hands from the steering wheel.

Mathematically the steering system for the front axle can be described by a second-order differential equation according to [13]:

$$J_s \cdot \ddot{\delta} + b_s \cdot \dot{\delta} + l_x \cdot f_y + M_f = l_y \cdot (f_{x,FL} - f_{x,FR}) \tag{5.1}$$

The difference in longitudinal force, $(f_{x,FL} - f_{x,FR})$, as a result of the applied differential wheel torque, will induce an alignment moment due to the scrub radius arm l_y. Furthermore, the equation display that the equilibrium contains inertia, J_s, damping, b_s and friction torque M_f in addition to the alignment moment from the lateral force, f_y, due to the moment arm l_x which is the sum of the pneumatic and mechanical trail. In other words, this equation displays that, when applying a certain difference in longitudinal force to the tires, the scrub radius will induce a mo-

ment around the tire's vertical axis, affecting the steering angle and, consequently, the cornering curvature. The inertia, damping and friction torque, in addition to the lateral force aligning moment, will "work against" this movement and therefore determine the steady state equilibrium resulting in a certain steering angle on the front tires.

In addition to the scrub radius effect on the steering angle, the second factor contributing to the vehicle's cornering curvature is the chassis yaw moment. The scrub radius effect can be seen as a scenario of having no hands on the steering wheel, i.e. not applying any steering wheel torque and letting the steering wheel move freely. As explained, the steering wheel will then move by itself due to the aligning moment from the difference in tire forces on the front axle, resulting in a certain steering wheel angle and a curvature for the vehicle. However, even when applying differential torque to the tires and having hands on the steering wheel, i.e. locking the steering wheel to zero degrees, the vehicle will turn with a certain cornering curvature. The vehicle will turn because the differential torque on the tires will induce a yaw moment on the chassis. Consequently, the two factors determining the vehicle's cornering curvature when applying differential torque are the suspension geometry and the scrub radius effect. The other contribution comes from the yaw moment on the chassis.

It has been observed both in [13] and in this thesis that the scrub radius effect significantly affects the cornering curvature. The difference between having hands-on and hands-off the steering wheel, i.e. the difference in yaw moment and scrub radius contribution to the cornering curvature, can be seen in Appendix E. The results in Appendix E showcase that the scrub radius effect can double the cornering curvature at lower velocities compared to only using the yaw moment on the front axle. However, the difference decreases when the velocity increases or with a lower differential torque. Since the scrub radius acts on the front axle, the front axle differential torque has a significant part of the steering capability, as opposed to applying differential torque on the rear axle, which will only increase the yaw moment contribution to the cornering curvature. Consequently, the capability is affected by the utilised configuration, i.e. only using the EM's on the front axle and/or using all four EM's in combination with the friction brakes.

5.3.2 Different Configurations

Since the test vehicle in this thesis has four EM's and friction brakes on both the front and rear wheels, many different configurations can be utilised to achieve the desired lateral motion from the backup system. Every configuration has the same goal of ensuring a fail-operational ability in the case of a steering failure. However, the capability to handle steering failures will vary between the different configurations. The configurations can be divided into three groups. The first one is configurations that only utilise the EM's, and the second group are configurations that only utilise friction braking. The third group utilises both friction brakes and EM's. An example of proposed configurations for the different groups of selective braking and/or

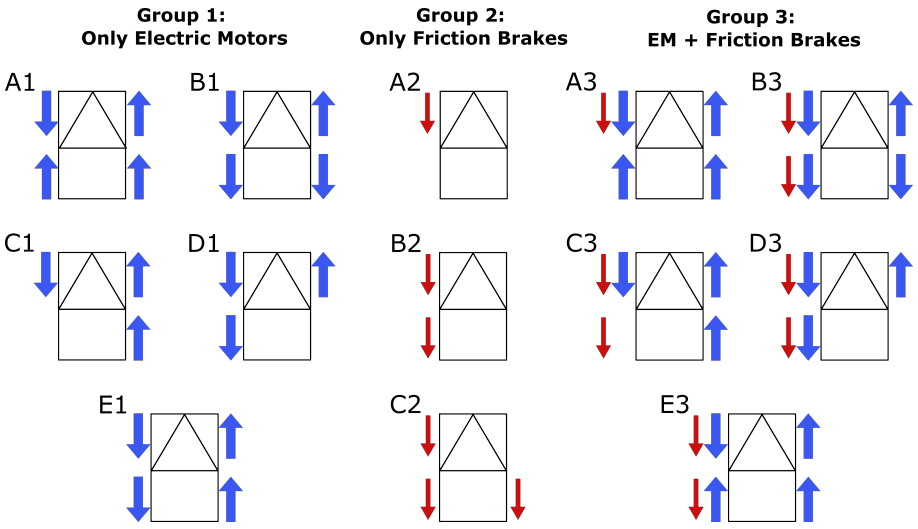

Figure 5.2: Steer by torque vectoring configurations

propulsion torque is presented in Figure 5.2.

Note that the arrows representing the wheel torques are displayed in a left turn scenario for all configurations, and that thick blue arrows represent the EM torque. The thinner red arrows represent friction brake torque. Furthermore, the configurations also differ if they keep a constant velocity or if they are braking the vehicle. Depending on the desired vehicle motion, i.e. if the safe state is to keep a constant velocity or braking, therefore affects which configurations that are possible to use. For example, configuration A1 can keep a constant velocity with the rear motors while the front motors are used to steer the vehicle. In contrast, configuration B1 use the rear motors to brake the vehicle instead while still using the front motors to steer the vehicle. Group 2 will always brake the vehicle since it only utilises the friction brakes, while configurations from group 3 have more options regarding the vehicle's velocity.

Additionally, since the torque on each side of the vehicle can have different amplitude, more options exist, further complicating the torque allocation. The most common configuration in previous research is only to use friction braking to steer the vehicle, i.e. configurations from group 2, but where the velocity also could be kept by applying propulsion torque. The reason is that when using a more conventional powertrain, it is much more complicated to apply the same differential torque from the powertrain as displayed in Figure 5.2, which can utilise the potential of having four EM's. The unique electric powertrain in this project with four EM's enables the lateral motion to be controlled by only the EM's, as displayed by group 1 in Figure 5.2. Therefore, in this project, the focus is only on configurations from group 1. More specifically, the evaluated configuration is A1, meaning that the front motors are used to steer the vehicle, and the rear motors are used to keep a constant velocity.

5.3.3 Finding the capability

It is essential to determine the steering capability to design the SbTV controller as it will affect the controller's ability to compute the wheel torque required for a certain curvature. Different methods can be applied to determine the capability. It can be mathematically modelled and obtained analytically, and it can be simulated with a vehicle model or by performing tests with a test vehicle. Different methods can supplement each other and serve as verification to validate the results. In this case, the capability for configuration A1 is obtained by performing simulations and tests with the test vehicle.

The steering capability corresponds to a certain curvature obtained by simulating the vehicle at certain operating points. The operating points are obtained using the same IPG CarMaker/Matlab Simulink simulation environment as in chapter 4. They consist of different constant velocities ranging from 20 km/h to 90 km/h, which are kept with the vehicle's rear motors according to the configuration. For each velocity, a constant differential torque is then applied at the front axle ranging from 200 Nm to 1000 Nm, where applying 200 Nm means a negative braking wheel torque of -100 Nm on one side and a positive propulsion wheel torque of 100 Nm on the other side. The steering wheel torque is set to 0 Nm so it can move freely. The resulting curvature of the vehicle is saved, and the simulation results are presented in Figure 5.3 and 5.4.

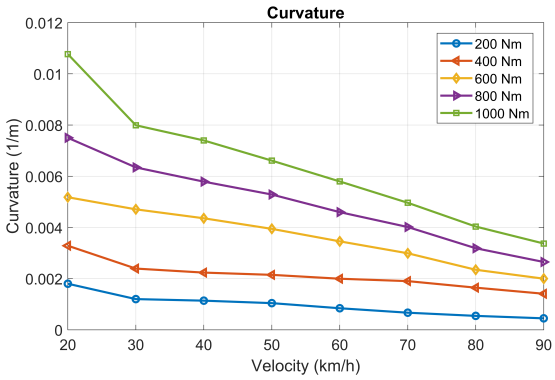

Figure 5.3: Steer by Torque Vectoring - Capability as a function of differential left-right torque

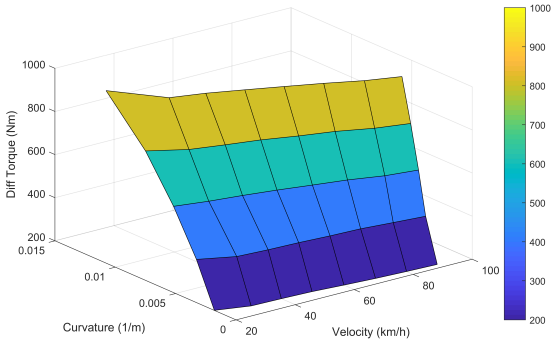

Figure 5.4: Steer by Torque Vectoring, Capability as a function of differential left-right torque in 3D

A similar process to the simulation setup is used for the test vehicle, with the same operating points. While driving at a constant velocity, a constant differential torque is applied on the front axle, while no steering wheel torque is applied. The curvature is then calculated by,

$$\rho = \frac{\dot{\psi}}{v} \tag{5.2}$$

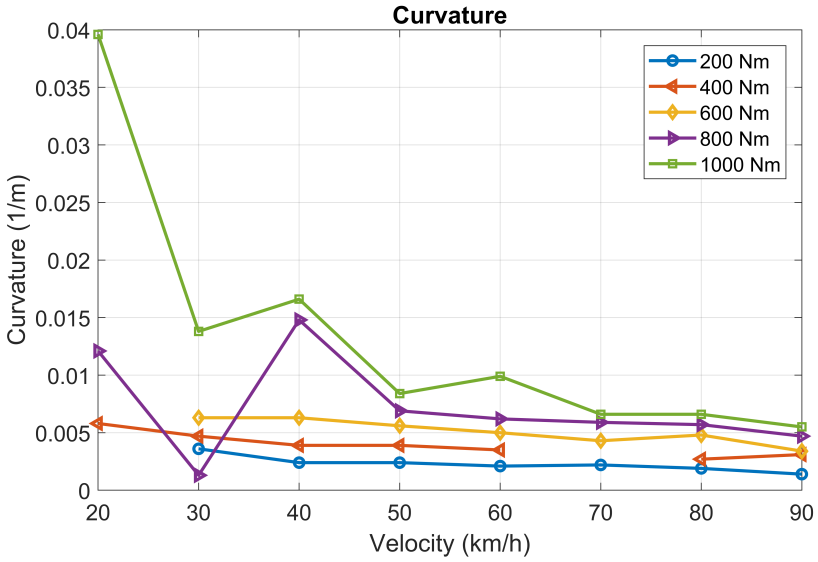

Figure 5.5: Steer by torque vectoring, test vehicle capability

and the test vehicle results are presented in Figure 5.5. Note that the data display the results from one test run for each operating point. Also, some operating points are missing from the test vehicle data because insufficient data were collected from the test runs at these specific operating points.

The comparison between the simulation and the test vehicle results displays a similar behaviour for the steering capability, where it decreases with an increase in velocity. It is also evident that the steering capability is higher when the differential torque is increased. In other words, the most significant curve possible with this configuration is at lower velocities and high differential torques. The simulation results display a maximum curvature of approximately 0.01 m, corresponding to a turn with a radius of 100 m when a differential torque of 1000 Nm is applied at 20 km/h. Furthermore, it is evident that the capability is higher for the test vehicle than the simulation results at all operating points.

As explained before, the steering capability increases with a higher differential torque and with the results showcased here, the limit is at 1000 Nm. In order to make turns with larger curvatures, this means that the differential torque has to increase. However, there are limitations on how high the applied differential torque can be. The first limitation is when the actuators get saturated, i.e. reach their limit. In this case, the power limit of the EM's is the limitation. If the EM's are saturated, the control input may not be fulfilled, which means that the differential torque request is not reached and the desired curvature is not fulfilled. The other limitation is the traction limit of the tires. If the applied wheel torque exceeds the torque limited by friction, the tire will slip instead and not contribute to turning the vehicle.

Finally, the curvature data for each operating point from the simulation and the test vehicle results are used to make a 2D look-up table which outputs a differential

torque for a given input of velocity and desired curvature. The following section describes the integration of the look-up table with the rest of the control architecture.

5.4 Control architecture - SbTV

As mentioned in section 5.3.3, the configuration that was used to find the steering capability was A1 which implies using the rear EM's to maintain the desired velocity, i.e. applying the same torque to the rear EM's and applying a differential torque ΔT on the front wheels to achieve a certain curvature. Therefore, the control allocator is designed to apply a differential torque on the front axle. Note that the magnitude of the torque to each front wheel is equal. However, the sign of the applied torque is opposite to fulfilling the desired curvature, hence the notation **differential** torque. The differential torque is calculated in the look-up table in the control allocator block using the vehicle velocity and the reference curvature, which is generated by the PTC. The architecture is illustrated in Figure 5.6. The sign of the reference curvature determines which wheel to apply positive or negative torque, i.e. turning left or right. Turning left would mean applying positive torque on the right wheel and negative torque on the left. The rear motor torques are equal and determined by the longitudinal force request from the driver interpreter.

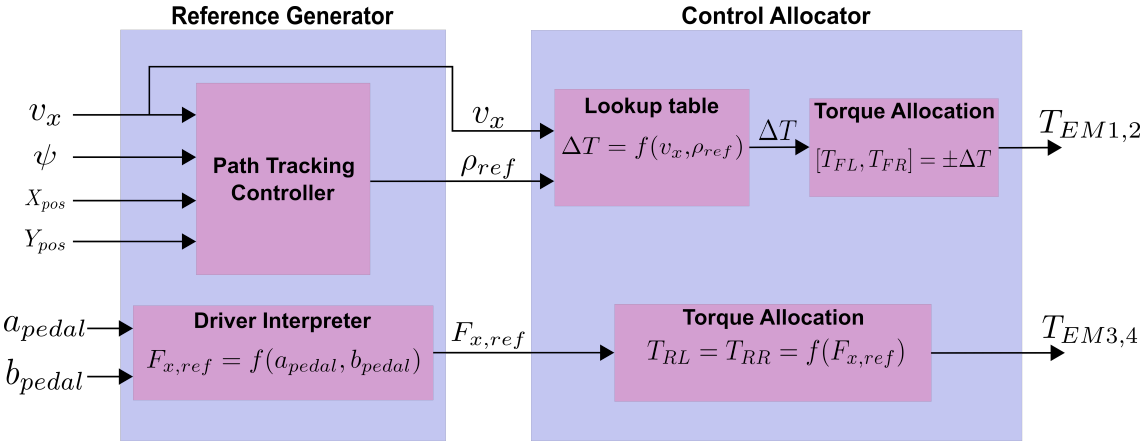

Figure 5.6: Control architecture of steer by torque vectoring control system

5.5 Test Cases

The SbTV controller's performance is evaluated by several different test cases. Since this controller is a backup system, ride comfort is not the most critical attribute to evaluate. In this case, the critical attributes are the controller's capability to steer the vehicle to ensure a fail-operational ability in case of steering wheel failures and therefore maintain a lateral deviation lower than the road boundaries. Therefore, in this case, only the controller's precision is considered compared to the PTC evaluation.

The first test case consists of the two 90° turns that were used when evaluating the path-tracking controller in chapter 4. Consequently, the same reference road definitions are used here as were presented in section 4.3.2, meaning a 90° turn with a radius of 50 m and 312.5 m, respectively. The complete settings for the test case are displayed in Table 5.1. For the radius of 50 m, the velocity is kept constant at 36 km/h, and for the 312.5 m turn, the velocity is set to 90 km/h such that the lateral acceleration is 2 m/s^2 in both scenarios. This test case aims to showcase the SbTV controller's behaviour in a steady state turn to evaluate its ability to steer the vehicle if the steering wheel actuation fails while turning.

Test case	Tuning	Velocity
90 ° turn - R=50 m	$T_p \in [0.6, 1.0]$ [s]	v = 36 $[km/h]$
90° turn - R=312.5 m	$T_p \in [0.6, 1.0]$ [s]	v = 90 $[km/h]$

Table 5.1: 90° turn test cases for the steer by torque vectoring controller

The second test case used to evaluate the SbTV controller is a lane change manoeuvre. This test case showcases the controller's ability to change lanes without using the steering actuator. If the controller can manage a lane change, it has a fail-operational ability and can control the vehicle's lateral motion to a safe state. A *safe state* in this scenario is defined as a lateral deviation smaller than the road boundaries, i.e. the vehicle can maintain its position on the road and either keep a constant velocity or brake to a stop (vehicle velocity = 0 km/h). The reference road definition is presented in Figure 5.8 and 5.7 and the test case settings are presented in Table 5.2. The distance between the points on the reference path is 1 m.

Test case	Tuning	Velocity
1: Lane change	$T_p \in [0.6, 1.0]$ [s]	v $\in [30, 60]$ $[km/h]$

Table 5.2: Lane change test cases

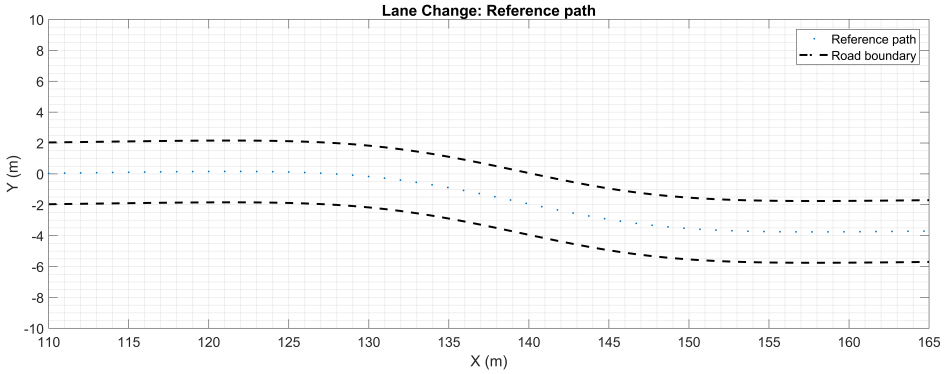

Figure 5.7: Lane change, reference path

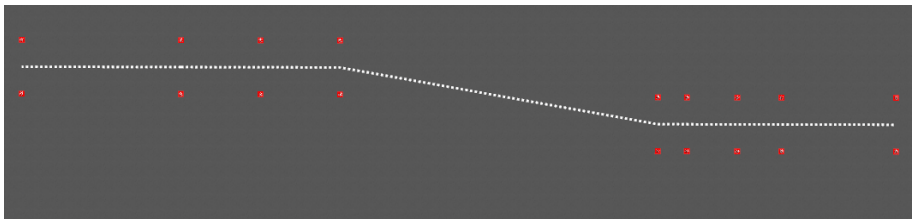

Figure 5.8: Lane change, reference path in IPG CarMaker

5.6 Simulation Results

In this section, the simulation results for the SbTV controller are presented for the different test cases.

Table 5.3 presents the results of the 90° turn with a radius of 50 m and 312.5 m, respectively. The difference between the RMSE and the max error for the two look-ahead times of $T_p = 0.6$ and $T_p = 1.0$ is insignificant for the first test case of a path radius of 50 m relative to the second test case with a larger path radius. For the larger path radius, the RMSE and the max error using $T_p = 0.6$ is approximately reduced by half compared to when $T_p = 1.0$ is used. The most obvious outcome of these results, however, is that the controller's precision using SbTV is notably worse than the precision using the steering wheel to control the lateral movement of the vehicle. Figure 5.9 and 5.10 below shows the lateral deviation of the manoeuvres mentioned above and Figure 5.11 and 5.12 the corresponding wheel torques.

90° turn (36 km/h, R=50 m)			**90° turn (90 km/h, R=312.5 m)**		
$\mathbf{T_p}$	**RMSE** $[m]$	**Max error** $[m]$	$\mathbf{T_p}$	**RMSE** $[m]$	**Max error** $[m]$
0.6	0.369	0.935	**0.6**	0.163	0.281
1.0	0.325	0.901	**1.0**	0.321	0.559
PPC	0.014	0.060	**PPC**	0.016	0.049

Table 5.3: Lateral deviation with steer by torque vectoring for the 90° turns

The simulation results for the vehicle's trajectory relative to the reference path for the lane change manoeuvre are presented in Figure 5.13 and 5.14 for 30 km/h and 60 km/h respectively. Note that the trajectory of two runs with different look-ahead times is presented in each figure, as specified in the test matrix for test case 1, which showcase the difference the look-ahead time has on the controller's ability to follow the reference path. The reference path is showcased with a single yellow line in the figures. Comparing Figure 5.13 and 5.14, it is evident that the SbTV controller's ability to follow the reference path is better at lower velocities, confirming the steering capability results displayed in Figure 5.3.

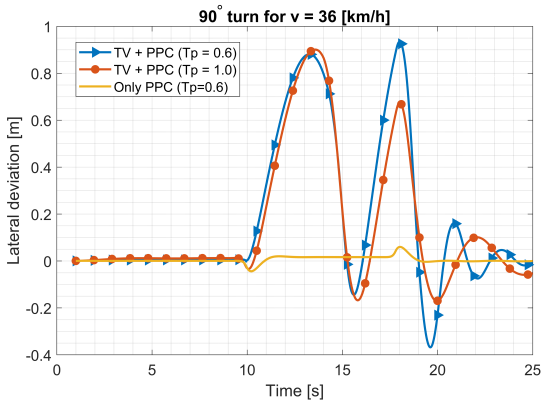

Figure 5.9: 90° turn at 36 km/h, lateral deviation using Differential Torque and PPC (TV + PPC) or a PTC alone (only PPC)

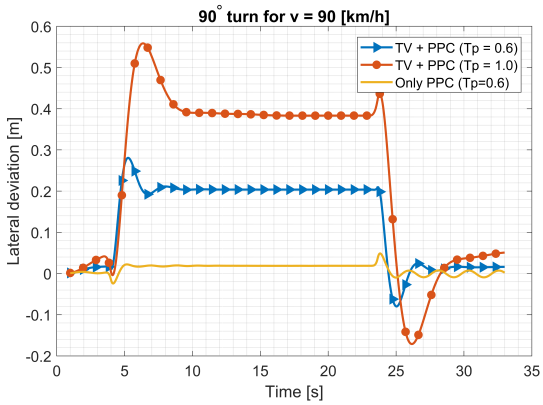

Figure 5.10: 90° turn at 90 km/h, lateral deviation using Differential Torque and PPC (TV + PPC) or a PTC alone (only PPC)

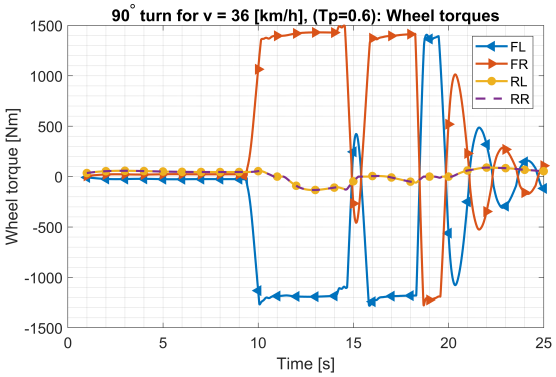

Figure 5.11: 90° turn at 36 km/h, wheel torques

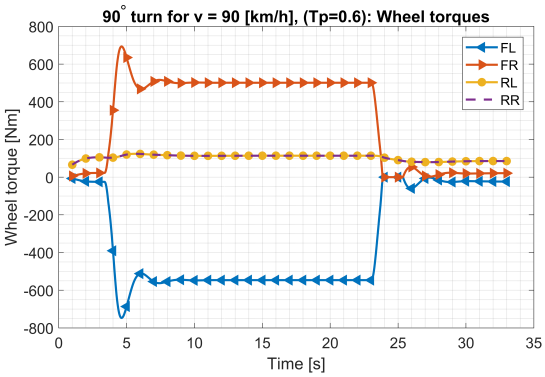

Figure 5.12: 90° turn at 90 km/h, wheel torques

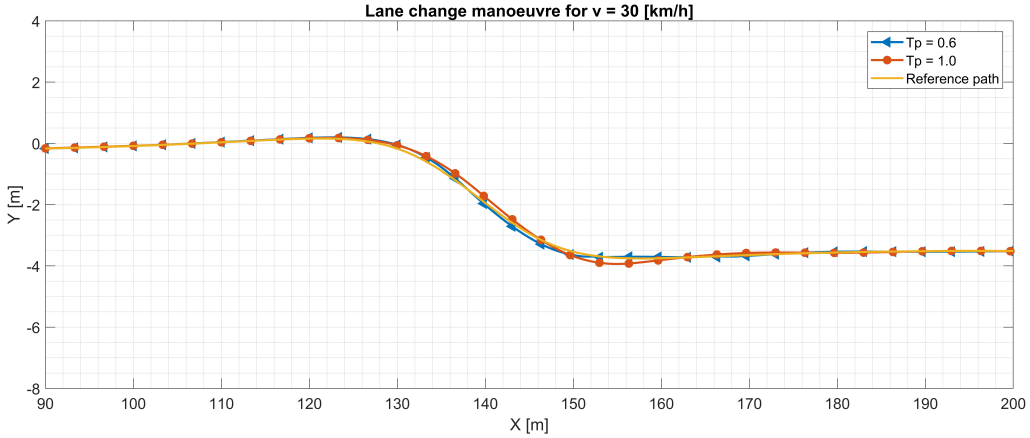

Figure 5.13: Lane change at 30 km/h, trajectory

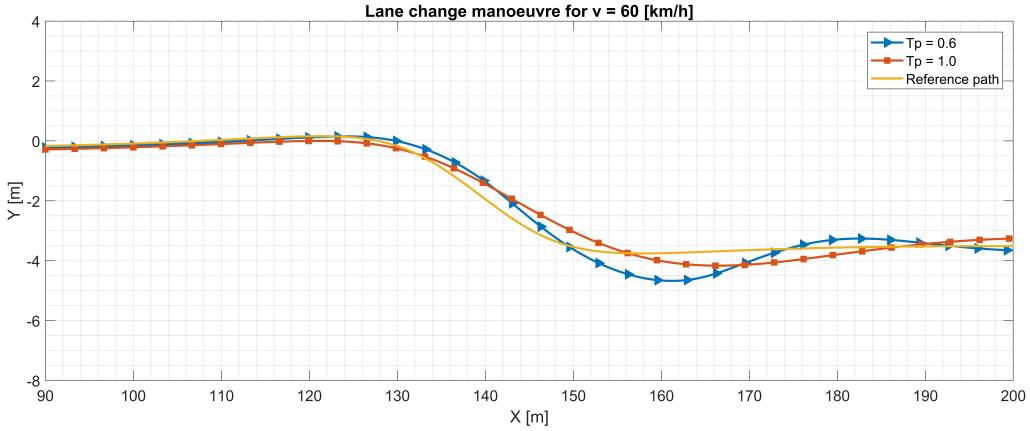

Figure 5.14: Lane change at 60 km/h, trajectory

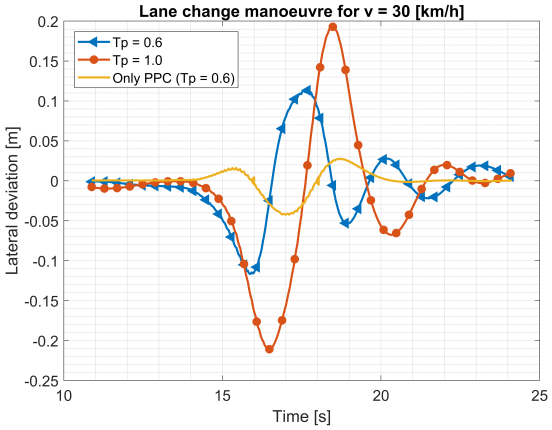

Figure 5.15: Lane change at 30 km/h, lateral deviation

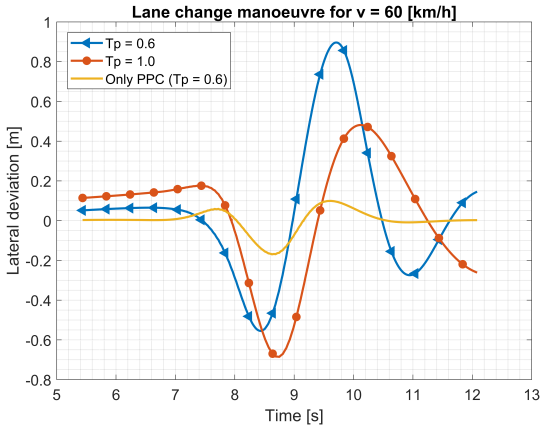

Figure 5.16: Lane change at 60 km/h, lateral deviation

Lane Change (30 km/h)			Lane Change (60 km/h)		
$\mathbf{T_p}$	**RMSE** $[m]$	**Max error** $[m]$	$\mathbf{T_p}$	**RMSE** $[m]$	**Max error** $[m]$
0.6	0.047	0.117	**0.6**	0.348	0.896
1.0	0.082	0.211	**1.0**	0.298	0.685
PPC	0.014	0.042	**PPC**	0.058	0.170

Table 5.4: Lateral deviation for the lane change manoeuvre

Figure 5.15 and 5.16 displays the lateral deviation of the lane change manoeuvre with the results presented in Table 5.4. The precision of the low-velocity manoeuvre is noticeably higher than that of the high-speed manoeuvre but, once again, inferior to the configuration of controlling the lateral movement of the vehicle using the steering wheel.

5.7 Chapter Conclusion

The results showcase that the SbTV controller can steer the vehicle in both a curve and a lane change scenario. Consequently, the SbTV controller has the capability to serve as a backup system and ensure fail-operational ability in case of steering actuator failures. The ability of the controller is, however, affected by the velocity. When the velocity increases, the controller will eventually not be able to maintain its ability to control the vehicle's lateral motion and follow the reference path. The decrease in capability when the velocity is increased is evident in Figure 5.3 for the vehicle model and Figure 5.5 for the actual test vehicle. Comparing the results for the 90° turn that were showcased in Table 5.3, the RMSE is greater than 0.3 m, independently of the look-ahead time for the path with radius R = 50 m. When the radius is increased to 312.5 m, however, the RMSE is decreased by approximately half to about 0.16 m. Note that a higher path radius implies a lower path curvature according to equation 4.2. With that being said, a path radius of 50 m results in a path curvature of 0.02 $\frac{1}{m}$, which is well above both the range of the wheel torques given by the capability matrix shown in Figure 5.3. Consequently, the motor torques increase beyond 1000 Nm, but they get saturated, which is visually apparent in Figure 5.11 where the wheel torques are saturated at around 10 seconds. However, when the path radius is larger, the requested torque is well within the range of the look-up table, and the motors are not saturated. In that case, the results are consistent with chapter 4, where a lower look-ahead time T_p provides better precision.

An aspect of the results which could be deceiving is the manoeuvres where the vehicle does not reach convergence. Figure 5.15, i.e. the lateral deviation of the 90° turn with a 50 m path radius, shows that the vehicle is not really in a steady state condition at any point during the primary manoeuvre. A low look-ahead time means rapid reactions with overshoot, and in short manoeuvres, the effect of a large overshoot on the results could be deceptive. However, compared to controlling the vehicle's lateral motion using the steering wheel as done in chapter 4, this system is much more unstable and less predictive. Some test cases could yield better results using a higher look-ahead time.

The vehicle's capability is also an important topic, as the capability is affected by the configuration, i.e. what actuators are utilised. For the results presented in the previous section, only the front motors were utilised to steer the vehicle, and the rear motors had an equal torque distribution to keep a constant velocity. Using another configuration can improve the results, for example adding friction brakes or distributing the rear motor torques as well. However, most of the capability is from

the front axle due to the scrub radius effect. Adding differential torque on the rear axle would only increase the contribution from the yaw moment on the chassis.

6

Energy Efficient Torque Vectoring

This chapter investigates the concept of reducing the vehicle's energy consumption by optimising the torque distribution between the four motors. The investigation includes the development of a torque vectoring controller that can allocate optimal wheel torques based on a reference yaw moment. Further, the torque vectoring controller is coupled with the PPC to investigate if combining the controllers for lateral and yaw motion control can reduce the vehicle's energy consumption. Consequently, in this chapter, the driver and the PPC can control the steering wheel actuation. The optimisation-based control allocation is designed with two offline optimisation strategies. The first is based on a set of distribution rules, and the other is based on a look-up table.

6.1 The Vehicle's Power Losses

The word **optimal** refers to the fact that an over-actuated system can obtain the desired reference value in infinite ways. Therefore, one of these approaches will be optimal concerning specific requirements. In this case, the requirement is energy efficiency, meaning that the total energy consumption for an arbitrary driving cycle needs to be reduced. The total energy consumption for a drive cycle can be computed by integrating the total work, P_{tot}, produced over time (from t_0 to t_e) to complete the cycle, according to equation 6.1. Since the energy consumption is minimised simultaneously, the power losses in the system are minimised. The purpose of the TVC is to allocate the wheel torque to minimise the power losses in the vehicle. An overview of the power flow for the vehicle used in this study is displayed in Figure 6.1.

$$E_{tot} = \int_{t_0}^{t_e} P_{tot}\, dt \tag{6.1}$$

As shown in Figure 6.1, there are different losses originating from various places in the vehicle, which can be categorised into different groups. There are electrical losses (motor, inverter and battery), transmission losses (gearbox), and tire losses (longitudinal and lateral slip and rolling resistance).

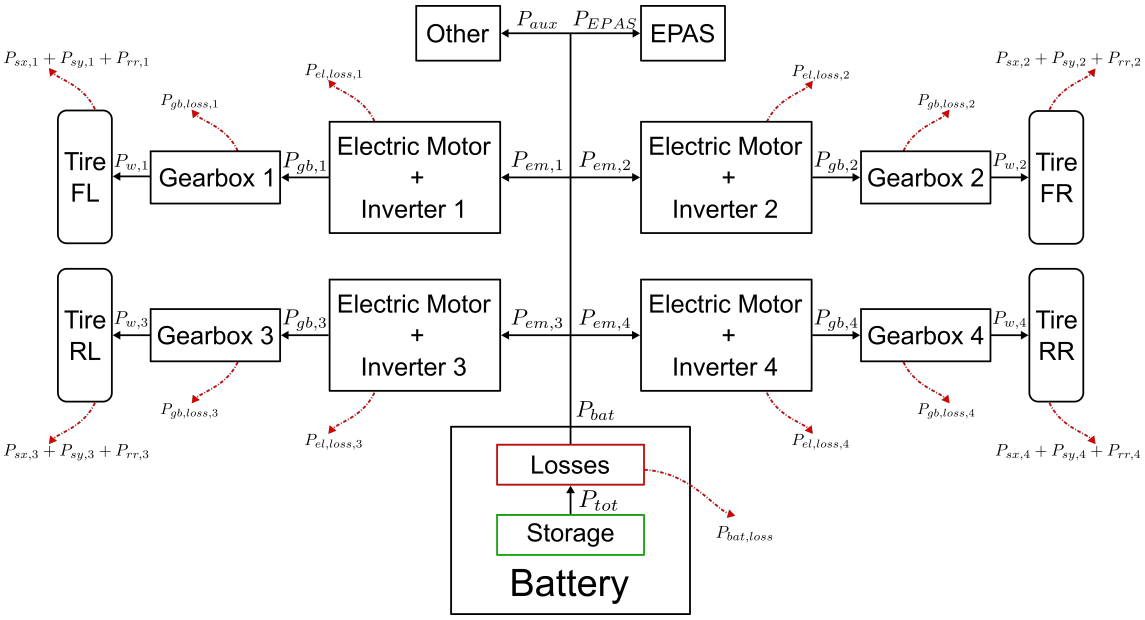

Figure 6.1: Power flow of the test vehicle used in this study

The total power, P_{tot}, is the battery power defined according to 6.2. Positive power is defined as a power flow from the battery to the wheels, and negative power is defined in the opposite direction, i.e. regenerative braking.

$$P_{tot} = \begin{cases} \sqrt{\eta_{bat}} P_{bat}, & \text{if } P_{bat} \leq 0 \\ \frac{P_{bat}}{\sqrt{\eta_{bat}}}, & \text{if } P_{bat} > 0 \end{cases} \tag{6.2}$$

The efficiency of the battery, η_{bat}, is the round-trip efficiency, i.e. the ratio of power flowing in and out of the system $P_{bat,out}/P_{bat,in}$. P_{bat} is the battery power going out or in from the battery, and it is defined according to equation 6.3.

$$P_{bat} = \sum_{i=1}^{4} P_{em,i} + P_{EPAS} + P_{aux}, \quad i \in \{1, ...4\} \tag{6.3}$$

The battery power is a sum of the input power, $P_{em,i}$ to motor $i \in \{1, ...4\}$ and the power to the EPAS as well as the auxiliary power, P_{aux} to other systems such as air conditioning. The auxiliary power is, however, neglected in this study and is therefore set to zero, $P_{aux} = 0$. The motor power is defined according to

$$P_{em,i} = P_{gb,i} + P_{em,loss,i}, \quad i \in \{1, ...4\} \tag{6.4}$$

where $P_{em,loss,i}$ is the power loss from one motor and inverter pair $i \in \{1, ...4\}$ and $P_{gb,i}$ is the input power to the gearbox which is defined according to

$$P_{gb,i} = \begin{cases} \frac{P_{w,i}}{\eta_{gb}}, & \text{if } P_{w,i} \leq 0 \\ \eta_{gb} P_{w,i}, & \text{if } P_{w,i} > 0 \end{cases} \tag{6.5}$$

where η_{gb} is the transmission efficiency and $P_{w,i}$ is the input power to the tire. The total power input to the tires is defined by

$$\sum_{i=1}^{4} P_{w,i} = \sum_{i=1}^{4} (P_{sx,i} + P_{sy,i} + P_{rr,i}) + P_{mech} + P_{res} \tag{6.6}$$

where $P_{sx,i}$ is the longitudinal slip power loss, $P_{sy,i}$ is the lateral slip power loss, $P_{rr,i}$ is the rolling resistance power loss for tire $i \in \{1, ...4\}$. P_{mech} is the mechanical power required for the vehicle's motion, and P_{res} is the power loss from aerodynamic drag and friction.

6.1.1 Battery power losses

In Figure 6.1, it can be seen that the battery power is the sum of the four motor power inputs and the power drawn from the EPAS module. The auxiliary power is neglected in this study. The battery power losses depend on the resistance in the battery cells, which varies with temperature, the state of charge and the current. The battery current depends on the motor power, which means that if the motor power consumption is reduced, it can be expected that the battery power losses will also be reduced. However, the effects of temperature, state of charge and battery current are neglected in this study. Instead, a round-trip efficiency for a lithium-ion battery of 95 % is used according to [36].

6.1.2 Electric power losses

In the electric motor and inverter pairs, power losses also exist due to iron and copper losses that will increase non-linearly with the torque and the motor's rotational speed. In this study, the electric losses are based on experimental data obtained in test bench experiments. The test data construct a power loss map for the motor and inverter pair, as shown in Figure 6.2. The power loss map shows that the power losses depend on the motor's torque and rotational speed.

6.1.3 Transmission losses

The transmission losses occur due to the friction in the gears and are acquired by experimental measurements. The efficiency of the gearbox is instantaneously calculated in a look-up table using the rotational speed and EM torque as input variables. The efficiency is then multiplied by the EM torque, which outputs the actual EM torque. The difference in torque before and after the gearbox efficiency is considered the power loss.

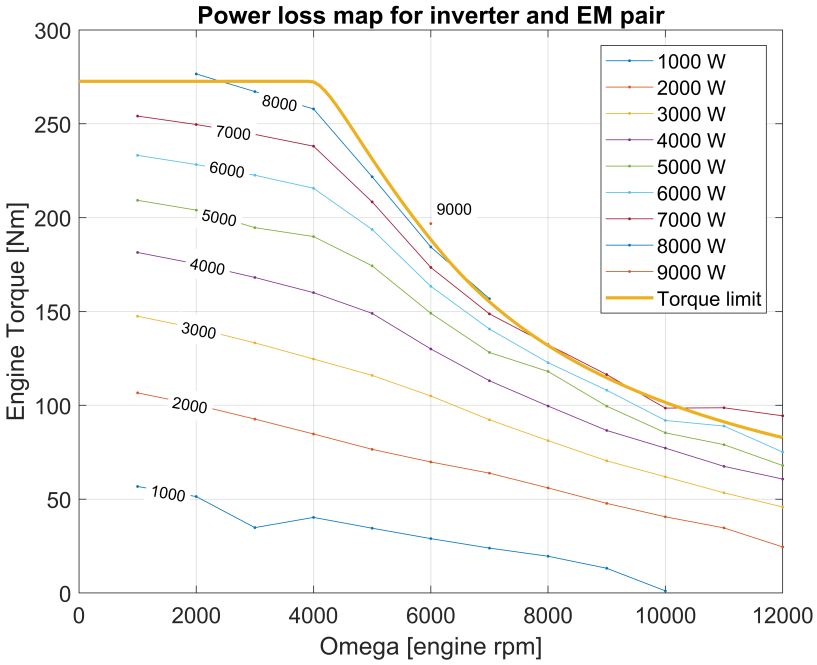

Figure 6.2: Test bench measured power loss data for inverter and EM pair

6.1.4 Tire losses

Rolling resistance, lateral slip and longitudinal slip power losses are all experienced in the vehicle's tires. Rolling resistance power losses occurs due to hysteresis. Hysteresis is a characteristic of deformable materials in how the deformation energy of the deflecting rubber elements of the tire coming in contact with the ground is greater than the energy of recovery when the rubber elements leave the contact patch and regain their original shape [36]. There are many factors affecting the rolling resistance losses. However, the most relevant factor for this project is the tire load and applied torque to the wheels.

The deflection of the rubber elements enables longitudinal and lateral forces. The longitudinal tire loss is a consequence of tire slip, which occurs due to a difference in tangential speed and longitudinal speed of the wheel centre relative to the ground.

The lateral slip angle is the main reason for the lateral slip power losses. When steering the vehicle, lateral tire forces will have to be developed, which is possible due to the rubber element deflection of the tires. These forces, however, will yield a co-directed force working against the direction of motion of the vehicle, resulting in lateral slip power losses.

6.1.5 EPAS consumption

As mentioned in section 5.3, an aligning torque is induced on the tires due to the suspension geometry, i.e. nonzero scrub radius and pneumatic trail. This phenomenon is experienced during cornering manoeuvres when one lets go of the steering wheel,

and the vehicle starts to align itself towards the instantaneous heading direction. The EPAS reacts to the driver's steering wheel angle input and produces a torque to overcome the aligning torque. Without EPAS, the driver would need to rotate the steering wheel and overcome the aligning torque without the aid of the EPAS, which is significantly more difficult. That is why EPAS is used; consequently, the power it consumes is needed to overcome the aligning torque. The direct yaw moment produced by applying a differential torque on the tires will make the tires turn until the aligning torque is equal to the direct yaw moment, assuming that the applied force on the steering wheel is zero, i.e. zero EPAS power consumption. However, if the EPAS is controlled by a driver model or a PTC with TV applied simultaneously whilst cornering in both transient and steady-state manoeuvres, the total power consumption of the EPAS could be reduced as the direct yaw moment produced by the TV aids in rotating the vehicle.

6.2 Optimisation strategy

Many different strategies can be utilised to solve the optimisation problem of minimising the power losses in the vehicle by allocating the wheel torques. The optimal torque distribution corresponds to an optimal yaw moment on the chassis; therefore, the optimisation problem can also be formulated to obtain an optimal yaw moment. As mentioned previously, the optimisation problem can be solved online or offline. One common approach is to implement a cost function that minimises the power losses by allocating the motor torques through online computations. Another online optimisation variant uses a quadratic program that analytically provides a solution through matrix operations. However, online optimisation methods can be more challenging to implement in a vehicle due to their complexity compared to offline optimisation strategies, which is why an offline strategy is chosen in this study. The offline solution can, for example, be obtained either by implementing distribution rules or by a look-up table that can be used online. The rule-based and the look-up table offline methods are used in this study and will be further explained in the following sections.

6.2.1 Offline optimisation - Rule based

The rule-based optimisation problem allocates the four motor torques based on a set of distribution rules. In this case, the distribution rules are defined in equation 6.7, and 6.8, where $F_{x,Left}$ and $F_{x,Right}$ are the longitudinal force requests on the left and right tires. $F_{x,req}$ is the total longitudinal force request and SWA_{thr} is the threshold for the steering wheel angle. In other words, these distribution rules allocate all longitudinal force requests on the right side of the vehicle if the steering wheel angle is above a certain threshold. If it is lower than the threshold, it will allocate all longitudinal force requests to the left side. Consequently, if the steering wheel angle is above, for example, 10 degrees, all torque requests will be sent to the right motors, and if the steering wheel angle is less than -10 degrees, all torque requests will be sent to the left motors. Note that the distribution rules presented here do not consider any optimal yaw moment.

$$F_{x,right} = \begin{cases} F_{x,req}, & \text{if } SWA > SWA_{thr} \\ 0, & \text{if } SWA < -SWA_{thr} \end{cases} \tag{6.7}$$

$$F_{x,left} = \begin{cases} 0, & \text{if } SWA > SWA_{thr} \\ F_{x,req}, & \text{if } SWA < -SWA_{thr} \end{cases} \tag{6.8}$$

The distribution between front and rear, i.e. the individual wheel force request $F_{x,ab}$ is done by using the distribution constant $d_{f-r} \in [0, 0.5, 1]$ and equation 6.9 - 6.12.

$$F_{x,FL} = F_{x,left} \cdot d_{f-r} \tag{6.9}$$

$$F_{x,FR} = F_{x,right} \cdot d_{f-r} \tag{6.10}$$

$$F_{x,RL} = F_{x,left} \cdot (1 - d_{f-r}) \tag{6.11}$$

$$F_{x,RR} = F_{x,right} \cdot (1 - d_{f-r}) \tag{6.12}$$

When $d_{f-r} = 0.5$, for example, 50 % of the longitudinal force request is sent to the rear and 50 % to the front. The indices a and b are notations for the different sides and axles of the vehicle. The individual EM torques are then defined by

$$T_{EM,FL} = \frac{F_{x,FL} \cdot r_w}{n_t} \tag{6.13}$$

$$T_{EM,FR} = \frac{F_{x,FR} \cdot r_w}{n_t} \tag{6.14}$$

$$T_{EM,RL} = \frac{F_{x,RL} \cdot r_w}{n_t} \tag{6.15}$$

$$T_{EM,RR} = \frac{F_{x,RR} \cdot r_w}{n_t} \tag{6.16}$$

with r_w being the wheel radius and n_t being the transmission ratio. The steering wheel angle threshold, SWA_{thr}, and the distribution constant, d_{f-r}, can be seen as tuning parameters. However, the steering wheel threshold is set to 5 degrees for all scenarios to avoid oscillations in the torque request at small steering wheel inputs.

6.2.2 Offline optimisation - Look-up table

The look-up table is based on a brute force offline optimisation where a yaw moment sweep is conducted to acquire the optimal yaw moment for each operating point. In contrast to the rule-based strategy, this method is an optimal yaw moment controller that allocates the motor torque based on an optimal yaw moment reference. In this case, the brute force optimisation is based on the trial-and-error method regarding

the control allocation because both the reference generator and the control allocation require an optimal control design. The initial process of developing the brute force offline optimisation is to define the operating points. First, an arbitrary front-rear torque distribution is decided. Since this optimisation strategy is time-consuming, a distribution constant, d_{f-r}, of 0.5 is decided, i.e. a 50/50 front/rear torque distribution. A sweep of constant direct yaw moments, $M_{z,dir}$, ranging from -1000 Nm to + 1000 Nm with increments of 100 Nm is then applied at a constant velocity and curvature, which defines the operating points. The curvature and velocities are then iterated for each yaw moment sweep. The torque allocation for the applied yaw moment is derived by expanding the single-track vehicle model to a two-track model according to Figure 6.3.

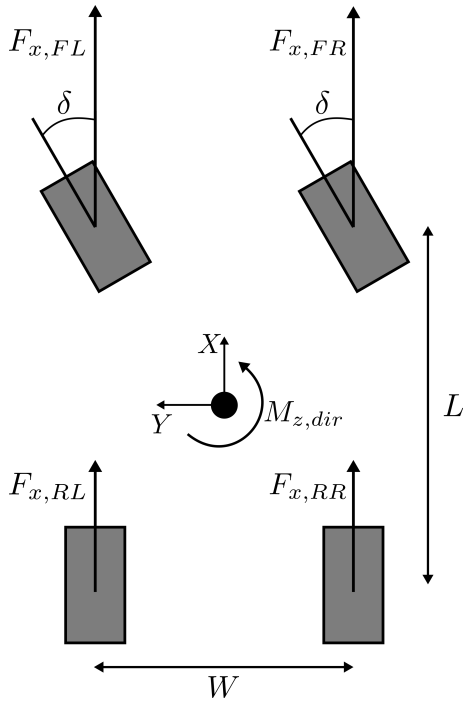

Figure 6.3: Force allocation for configuration used in the Energy Efficient Torque Vectoring controller

The total longitudinal force request, $F_{x,tot}$ for the vehicle can be expressed as the sum of the left and right tire forces, which leads to the relation between the left, right and total force requests, which is presented in equation 6.17.

$$\begin{aligned} F_{x,tot} &= F_{x,Left} + F_{x,Right} \\ F_{x,Left} &= F_{x,tot} - F_{x,Right} \\ F_{x,Right} &= F_{x,tot} - F_{x,Left} \end{aligned} \tag{6.17}$$

The direct chassis yaw moment, $M_{z,dir}$, is defined in equation 6.18.

$$M_{z,dir} = (F_{x,FR} + F_{x,RR}) \cdot \frac{w}{2} - (F_{x,FL} + F_{x,RL}) \cdot \frac{w}{2} \tag{6.18}$$

Since $F_{x,FR} + F_{x,RR} = F_{x,Right}$ and $F_{x,FL} + F_{x,RL} = F_{x,Left}$, one can insert the expressions for $F_{x,Left}$ and $F_{x,Right}$ from equation 6.17 in equation 6.18 and obtain the following expressions for the left and right longitudinal forces:

$$\begin{aligned} F_{x,Right} &= F_{x,tot} \cdot \frac{w}{2} + \frac{M_{z,dir}}{w} \\ F_{x,Left} &= F_{x,tot} \cdot \frac{w}{2} - \frac{M_{z,dir}}{w} \end{aligned} \tag{6.19}$$

The individual wheel forces and motor torques are then computed by equations 6.9 - 6.13 that were presented for the rule-based distribution.

The yaw moment sweep is performed with the same IPG Carmaker/Matlab Simulink model used in chapter 4 and 5, and for each sweep, the power consumption is measured. The yaw moment with a torque allocation that yields the lowest power consumption is then saved for that specific velocity and curvature operating point. The saved data containing the optimal yaw moments are then used to create a look-up table. The look-up table, therefore, generates an interpolated optimal reference yaw moment $M_{z,ref}$ for each combination of instantaneous vehicle velocity and reference curvature ρ_{ref}, assuming the requests are within the curvature capability of the vehicle. The look-up table is visualised in Figure 6.4. Note that the look-up table presented here is for a 50/50 front/rear torque distribution since d_{f-r} is set to 0.5. The possibility, however, exists to have one look-up table for different front/rear torque distributions, but this is not evaluated in this study.

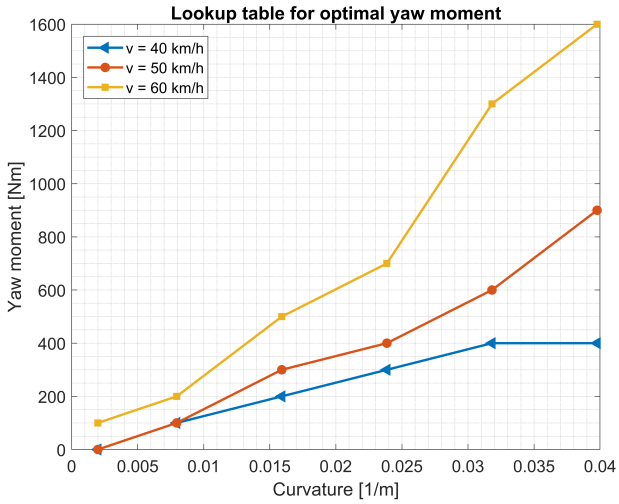

Figure 6.4: Lookup table for interpolating optimal reference yaw moments

6.3 Control architecture - Energy Efficient TV

As the two optimisation strategies used in this study have been presented, it is time to introduce the controller design. Since the purpose of the TVC in this concept is to allocate the motor torques to generate an optimal distribution regarding the power consumption, the controller is called an Energy Efficient Torque Vectoring Controller (EETVC). The EETVC utilises both optimisation strategies presented in the previous section, i.e. it can either use the rule-based or the look-up table method to allocate the motor torques. As mentioned, the look-up table consists of optimal yaw moments obtained offline through a brute force method. Consequently, when the EETVC utilises the look-up table, it allocates the motor torque to achieve the optimal yaw moment reference. However, the controller does not have any feedback regarding the yaw moment, i.e. it is a feed-forward controller. When the controller uses the rule-based method, it distributes the torques based on the total longitudinal force reference from the driver model based on the distribution rules presented in section 6.2.1. The control architecture for the EETVC is displayed in Figure 6.5.

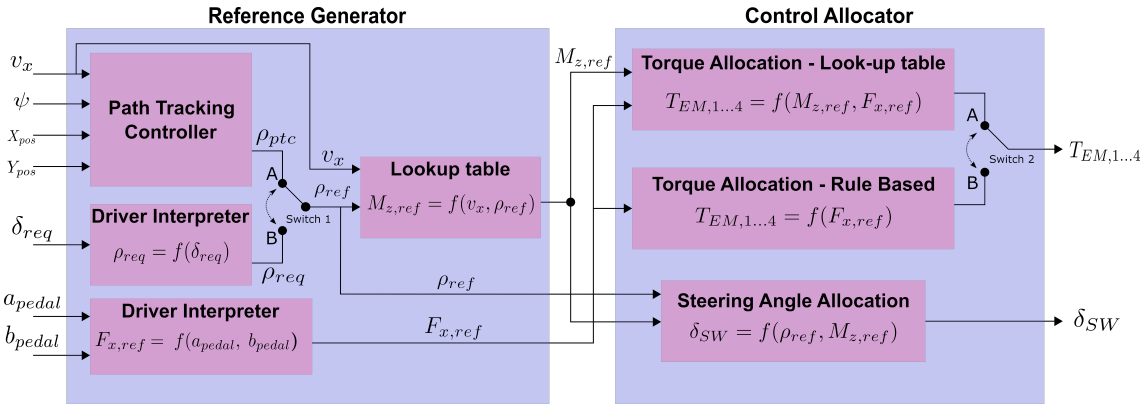

Figure 6.5: Control architecture for the energy efficient torque vectoring control system

The EETVC architecture consists of a reference generator and a control allocator, similar to the PTC and the SbTV control architectures. The reference for the rule-based EETV is the total longitudinal force request, $F_{x,ref}$, computed by the driver interpreter and the pedal position inputs from the driver. The longitudinal force reference is used in the control allocator to distribute the EM torques, $T_{EM,1...4}$, based on the distribution rules that were presented in section 6.2.1. The look-up table EETV also has the longitudinal force reference as an input. However, it also has the optimal yaw moment reference, $M_{z,ref}$, from the look-up table as an input which is computed based on the velocity and curvature reference. The optimal yaw moment reference and the longitudinal force reference are used in the control allocator, which will distribute the EM torques, $T_{EM,1...4}$ based on equations, 6.9 to 6.16 and 6.19. The reference curvature is obtained either by the PTC, ρ_{ptc} or by the

driver model, which requests a steering angle δ_{req}, which is later converted into a requested driver curvature ρ_{req} based on the relationship described in equation 4.3.

The reference curvature ρ_{ref} is chosen depending on the configuration, i.e. either a configuration where the PTC allocates the steering wheel angle request, δ_{SW} or when the driver allocates the steering wheel angle request. The torque allocation can also be changed between the rule-based or the look-up table optimisation strategy. Consequently, four different configurations exist for the EETVC indicated by switches 1 and 2 in Figure 6.5. For example, having both switches 1 and 2 in mode A means that the steering wheel angle request is defined by the PTC, and the torque allocation is made by the look-up table optimisation strategy.

Finally, with the EETV configurations presented here, the lateral motion of the vehicle is controlled with both the steering wheel and the yaw moment produced by the torque distribution. Consequently, the required steering angle to follow an arbitrary curvature will be less with the added yaw moment than with no differential torque distribution. Therefore, the driver can decrease the steering wheel angle and maintain the same curvature. To account for the added yaw moment when using the PTC, i.e. having mode A on switch 1, a correction term can be added to the steering wheel angle formulation, which will counter the effect of the added yaw moment. The correction term, $M_{z,cor}$, is defined in equation 6.20, and this is then added to the wheel angle formulation in equation 6.21.

$$M_{z,cor} = \frac{M_{z,ref} \cdot (C_{yf} + C_{yr})}{(C_{yr} \cdot C_{yf} \cdot L)} \tag{6.20}$$

$$\delta_{SW} = arctan((L + K_u \cdot v^2) \cdot \rho_{ref}) - M_{z,cor} \tag{6.21}$$

6.4 Test cases

The EETVC's effect on the vehicle's energy consumption is evaluated by two different test cases defined in this section. The test cases are evaluated in the same simulation environment that was used to evaluate the PTC and SbTV controllers.

6.4.1 Test Case 1: Steady state power consumption

The first test case aims to evaluate the possible differences in power consumption when applying different torque distributions by measuring the instantaneous power consumption when driving at a constant velocity in a constant radius, i.e. the steady-state power consumption. In this scenario, the four motor torques are allocated by the control allocation block as a function of the requested longitudinal force and the yaw moment reference, see Figure 6.5. However, the applied reference yaw moment, $M_{z,ref}$, to obtain different torque distributions is set to a constant value for each simulation run and not computed online through the look-up table. Instead, in

this test case, a sweep of different constant yaw moments at different velocities is applied, which results in different torque distributions that will affect the power consumption. Therefore this test case will display the optimal yaw moment for a particular torque distribution with optimal steady-state power consumption. The test case will also display how the power losses change for different yaw moments.

A reference test run must be performed without the EETVC activated to enable a comparison between the power consumptions with and without the EETVC. The reference test case is therefore defined as having equal torque on the left and right motors, which is done by setting the yaw moment reference to zero, i.e. the power consumption when the yaw moment is zero is the reference test case. The test case is performed at three different front/rear torque distributions of 0-100, 50-50 and 100-0, i.e. RWD, AWD and FWD. The radius for the test case is set to 100 m, and the velocities are set to 51, 72, and 89 km/h. For this test case, the IPG Driver model controls the steering wheel angle, i.e. switch 1 is in mode B. The velocity is also kept constant by the IPG Driver model. The yaw moment sweep is performed from -1000 Nm - 1000 Nm with increments of 100 Nm, and the test case matrix is displayed in Table 6.1.

Test Matrix

Configuration	Reference test case	Yaw Moment Sweep
Velocity	v = [51, 72, 89] $[m/s]$	v = [51, 72, 89] $[m/s]$
Path radius	r = 100 [m]	r = 100 [m]
Lateral acceleration	a_y = [2, 4, 6] $[m/s^2]$	a_y = [2, 4, 6] $[m/s^2]$
Front/Rear distribution	d_{f-r} = [0-100, 50-50, 100-0]	d_{f-r} = [0-100, 50-50, 100-0]
Applied direct yaw moment	0 [Nm]	Sweep -1000 [Nm] $\rightarrow$ 1000 [Nm]

Table 6.1: Test case 1: Test matrix using IPG Driver

6.4.2 Test Case 2: Energy consumption at HandlingTrack1

The second test case evaluates the energy consumption for the different EETVC configurations at Handling Track 1 from Hällered Proving Ground, which was also used in the PTC evaluation. The energy consumption for each configuration is measured for one lap and compared to the reference test case, which is defined as similar to the previous test case when the yaw moment is zero, i.e. the torque is equal on the left and right motors. For this test case, the vehicle velocity is also kept constant by the IPG Driver. The velocity is set to 50 km/h, which is the same as in the PTC evaluation. The velocity is constant to separate this test case from any transient manoeuvres, i.e. the longitudinal acceleration is constant, and to ensure that the lateral acceleration is kept within reasonable limits. The lateral acceleration for this test case is displayed in Figure 6.6.

The first configuration for the EETVC evaluated in this test case is when the steering

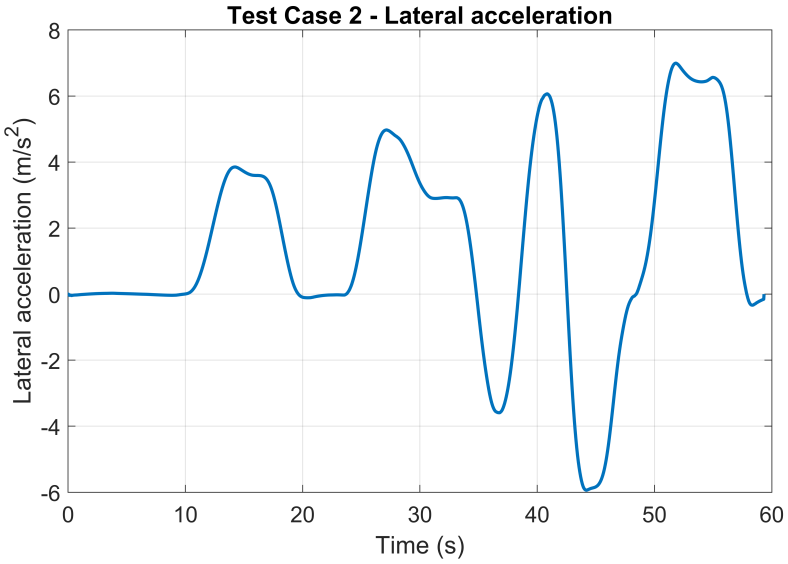

Figure 6.6: Test Case 2 - Lateral Acceleration

wheel angle request is controlled by the IPG Driver and the rule-based optimisation strategy is used, i.e. switch 1 and 2 are set on mode B in the control architecture. The first configuration is evaluated for FWD, AWD and RWD, and the test matrix for this test case is presented in the second column in Table 6.2, "Rule-based EETVC". Note that the reference test case is defined by the two rows "Reference for $T_{EM,1...4}$" and "Reference for δ_{SW}". Consequently, for this case, the reference has equal torque distribution on the left and right motors, and the IPG Driver controls the steering wheel angle allocation for the path following.

The second configuration for the EETVC is when the vehicle still is steered by the IPG Driver model. However, in this scenario, the EETVC is coupled with the look-up table optimisation strategy, i.e. switch 1 is in mode B and switch 2 is in mode A. Note that this configuration is only tested for a 50-50 front/rear distribution since the look-up table is derived only with that configuration. The settings for this configuration can be seen in column three in Table 6.2.

Test Matrix (IPG Driver)

Configuration	Rule Based EETVC	Look-up table EETVC
Velocity	$v = 50$ $[m/s]$	$v = 50$ $[m/s]$
Front/Rear distribution	d_{f-r} = [0-100, 50-50, 100-0]	d_{f-r} = [50-50]
Reference ($T_{EM,1...4}$)	$F_{x,Left} = F_{x,Right}$	$F_{x,Left} = F_{x,Right}$
Reference (δ_{SW})	IPG Driver	IPG Driver
Steering Control (Switch 1)	B (IPG Driver)	B (IPG Driver)
Optimisation strategy (Switch 2)	B (Rule Based)	A (Look-up table)

Table 6.2: Test case 2 - Handling track 1: EETVC Test matrix coupled with the IPG Driver

The third EETVC configuration is when the path following is done by the PTC, which in this test case is the PPC, and the rule-based optimisation strategy is used. The settings for this test case can be seen in column two in Table 6.3. Since the EETVC is coupled with the PPC in this case, the tuning must be performed with both controllers in mind. Therefore the reference case for this configuration is defined by setting the look-ahead time, $T_p = 0.6s$, while the torque allocation is equal on the left and right motors. The EETVC is then tested for two different PPC combinations when $T_p = 0.6s$ and when $T_p = 1.0s$. Also note that this configuration is tested for FWD, AWD and RWD configurations.

The fourth and final EETVC configuration is when the look-up table optimisation strategy is used together with the PPC. The settings for this configuration are displayed in the third column in Table 6.3. Note that the reference in this scenario is when $T_p = 0.6s$ and that it is only tested for a 50-50 front/rear distribution.

Test Matrix (PTC)

Configuration	Rule Based EETVC	Look-up table EETVC
Velocity	$v = 50$ $[m/s]$	$v = 50$ $[m/s]$
Front/Rear distribution	d_{f-r} = [0-100, 50-50, 100-0]	d_{f-r} = [50-50]
Reference ($T_{EM,1...4}$)	$F_{x,Left} = F_{x,Right}$	$F_{x,Left} = F_{x,Right}$
Reference (δ_{SW})	(PPC, $T_p = 0.6$)	(PPC, $T_p = 0.6$)
Steering Control (Switch 1)	A (PPC, $T_p = [0.6, 1.0]$)	A (PPC, $T_p = [0.6, 1.0]$)
Optimisation strategy (Switch 2)	B (Rule Based)	A (Look-up table)

Table 6.3: Test case 2 - Handling track 1: EETVC Test matrix coupled with the PPC

6.5 Simulation results

The simulation results for the different test cases are presented in this section.

6.5.1 Steady State Power Consumption

The steady-state power consumption simulation results for a radius of 100 m are presented in Table 6.4. The table display results for the three different front/rear torque distributions and three different lateral accelerations for a sweep of constant yaw moment between ± 1000 Nm, defined in section 6.4.1. Note that the table presents both the difference in percentage and the total power saving for the optimal yaw moment compared to applying zero yaw moment. The obtained optimal yaw moment from the sweep, corresponding to each cell in Table 6.4 is displayed in Figure 6.7. The power consumption saving at 2 m/s^2 is deficient but increases with a higher lateral acceleration. It is also evident that the power consumption difference depends on which front/rear torque distribution that is used.

Front/Rear Torque Distribution	$v = 51km/h$ $ay = 2m/s^2$	$v = 72km/h$ $ay = 4m/s^2$	$v = 89km/h$ $ay = 6m/s^2$
0 - 100	0.06 % (3.38 W)	0.12 % (15.52 W)	0.15 % (40.03 W)
50 - 50	0.04 % (2.45 W)	0.08 % (12.02 W)	0.17 % (45.77 W)
100 - 0	0.01 % (0.72 W)	0.05 % (6.15 W)	0.12 % (33.06 W)

Table 6.4: Steady state total power consumption difference in percent and absolute power for a 100 m radius turn

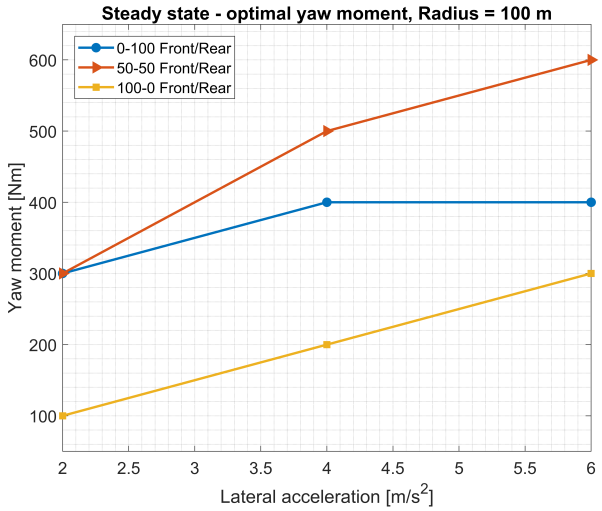

Figure 6.7: Steady-state optimal yaw moment, Radius = 100 m

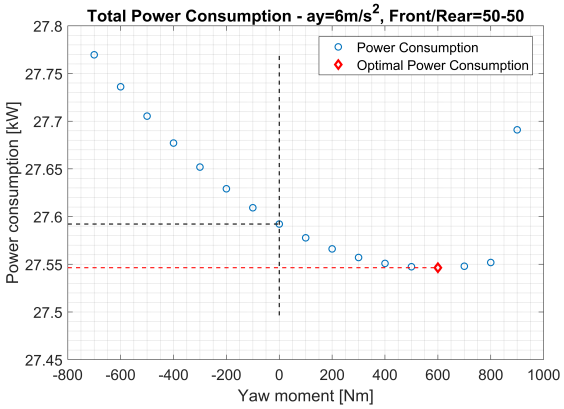

Figure 6.8: Total power consumption for $a_y = 6m/s^2$ and 50-50 front/rear distribution

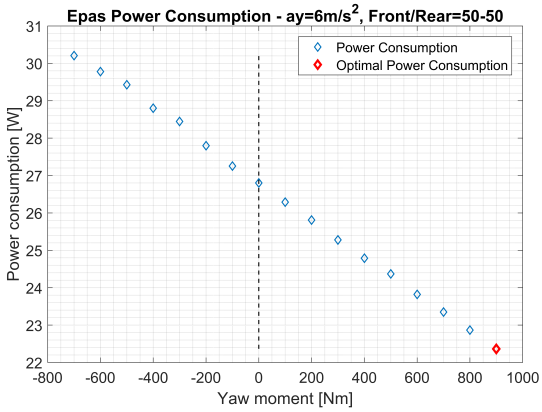

Figure 6.9: EPAS power consumption for $a_y = 6m/s^2$ and 50-50 front/rear distribution

In Figure 6.8 and 6.9, the total power consumption and the EPAS power consumption for the yaw moment sweep are presented for the 50-50 front/rear torque dis-

tribution and a lateral acceleration of 6 m/s^2. The total power consumption is displayed in the unit kW and the EPAS consumption in W. The figure shows that the total power consumption decreases when the yaw moment is increased. There is, however, an optimal point for the power consumption, which means that when the yaw moment is increased *"too much"*, the power consumption will increase again as displayed in Figure 6.8. The same behaviour is not valid for the EPAS consumption. When the added yaw moment increases, the EPAS power consumption will continue to decrease, as displayed in Figure 6.9.

6.5.2 Handling Track 1 Energy Consumption

This section presents the energy consumption for the simulation results from Handling Track 1 for both EETV controllers. The test case configuration settings were presented in section 6.4.2 for test case 2. However, only the results for a 50-50 front/rear torque distribution are presented in this section. The results from the other distributions, i.e. RWD and FWD, can be found in Appendix F instead.

Test Case 2: Results with IPG Driver
The results from test case 2 with the IPG Driver scenario, i.e. what was described in Table 6.2, are presented in Table 6.5 and 6.6 for the rule-based and Look-up table EETV concepts respectively. The tables describe the comparison in energy consumption for one lap at Handling Track 1 when no EETVC is activated and when the Rule Based or the Look-up table EETVC is activated. Note that in this case, the IPG Driver allocates the steering wheel angle request and that a negative value in the "Difference" column indicates a decrease in, for example, energy consumption. The rule-based EETVC reduces the energy consumption by 0.31 %, and the EPAS energy losses are reduced by 9.98 %. The look-up table optimisation strategy yields similar results, where the total energy consumption is reduced by 0.32 % and the EPAS losses are reduced by 9.34 %. In Table 6.5 and 6.6, the lateral deviation in terms of RMSE and maximum deviation is also presented. However, both strategies yield similar results where the EETV neither worsens nor improves the path following.

In Figure 6.10 and 6.11, the difference for all energy losses that are present in the vehicle is displayed for the rule-based and look-up table optimisation strategies. Note that both the absolute and percentage differences in energy consumption are showcased. It is evident that the EM and inverter losses reduce the most when the EETV is activated. Consequently, the reduction in EM and inverter losses contribute the most to the overall reduction in the vehicle's energy consumption. For the rule-based method, the EM and inverter losses reduce by 0.30 kJ; for the look-up table method, the losses are reduced by 0.27 kJ. Furthermore, the EPAS losses have the most considerable reduction in percentage for both strategies. A final observation when comparing the results is that the longitudinal slip losses, S_x, increase with the rule-based strategy while it does not change with the look-up table method.

EETV: Rule Based + IPG Driver - Energy Consumption [kJ]			
Comparison	**No TV**	**With TV**	**Difference**
Total Consumption	438.98 [kJ]	437.60 [kJ]	-0.31 [%]
EPAS Consumption	0.69 [kJ]	0.62 [kJ]	-9.98 [%]
Lateral Deviation (RMSE)	0.170 [m]	0.166 [m]	-0.004 [m]
Lateral Deviation (Max)	0.517 [m]	0.498 [m]	-0.019 [m]

Table 6.5: Handling Track 1 - Rule Based Torque Distribution, Energy Consumption with IPG Driver for a 50-50 front/rear distribution

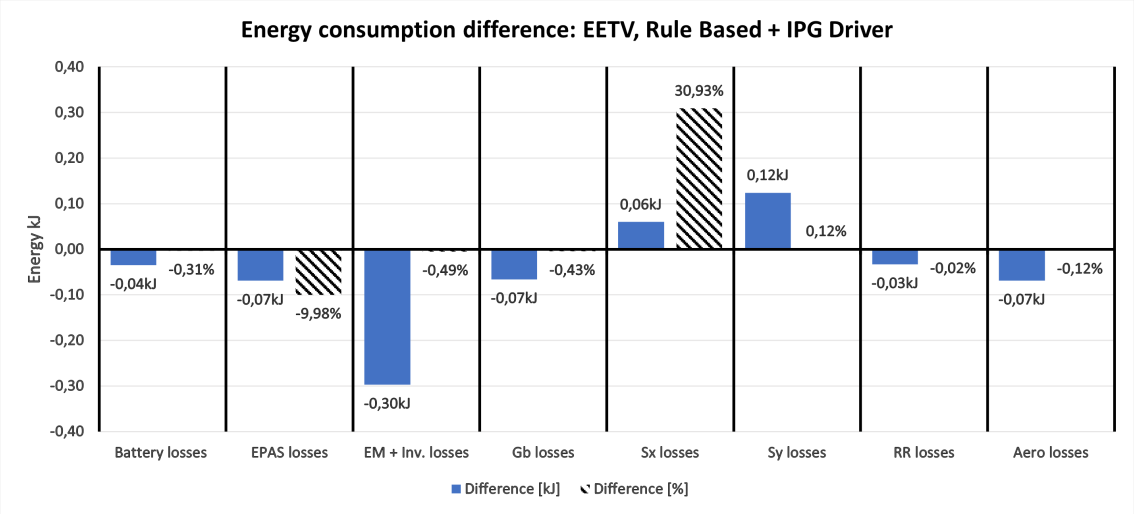

Figure 6.10: Difference in energy losses without EETV + IPG Driver compared to with Rule Based EETV + IPG Driver for a 50-50 front/rear distribution

EETV: Look-up Table + IPG Driver - Energy Consumption [kJ]			
Comparison	**No TV**	**With TV**	**Difference**
Total Consumption	438.98 [kJ]	437.56 [kJ]	-0.32 [%]
EPAS Consumption	0.69 [kJ]	0.63 [kJ]	-9.34 [%]
Lateral Deviation (RMSE)	0.170 [m]	0.172 [m]	+0.002 [m]
Lateral Deviation (Max)	0.517 [m]	0.520 [m]	+0.003 [m]

Table 6.6: Handling Track 1 - Look-up Table Torque Distribution, Energy Consumption with IPG Driver for a 50-50 front/rear distribution

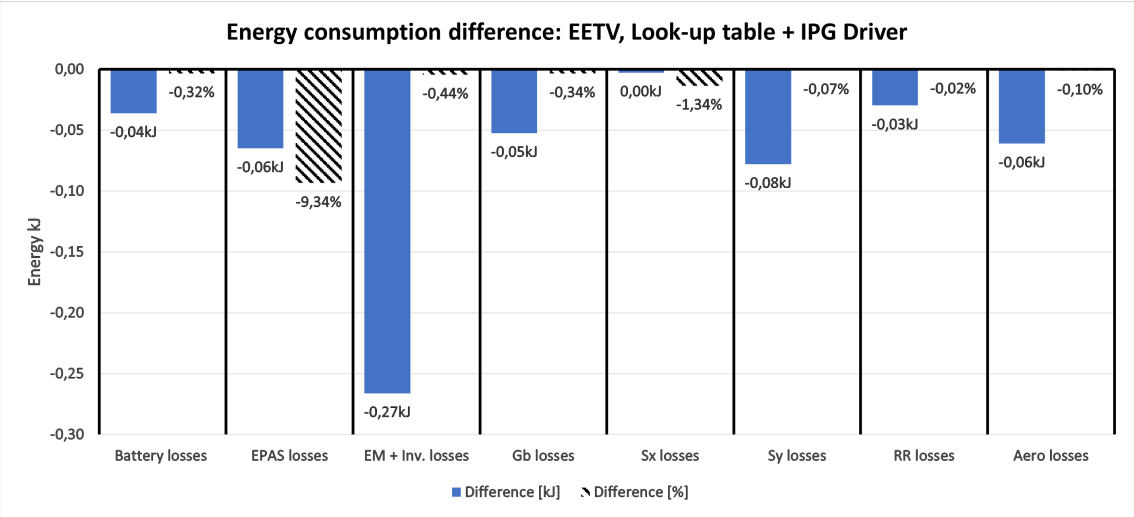

Figure 6.11: Difference in energy losses without EETV + IPG Driver compared to with Look-up table EETV + IPG Driver for a 50-50 front/rear distribution

Test Case 2: Results with PPC

The simulation results from test case 2 with the PPC scenario, i.e. when the EETVC is used in combination with the PPC is presented in Tables 6.7 - 6.10. In Table 6.7 and 6.8 the look-ahead time, T_p, is 0.6 s, and in Table 6.10 and 6.10 $T_p = 1.0$. The configuration settings for this test case were described in Table 6.3. In this scenario, the reference measurement is with no active EETV, i.e. equal torque on all four wheels, and the PPC always has a look-ahead time of 0.6 s, i.e. $T_p = 0.6$. When the rule-based EETVC is combined with the PPC, which has a $T_p = 0.6$, it yields a reduction of 0.34 % for the vehicle's total energy consumption for one lap at Handling Track 1. With the same settings but instead using the EETVC with the look-up table strategy, the results are similar, with an energy consumption reduction of 0.33 %. Consequently, the total energy consumption reduction when using the EETVC in combination with the PPC is similar to when combined with the IPG Driver. The total energy consumption is, however, different. With the IPG Driver scenario, the lowest total energy consumption is 437.56 kJ when the look-up table EETVC is used, while for the PPC scenario, the lowest energy consumption is 441.35 kJ when the rule-based EETVC is used instead. Another difference between the IPG Driver and the PPC scenario is that the lateral deviation is higher with the IPG Driver than with the PPC. Similar to the IPG scenario, the lateral deviation is not affected as much when EETV is activated in combination with the PPC.

In Figure 6.12 and 6.13, the different energy losses for the vehicle are presented when $T_p = 0.6$ for the rule-based and look-up table strategy, respectively. Similar to the previous results, the EM and inverter losses reduce the most, and the EPAS losses have the highest percentage difference. Similar to the previous scenario, the longitudinal slip losses also increase with the rule-based strategy while they stay consistent while using the look-up table EETVC.

EETV: Rule Based + PPC - Energy Consumption [kJ]			
Comparison	**No TV ($T_p = 0.6$)**	**With TV ($T_p = 0.6$)**	**Difference**
Total Consumption	442.87 [kJ]	441.35 [kJ]	-0.34 [%]
EPAS Consumption	0.76 [kJ]	0.68 [kJ]	-10.62 [%]
Lateral Deviation (RMSE)	0.061 [m]	0.059 [m]	-0.002 [m]
Lateral Deviation (Max)	0.154 [m]	0.151 [m]	-0.003 [m]

Table 6.7: Handling Track 1 - Rule Based Torque Distribution, Energy Consumption with PPC ($T_p = 0.6$) for a 50-50 front/rear distribution

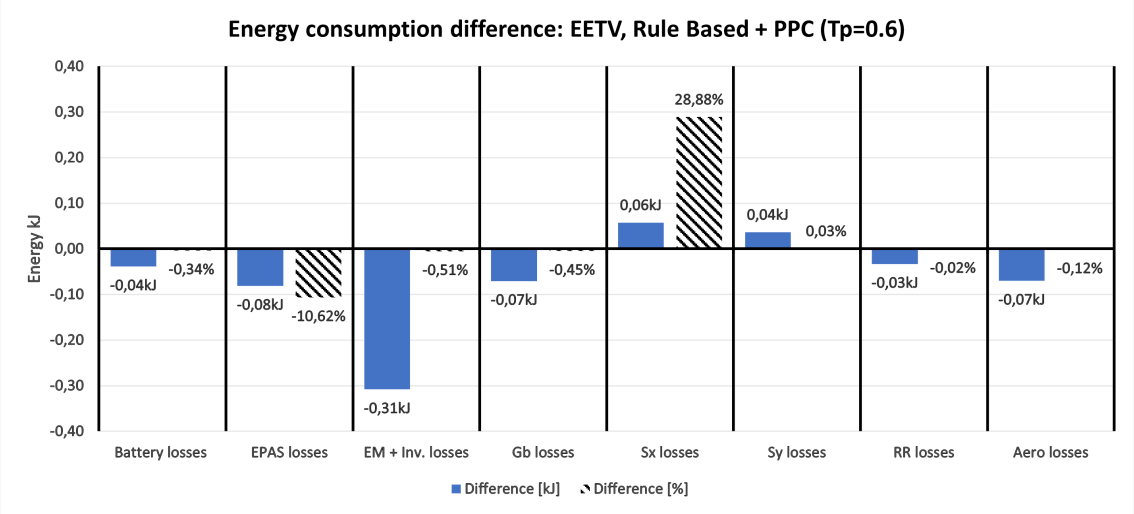

Figure 6.12: Difference in energy losses without EETV + PPC ($T_p = 0.6$) compared to with Rule Based EETV + PPC ($T_p = 0.6$) for a 50-50 front/rear distribution

EETV: Look-up table + PPC - Energy Consumption [kJ]			
Comparison	**No TV ($T_p = 0.6$)**	**With TV ($T_p = 0.6$)**	**Difference**
Total Consumption	442.87 [kJ]	441.42 [kJ]	-0.33 [%]
EPAS Consumption	0.76 [kJ]	0.69 [kJ]	-9.71 [%]
Lateral Deviation (RMSE)	0.061 [m]	0.061 [m]	0.000 [m]
Lateral Deviation (Max)	0.154 [m]	0.151 [m]	-0.003 [m]

Table 6.8: Handling Track 1 - Look-up table Torque Distribution, Energy Consumption with PPC ($T_p = 0.6$) for a 50-50 front/rear distribution

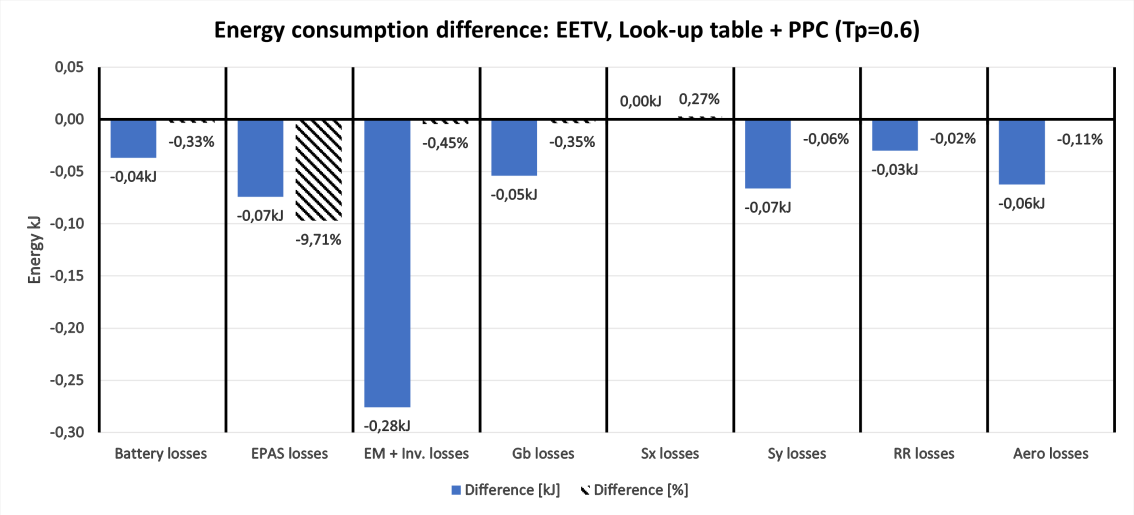

Figure 6.13: Difference in energy losses without EETV + PPC ($T_p = 0.6$) compared to with Look-up table EETV + PPC ($T_p = 0.6$) for a 50-50 front/rear distribution

When the rule-based EETVC is combined with the PPC with $T_p = 1.0$ s, the total energy consumption is reduced by 1.15 %. When the PPC with $T_p = 1.0$ s is combined with the look-up table EETVC instead, the energy consumption is reduced by 1.13 %. Consequently, the energy consumption is reduced more with a different PPC tuning. The lateral deviation is, however, increasing with a larger T_p, which can be seen in Table 6.9 and 6.10. With a larger look-ahead time, the RMSE for the lateral deviation has increased by 0.107 m when using the rule-based strategy.

In Figure 6.14 and 6.15 the different energy losses for the rule-based and the look-up table strategy are presented when $T_p = 1.0$. In contrast to the previous scenarios, the most significant energy loss reduction here is for the lateral slip losses, s_y. However, similar to before, the longitudinal slip losses increase by almost 30 % when using the rule-based method, while it stays consistent using the look-up table method.

EETV: Rule Based + PPC - Energy Consumption [kJ]			
Comparison	**No TV** ($T_p = 0.6$)	**With TV** ($T_p = 1.0$)	**Difference**
Total Consumption	442.87 [kJ]	437.80 [kJ]	-1.15 [%]
EPAS Consumption	0.76 [kJ]	0.66 [kJ]	-13.93 [%]
Lateral Deviation (RMSE)	0.061 [m]	0.168 [m]	+0.107 [m]
Lateral Deviation (Max)	0.154 [m]	0.612 [m]	+0.458 [m]

Table 6.9: Handling Track 1 - Rule Based Torque Distribution, Energy Consumption with PPC ($T_p = 1.0$) for a 50-50 front/rear distribution

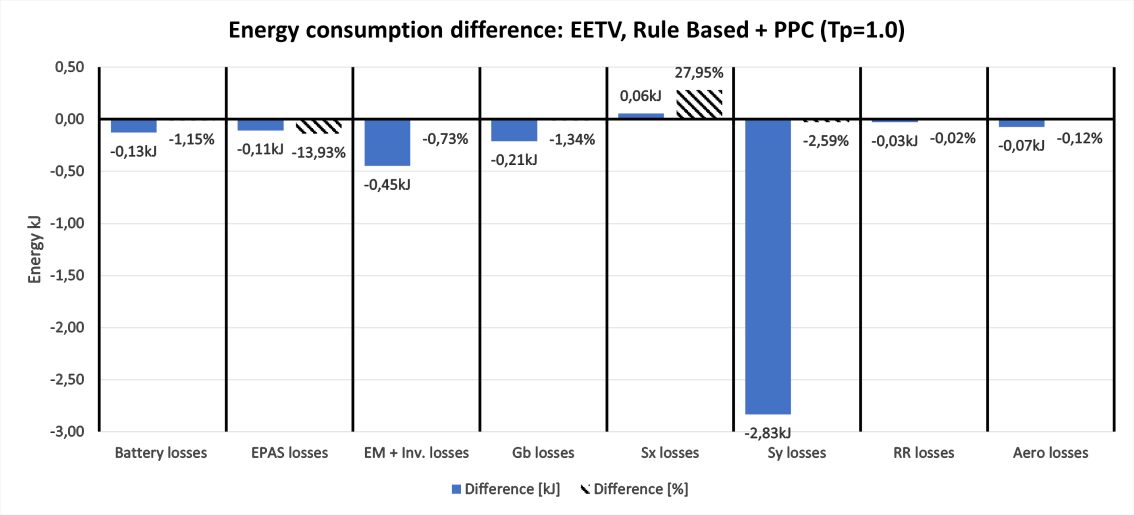

Figure 6.14: Difference in energy losses without EETV + PPC ($T_p = 0.6$) compared to with Rule Based EETV + PPC ($T_p = 1.0$) for a 50-50 front/rear distribution

EETV: Look-up table + PPC - Energy Consumption [kJ]			
Comparison	**No TV** ($T_p = 0.6$)	**With TV** ($T_p = 1.0$)	**Difference**
Total Consumption	442.87 [kJ]	437.85 [kJ]	-1.13 [%]
EPAS Consumption	0.76 [kJ]	0.66 [kJ]	-13.13 [%]
Lateral Deviation (RMSE)	0.061 [m]	0.170 [m]	+0.109 [m]
Lateral Deviation (Max)	0.154 [m]	0.620 [m]	+0.466 [m]

Table 6.10: Handling Track 1 - Look-up table Torque Distribution, Energy Consumption with PPC ($T_p = 1.0$) for a 50-50 front/rear distribution

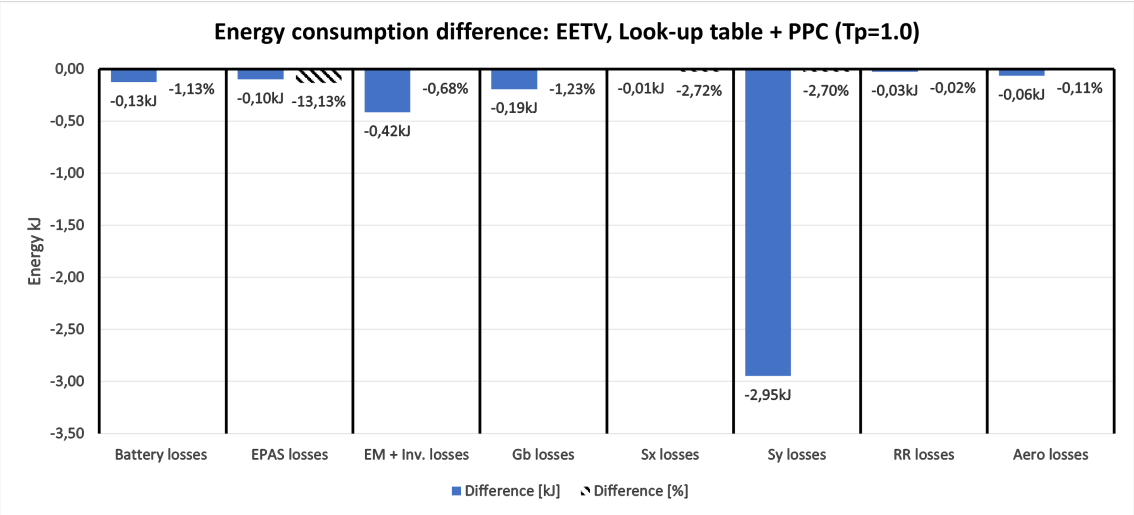

Figure 6.15: Difference in energy losses without EETV + PPC ($T_p = 0.6$) compared to with Look-up table EETV + PPC ($T_p = 1.0$) for a 50-50 front/rear distribution

6.6 Chapter Conclusion

In this chapter, two torque vectoring concepts based on an offline optimisation strategy have been presented. The first is the rule-based EETV controller that distributes all torque requests to either the left or right motors, depending on the steering angle. The second TV controller allocates the motor torques based on a look-up table with predefined yaw moments obtained with measurement data for optimal energy consumption. The two EETVC concepts aim to allocate the motor torque to minimise the power losses and thereby minimise the overall power consumption for the vehicle.

The potential energy savings by allocating the motor torques were investigated and presented by the first test case, which applies a range of constant yaw moments for a constant radius and velocity. The results showcase the instantaneous steady-state power consumption, and the conclusion is that the potential energy savings are insignificant. The most considerable reduction for the power consumption is 0.17 % or 45.8 W at a yaw moment of 600 Nm. However, the total power consumption at this operating point is 27.5 kW. Another conclusion from the results is that the power consumption reduces more when the lateral acceleration increases and that the optimal yaw moment increases with a 50-50 front/rear torque distribution. However, there is no significant difference in the power consumption between having different front/rear torque distributions. Finally, this investigation showcase that the power consumption reduces when allocating more torque to the outer motors while turning than to the inner motors, but it increases again when applying negative torque on the inner motors since the regenerative braking losses are assumed to be equal in this research. Consequently, the optimal torque distribution to minimise the power losses is a yaw moment that yields an allocation that distributes more torque on the outer motors and less on the inner motors while turning. The optimal distribution found in this study is to apply all of the torque requests on the outer motors and zero torque on the inner motors, i.e. when turning left, apply around 95 % of the torque request to the right motors. Note that since the steps in the yaw moment are relatively high, the utilised method indicates the optimal yaw moment but does not yield an absolute optimal value, i.e. the optimal yaw moment can be between, for example, 600 and 700 Nm. However, as aforementioned, the aim is to indicate the potential power consumption savings rather than the exact optimal yaw moment. Therefore, the resulting decrease in power consumption could have improved if the smaller steps in yaw moments had been applied.

The EETV controller's performance, i.e. how much the energy consumption changed with the controllers activated compared to an equal torque distribution between the left and right motors, was evaluated by simulating one lap at Handling Track 1, both with manual steering with the IPG Driver or in combination with the PPC. The results showcase that the vehicle's total energy consumption was reduced by around 0.33 % while using the EETVC controller in combination with the IPG Driver, i.e. manual steering. When the EETVC controller is combined with the PPC, the total energy consumption is reduced by approximately 1.14 % instead.

Consistent for all scenarios when evaluating the EETVC is that the EPAS energy losses reduce when the controller is activated. On average, the EPAS energy losses are reduced by 11.12 %, which is the most significant reduction in percentage. However, the EPAS consumption is relatively small compared to the other energy losses in the vehicle. Otherwise, the EM and inverter losses reduce the most in absolute energy, except for the case when the PPC has a look-ahead time of 1.0 s. In that scenario, it is the lateral slip losses that reduce the most instead. It is also important that a significant energy loss reduction in percentage does not mean that it contributes to the total energy consumption reduction for the vehicle. One such example is the longitudinal slip losses. In percentage, it increases by approximately 30 % in some scenarios. However, the longitudinal slip losses are only approximately 0.05 % of the vehicle's total energy losses, while the EM and inverter losses are approximately 15 % of the total energy losses. Therefore, even though the longitudinal slip losses may have a significant percentage difference compared to the EM and inverter losses, it contributes less to the total reduction of the energy consumption. The most significant contribution to the reduced energy consumption, in order of magnitude, is the EM and inverter losses, the gearbox losses and the lateral slip losses. Another observation when comparing the results is that the difference between using the rule-based or the look-up table optimisation strategies is insignificant. The difference in the energy reduction is 0.02 percentage units between the two methods in both the IPG Driver and PPC scenarios. With the rule-based strategy, the longitudinal slip losses increase, however, compared to the look-up table strategy, which has no significant difference.

When using the EETVC in combination with the PPC, the vehicle's energy consumption reduces the most when the look-ahead time is 1.0 s. One significant factor contributing to why this configuration had such good energy consumption is the reduction of the lateral slip losses. When $T_P = 1.0$, the lateral slip losses are reduced compared to when $T_p = 0.6$, i.e. the vehicle trajectory results in more minor lateral slip losses, which is why that configuration has a smaller energy consumption. However, the higher look-ahead time in this scenario, as the PTC evaluation in chapter 4 also showcased, means that the lateral deviation is increasing. Consequently, there is a trade-off between having good precision for the path following and optimising the vehicle's energy consumption when combining the EETCV and PPC. The vehicle's trajectory will also affect the energy consumption, which means that if the reference path also is optimised to reduce the energy consumption, both the path following precision and the energy consumption requirements can be fulfilled. Comparing the total energy consumption for all scenarios, the rule-based ETTVC, in combination with the IPG Driver, have the smallest overall energy consumption of 437.56 kJ. In comparison, the best EETVC and PPC combination is the rule-based method with an energy consumption of 437.80 kJ. Therefore, how much the energy consumption reduces also depends on which reference measurement it is compared with. For example, comparing the EETVC combined with the PPC with the EETVC combined with the IPG Driver would yield different results.

Finally, from the study, it is evident that the potential reduction in the vehicle's power consumption is insignificant in a steady-state driving condition. However, during a drive cycle, in this case, one lap of the Handling Track 1, it is possible to reduce the vehicle's total energy consumption by 1.14 %, and the EPAS energy losses can be reduced by 11.12 %. The difference between the two evaluated optimisation strategies is, however, insignificant. Furthermore, the study showcased that for the test vehicle and powertrain used in this study, the optimal yaw moment reference for the energy consumption is to allocate all torque requests on the outer motors while turning. There is also a trade-off between the precision of the path following and the energy consumption. The potential energy consumption reduction can increase when using the EETVC in combination with the PPC. However, combining the controllers requires tuning, where both the reference path, the PPC, and the EETVC can be tuned to optimise the path following for precision comfort and energy.

7
Discussion

The concepts of geometric path tracking, steer by torque vectoring, and energy efficient torque vectoring for lateral and yaw motion control have now been presented. The concepts aim to serve as a centralised controller for precise and comfortable path following, a backup system in case of steering actuator faults and distribute the motor torques for an optimal energy consumption. In this chapter, the topics presented in this study are discussed.

7.1 Geometric Path Tracking

This section discusses topics related to the geometric path tracking presented in chapter 4.

7.1.1 Kinematic bicycle model

There are several reasons why the simplifications regarding small steering angles were made. The primary and intuitive reason is associated with the fact that the small steering angle approximation provides a linear system, as all the trigonometric functions are replaced with their respective simplifications. A linear approximation disentangles the process of designing a controller since the need to use complex methods, such as Lyapunov's method, to linearize the system is withdrawn. Linear systems have analytical solutions, are intuitively interpreted, are quick to compute and can be good approximations of non-linear systems. The second significant reason for the validity of a linear system is derived from the fact that a path tracking algorithm is to be implemented in the simulation software IPG CarMaker before being tested in the actual test vehicle. Since IPG CarMaker is equipped with a fully developed and comprehensive non-linear vehicle model, the simple kinematic bicycle model is sufficient to ensure the proper functionality of the controllers, which is the sole purpose of the early development stages.

7.1.2 Modified Path Tracking Controllers

Even though only the PPC and the SC were thoroughly evaluated in this project, several modified concepts were developed during the study. All modified PTC's were developed with either the steering angle formulation of the PPC or the SC as a basis. One concept that was developed but not included in the evaluation in chapter 4 was the PPC as a PI-controller as opposed to all the previous concepts,

which were developed as simple P-controllers. In this concept, the lateral deviation from the reference point on the vehicle to the reference path is used as the measured variable and controls the steering angle until the integral sum of error becomes constant. The PI-controller made sure that the steady-state error was removed, which was evident as the lateral deviation decreased drastically when implemented and evaluated at Handling Track 1. However, the stability deteriorated as the vehicle started oscillating with low frequencies at cornering manoeuvres. The reason was that the PPC with the understeer gradient performed relatively well at cornering manoeuvres but experienced small issues with corner cutting, which triggered the integral term, leading to a relatively high or low instantaneous steering angle request which resulted in oscillations. Therefore, this concept was not further evaluated and, consequently, not included in the results.

Another interesting concept that was developed was the front-axle PPC. This method used the front axle as the reference point on the vehicle instead of the rear axle. Note that an important characteristic of the PPC is its use of a look-ahead point, which is also the reason for its corner cutting tendencies. Using the front axle as the reference point increased the magnitude of corner cutting. When the distance to the look-ahead point was shortened, that issue was partly resolved, but oscillations were introduced as the look-ahead distance was decreased. It was therefore decided that the trade-off between stability and precision was not admissible, as the modification of the vehicle's reference point only worsened the controller's overall performance.

Several other modifications were made, but eventually, the performance of the Pure Pursuit and Stanley controllers using a simple P-controller was superior.

7.1.3 Tuning parameters

Tuning parameters have been widely mentioned and used throughout this project, referring to the understeer gradient K_u but, more importantly, the look-ahead time T_p. The look-ahead time is not constrained to a domain and ignoring the argument of reasonable values as defined in the referred literature, the look-ahead time could be set to any arbitrary value $T_p \in (0, \text{inf})$. However, the look-ahead time was set between 0.6 s and 1.2 s throughout this project because of the statement made in section 4.6, which explains that the tuning of the look-ahead time T_p is dependent on the trade-off between precision and comfort. In section 4.4.2, it appears as the precision of the controllers is improved as the look-ahead time is decreased. However, the reason for using a look-ahead time of 0.6 s as a minimum is based on the observation that the comfort of the controller deteriorates as the look-ahead time decreases. Intuitively, using a lower look-ahead time would improve the precision. However, looking at Figure 7.1, which is a rerun of the 90° turn test case at 128 km/h where the look-ahead time $T_p = 0.4$ s, the precision as well as the comfort deteriorates when the look-ahead time is decreased below 0.6 s. For this reason, the minimum set value of T_p is 0.6 s.

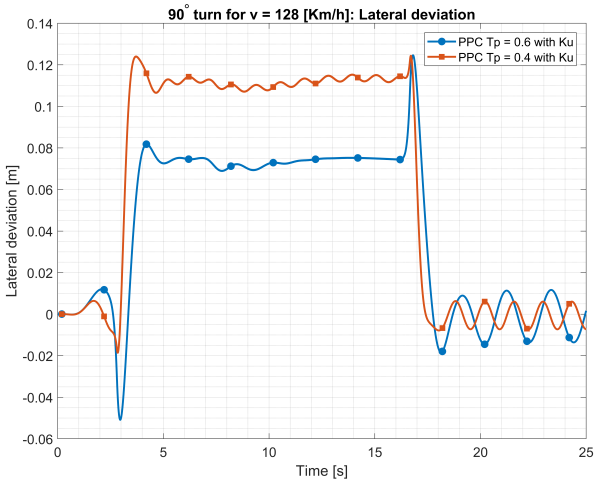

Figure 7.1: Lateral deviation comparison for the Pure Pursuit Controller between having a look-ahead time of 0.6 and 0.4 s

7.1.4 Precision performance - Geometric Path Tracking

Throughout this thesis, it has been concluded that the path tracking precision of the PPC is superior to the SC, even though the precision is close at lower velocities. In most test cases, the initial threshold for maximum lateral deviation of 37.5 cm, which was listed on the requirements of an automated lane keeping system stated in the UN regulations, was not exceeded. Hence, the precision is a solid argument for the quality of the developed PPC in this project. The test cases used were more dynamic, further strengthening the argument that the performance of the PPC was up to the mark. In such a conclusion, however, it is very appropriate to discuss the sources of error as well. The path tracking performance of the PPC depends on both modelling and external factors. Even though a look-ahead time of 0.6 s yielded the best result, concerning the precision, it was not tuned for optimal performance since this would be very time-consuming. The same goes for the other tuning parameters. The lateral deviation for the PPC occurs due to corner cutting. With a larger look-ahead time, the corner cutting increases since the controller ”notice” the turn earlier and starts turning. By reducing the look-ahead, the corner cutting behaviour can be mitigated. For the external factors, when testing in the test vehicle, the weight, road conditions, wind disturbances and accuracy of the GPS are all factors that could not be controlled and therefore, it is assumed that for a single test case, the path tracking performance could be improved.

7.1.5 Stanley controller at high velocities

The comfort of the SC, as specified in section 4.6, was worsened at high velocities. Interestingly, at low velocities, it is slightly superior to the PPC due to two factors. The first one is related to the steering angle formulation being a sum of two correcting terms, namely the heading error ψ_e and the lateral error d_f, as opposed to the single correcting term of the PPC. The second factor is the dominant one, referring to the

fact that the SC does not have a look-ahead point but rather calculates a steering angle request dependent only on the point on the path closest to the reference point on the vehicle. Without a look-ahead point, the steering angle becomes sensitive to sudden heading or cross-track errors, i.e. when the road ahead is not smooth. At high velocities, this is visible even for smooth paths. Figure 7.2 below visualises the trajectory of the SC at 90 km/h in the 90° turn, and Figure 7.3 is a zoomed illustration which clearly shows the phenomenon of the instabilities of the SC at high velocities.

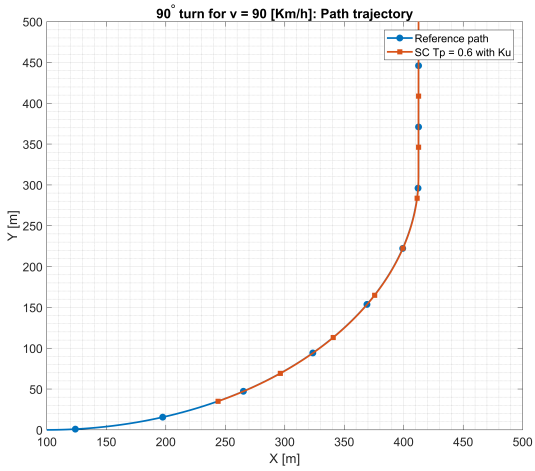

Figure 7.2: 90° turn - SC: Reference path and vehicle trajectory at high velocities

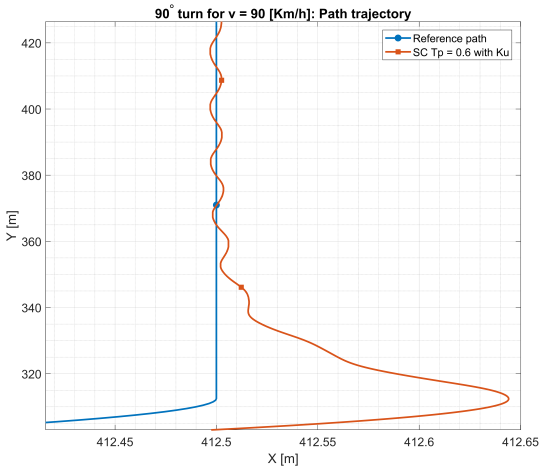

Figure 7.3: 90° turn - Close-up of oscillations and overshoot of SC at high velocities

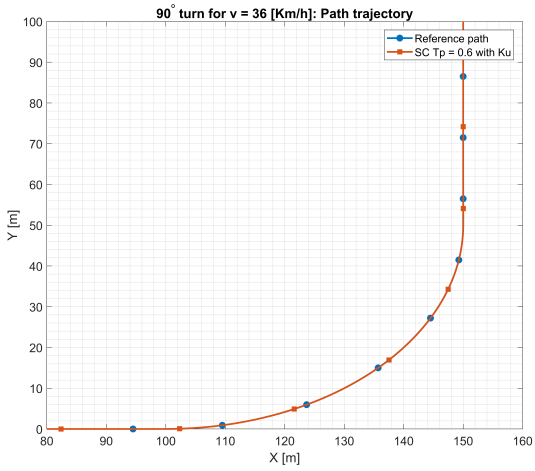

Figure 7.4: 90° turn - SC: Reference path and vehicle trajectory at low velocities

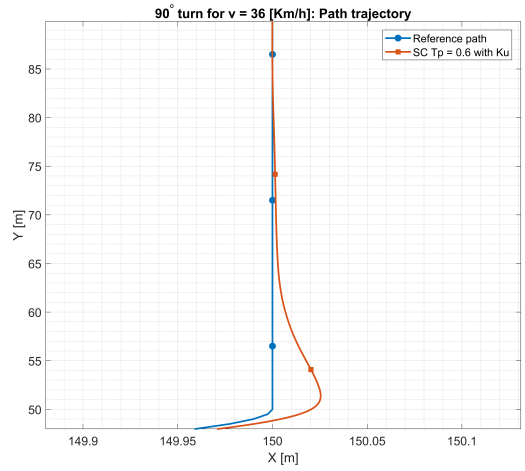

Figure 7.5: 90° turn - Close-up of oscillations and overshoot of SC at low velocities

Comparing this with the vehicle's trajectory at low velocities using the SC, oscillations are absent, and the overshoot amplitude is significantly decreased, which is visualised in Figure 7.4 and 7.5. Note that the range of the X-axis of Figure 7.3 and 7.5 is equal for a fair comparison.

7.1.6 Path definition

A vital area of this project is the path definition, i.e. the reasoning behind how the reference path was defined and generated. In section 4.1.2, it is explained that the reference path is a set of vectors constituting the x -and y positions of the different coordinates that make up the path. The distance between each point on the defined paths used in this project is 0.5 m. Figure 7.6 below shows how the controller behaviour changes when the distance between each point on the reference path is increased to 1 m and decreased to 0.05 m respectively. Table 7.1 presents each case's RMSE and maximum error.

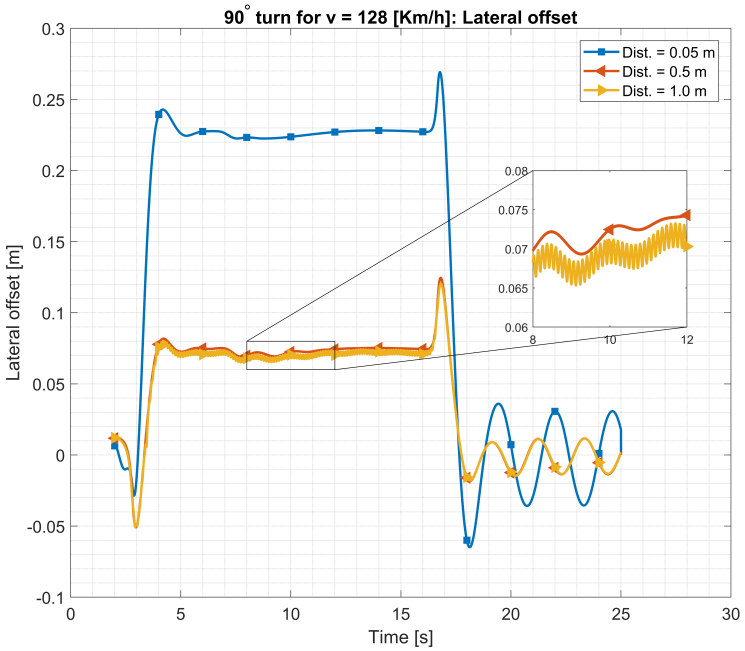

Figure 7.6: Influence of distance between points on reference path

The precision is significantly worsened as the distance between the points is decreased. However, when the distance between the points is increased to 1 m, the RMSE is slightly decreased, but the downside is that the vehicle experiences weak, high-frequency oscillations. In conclusion, a distance of 0.5 m between each coordinate of the reference path is a perfect compromise between precision and oscillations.

RMSE [m] (128 km/h)		Max error [m] (128 km/h)	
$\mathbf{d_{points}}$	**PPC**	$\mathbf{d_{points}}$	**PPC**
0.05	0.177	**0.05**	0.269
0.5	0.059	**0.5**	0.125
1.0	0.057	**1.0**	0.121

Table 7.1: RMSE and maximum error of test case with different distance between points on reference path

7.2 Steer by Torque Vectoring

This section discusses topics related to the development of the steer by torque vectoring controller that was developed in chapter 5.

7.2.1 Influence of suspension geometry on curvature capability

In chapter 5, a steer by torque vectoring controller was created to explore the possibility of a redundant backup steering system in the case of steering failures. It was explained that a differential torque could be allocated to the vehicle's left and right EM's, which would steer the vehicle laterally. The steering capability is affected by the suspension geometry, i.e. the effect of having a non-zero scrub radius, pneumatic, and mechanical trail. The direct yaw moment on the chassis that is generated from the differential torque also aids the amplitude of the lateral movement. If the steering wheel is locked, i.e. when the steering angle is locked at 0 degrees, then the steering effect of the suspension geometry becomes zero, and the lateral movement of the vehicle is the result of a pure direct yaw moment on the chassis. Figure 7.7 shows the curvature capability when the steering wheel is locked.

The curvature capability is significantly lower with the wheels locked compared to the curvature capability with the additional effect of the scrub radius, pneumatic trail and mechanical trail shown in Figure 5.3. An interesting aspect of this phenomenon is associated with the **Group 1** configurations of torque allocation displayed in Figure 5.2. Note that the rear wheels do not induce additional steering capability due to the suspension geometry because they do not rotate around their vertical axis, i.e. no steering angle. The configuration used in this project applied a differential torque on the front EM's and used the rear EM's to maintain the velocity, i.e. propel the vehicle with the same amount of torque on both rear EM's. Using this discussion as a basis for determining the best configuration for steering capability, it is clear that **E1** in Figure 5.2 should result in the highest curvature capability. However, with such an unstable and fragile system, as mentioned in chapter 5.7, an increase in curvature capability as in configuration **E1** would result in an even more unstable system. The capability of using configuration **A1** is sufficient for the use

cases defined as a result of steering failure, i.e. a lane change and a 90° turn.

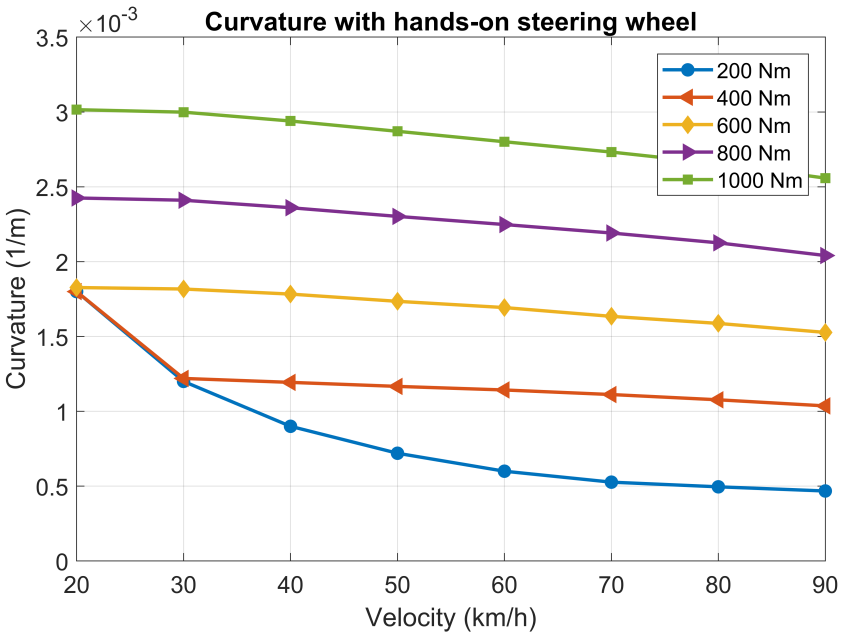

Figure 7.7: Steer by Torque vectoring - Capability (locked steering wheel) as a function of differential left-right torque

7.3 Energy Efficient Torque Vectoring

This section discusses topics related to the Energy Efficient Torque Vectoring controller presented in chapter 6.

7.3.1 Offline vs Online optimisation

In this project, an offline optimisation method was used to determine the optimal yaw moment for a given operating point. Offline optimisation refers to the fact that complete information is assumed, i.e. the generated optimal output signal is dependent on predefined results. In this project, this corresponds to the yaw moment sweep that was conducted in a nested loop with direct yaw moment applied, road curvature and vehicle velocity as loop variables. This method will not mathematically provide the optimal value as the generated dataset (look-up table) is discrete and uses interpolation and extrapolation to generate the optimal yaw moment. Luckily, the use of online optimisation methods for energy-efficient TV is well documented, and a fair comparison can therefore be conducted to evaluate the level of precision of the offline optimisation method conducted in this project.

7.3.2 Potential of decreasing power consumption

One vital point to understand about the energy efficient torque vectoring concept is the fact that the energy efficiency in the context of this project is purely related to

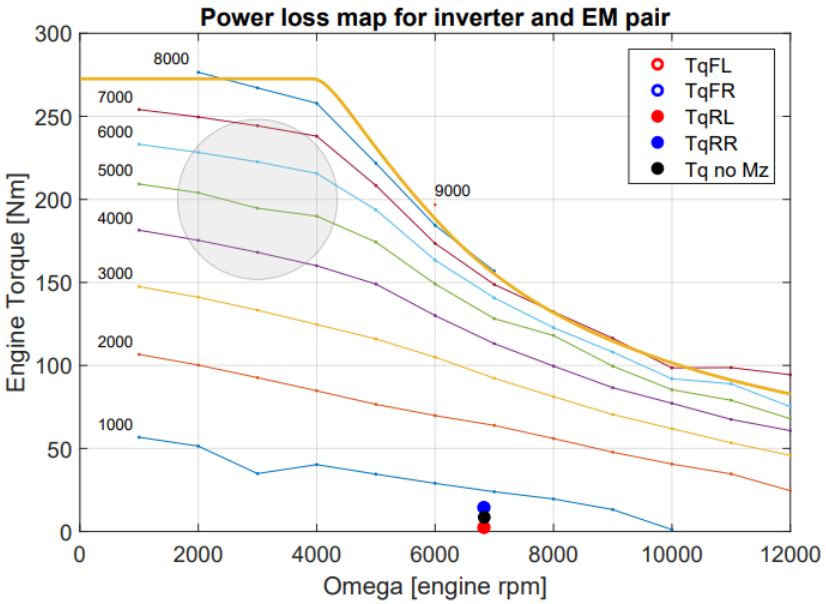

Figure 7.8: Motor/inverter power loss map - Operating points

the **power losses** of the vehicle. The energy consumption is compared for the same drive cycle with identical velocities with and without the EETVC. By definition, that means that the power required to propel the vehicle depends on the power losses, such as motor/inverter, tire and drag losses. Taking an arbitrary test as an example, imagine that the EM's require a certain power request to maintain some operating point. The amount of power loss from the tires, drag and transmission, for example, is limited by the amount of power that is actually being delivered by the power source, i.e. the battery. Consequently, if the power request is huge, the losses, and therefore the potential to decrease the losses with an EETVC, are increased. Figure 7.8 represents a test case of a constant radius with $a_y = 6m/s^2$ and a front-rear distribution of $d_f = 0.5$. It is clear that the operating points with and without TV are located in a relatively low power loss region of the power loss map. This is consistent throughout the test cases in this project due to the steady state driving, i.e. constant velocity. However, if the driving manoeuvre were more dynamic up until the point where the torque requests would be in the marked circle in Figure 7.8, then the potential to reduce the power consumption would be more significant. If, for example, the tire, drag and transmission losses were higher, the potential to decrease the total energy consumption would be higher as well due to the high energy loss operating point of the motors/inverters.

7.4 Future work

The technical part of this project has had an excessively conceptual basis. With conceptual work comes questions and curiosity regarding methods and potential improvements.

With the conditions set in this project and the basis created for the path tracking controllers, the dominant controller configuration for both the PPC and SC was a simple P-controller. Even though a PI-controller was developed and proved to perform worse than the simple P-controller, a PID or even a PD-controller could be implemented and improve the path tracking performance and comfort. Other control methods could also be compared, such as linear quadratic regulators or model predictive control, which was mentioned in the background.

Another area that could be developed is the tuning of all the controllers. Tuning the look-ahead time, the gain at the output of the several look-up tables and several other in-code parameters could significantly affect the outcome, as seen by simply changing the look-ahead time from 1.0 s to 0.6 s.

Unlike the test vehicle, most cars are not equipped with an EM on each wheel. Therefore the method of steering the lateral motion of the vehicle using a differential torque is outside the capability of most cars. There is, however, a method based on the same concept where the yaw moment needed is obtained by friction braking instead. In this method, the yaw moment is a function of pressure applied to the brake discs, and since the majority of vehicles are equipped with brake discs, this is a cheaper and easier method. How the capability of the configuration used in this study compares to other configurations, such as friction braking, needs further analysis.

Since no optimisation problem was defined for the energy efficient torque vectoring controller but rather an offline optimisation using a look-up table, every single configuration change was very time-consuming. A simple configuration change, such as a change in the torque distribution, would be very inefficient regarding time. Developing and solving an optimisation problem, which would, by definition, optimally allocate the torque, would not only have saved time but could also obtain better results for each test case without needing a trial and error method.

Finally, much work in this project was spent on testing and implementing the controllers in the test vehicle. Unfortunately, as this is a very time-consuming process, this did not yield satisfactory results for the steer by torque vectoring and the energy efficient torque vectoring controllers, which is why these results are absent in the report. Consequently, more work is needed to further evaluate the controllers in the test vehicle.

8

Conclusion

In this project, three different concepts for centralised yaw and lateral motion control have been developed and evaluated. The first concept is geometric path tracking for lateral motion control in an AD scenario. Two geometric path tracking controllers, i.e. the Pure Pursuit and Stanley controller, were developed and evaluated concerning their precision, comfort and robustness when following a predefined reference path. The path tracking controller's output is a curvature reference that is converted to a steering wheel angle request in the control allocation for the primary path following. The second concept investigates the steering capability of a backup system for lateral motion control to ensure fail-operational ability in case of failures in the steering system. In this concept, the curvature reference from the geometric path tracking is used to control the vehicle's lateral motion using torque vectoring instead of the steering wheel, i.e. a steer by torque vectoring controller. The potential benefit of this concept is to have a highly redundant steering system for AD or steer-by-wire systems in future electric vehicles, which means that the vehicle can follow the reference path even if the primary system fails. The third concept is an energy efficient torque vectoring controller, which aims to reduce the vehicle's energy consumption by distributing the EM torques and thereby controlling the vehicle's yaw moment, i.e. an optimal yaw moment controller. An offline optimisation strategy was used, and the lateral motion was controlled either by the driver or the geometric path tracking controller. Consequently, the third concept investigates the potential of combining torque vectoring with path tracking for optimal path following and energy consumption.

The three controllers were developed in Matlab Simulink and evaluated in a simulation environment which combines Matlab Simulink with IPG CarMaker consisting of the Polestar 1 vehicle model. Furthermore, the control architecture was also modified and implemented in the Polestar 1 test vehicle for further evaluation. The conclusions drawn from the collection of results in this project indicate that a relatively simple geometric path tracking controller can fulfil the precision and comfort regulations for wheeled vehicles given by the UN. The backup safety system for steering, i.e. the steer by torque vectoring controller, has the steering capability to control the lateral movement of the vehicle in a curve and lane change manoeuvre. However, the steering capability deteriorates as the velocity increases. Finally, the potential of reducing the vehicle's energy consumption using an energy efficient torque vectoring controller based on an offline optimisation strategy is very limited and cumbersome. However, the results in this study showcase which torque distribution that reduces the vehicle's energy consumption and the potential reduction

for one lap at the test track.

The comparison between the two geometric path tracking controllers, i.e. the PPC and the SC, was done with simulations in both low and high velocities with more dynamic driving for several different test cases. The controllers were tuned with the look-ahead time and by adding the understeering gradient. Linking back to the research problem stated at the beginning of this report, on which controller is superior concerning precision, comfort and robustness, the evaluation has concluded that the PPC is superior to the SC. Even though the precision of the SC is better than the PPC at lower velocities, the PPC can maintain good precision and comfort at higher velocities which is not the case for the SC. Developing a PTC for use in real-time applications in a test vehicle also meant that a stability analysis was conducted where the delay margins of the different PTC's were acquired. It was primarily calculated theoretically for the vehicle model to ensure stability in the base of the entire architecture and subsequently for the PTC's using the trial-and-error method. Similar to the precision, both controllers have a high delay margin at low velocities. However, the delay margin of the SC drastically reduces at higher velocities compared to the PPC. Finally, the controllers were implemented in the test vehicle and evaluated at Handling Track 1 at Hällered Proving Ground. The results showcased that the PPC had a RMSE of $\approx 0.15\ m$ for one lap, while the SC had a RMSE of $\approx 0.41\ m$. More oscillations in the lateral acceleration and higher jerk than the PPC was also experienced with SC. However, increasing the look-ahead time increased the comfort but decreased the precision, which means tuning the controllers is a trade-off between precision and comfort. Consequently, the PPC is the superior path tracking controller as it can maintain its precision, comfort and robustness in a broader range of driving scenarios.

The concept of controlling the vehicle's lateral motion using only differential torque can be constructed in many ways. In this project, several configurations of distributing differential torque on the vehicle were presented. However, the chosen configuration in this study for the steer by torque vectoring controller was to apply differential torque on the front wheels, creating a yaw moment on the chassis and a steering wheel angle due to the scrub radius effect, which contributes to a resulting curvature for the vehicle. The rear motor torques are instead equal to maintain the desired velocity. This configuration is relatively effective with its low complexity as there are several other configurations, illustrated in Figure 5.2 that include rear differential torque, friction brakes and combinations of these configurations. The differential torque ΔT was not obtained analytically but rather numerically, using a look-up table based on experimental data from simulations and test data from the test vehicle. The steering capability of the test vehicle is highest at low velocities and deteriorates as the velocity increases. Since the steer by torque vectoring controller acts as a safety backup steering system, the system's attributes do not include any requirements on comfort. The most crucial attribute is instead that it has enough steering capability to follow the reference path without deviating from the road. Therefore, relatively simple turns and a lane change manoeuvre were used to assess the functionality. Even though the steer by torque vectoring controller

was more prone to unstable conditions than steering the vehicle using the steering wheel, it could handle the defined driving scenarios at a range of velocities, using different look-ahead times. Since this system should only be activated due to system failure, basic path tracking without regard to optimal precision is sufficient. In the evaluated scenarios, the deviation never exceeds 1 m, which shows that the steering capability requirement is fulfilled. However, the capability will be affected if the curvature is too small or if the velocity increases. The actuators can also get saturated due to limitations of available power or traction, affecting the curvature.

Reducing the vehicle's energy consumption using an energy efficient torque vectoring controller involves consideration of the different power losses present in the vehicle, such as EM and inverter losses, longitudinal and lateral slip losses and rolling resistance losses. Optimally distributing the wheel torques can reduce the power losses, consequently reducing the vehicle's energy consumption, which is the aim of the developed energy efficient torque vectoring controller. The controller was developed with two offline optimisation strategies, a rule-based and a look-up table based method. The power losses reduce by allocating more torque to the outer motors than the inner motors while turning. However, the results show that in a steady-state driving condition, the potential reduction of the vehicle's instantaneous power consumption is insignificant. While applying the rule-based and look-up table optimisation strategies to allocate the wheel torques during a drive cycle of one lap at Handling Track 1 at Hällered Proving Ground, the potential energy saving increased. The difference in the two optimisation strategies was, however, insignificant. The simulation results showed that when using the EETVC combined with the IPG Driver, the vehicle's energy consumption was reduced by 0.33 %. However, when combining the EETVC with the PPC, the reduction increased to 1.14 % instead. Consequently, the combined PPC and EETVC provided a good insight into how the losses depend on the manoeuvre itself since the power consumption directly depended on the PTC's performance. Even though the velocity profile and the total distance travelled for two different test runs were relatively identical, a test run with more tolerance for lateral deviation allowed for a more energy-efficient test run due to the decreased power losses. The vehicle's energy consumption can be decreased but in more than one way. It can be done by directly minimising the different power losses associated with torque vectoring and also indirectly by changing the tuning of the PTC. To answer the research questions stated at the beginning of the project. An energy efficient torque vectoring controller can reduce the vehicle's energy consumption. However, at steady-state conditions, i.e. constant velocity, the reduction in this study and for this powertrain is insignificant. However, combining the EETVC with the PPC has the potential to save more energy when tuning the controllers for both energy efficiency and optimal path following.

Bibliography

[1] D. Wanner *et al.*, "Control allocation strategies for an electric vehicle with a wheel hub motor failure," Tech. Rep. 3, 2015, pp. 9–12.

[2] C. Chatzikomis *et al.*, "Comparison of Path Tracking and Torque-Vectoring Controllers for Autonomous Electric Vehicles," *IEEE Transactions on Intelligent Vehicles*, vol. 3, no. 4, pp. 559–570, Dec. 2018, ISSN: 23798858. DOI: 10.1109/TIV.2018.2874529.

[3] J. E. Naranjo *et al.*, "Power-steering control architecture for automatic driving," *IEEE Transactions on Intelligent Transportation Systems*, vol. 6, no. 4, pp. 406–415, Dec. 2005, ISSN: 15249050. DOI: 10.1109/TITS.2005.858622.

[4] A. Khodayari *et al.*, "A historical review on lateral and longitudinal control of autonomous vehicle motions," in *ICMET 2010 - 2010 International Conference on Mechanical and Electrical Technology, Proceedings*, 2010, pp. 421–429, ISBN: 9781424481019. DOI: 10.1109/ICMET.2010.5598396.

[5] A. Parra, A. Zubizarreta, and J. Perez, "A comparative study of the effect of Intelligent Control based Torque Vectoring Systems on EVs with different powertrain architectures," in *2019 IEEE Intelligent Transportation Systems Conference, ITSC 2019*, Institute of Electrical and Electronics Engineers Inc., Oct. 2019, pp. 480–485, ISBN: 9781538670248. DOI: 10.1109/ITSC.2019.8917381.

[6] E. Sabbioni *et al.*, "Comparison of Torque Vectoring Control Strategies for a IWM Vehicle," *SAE International Journal of Passenger Cars - Electronic and Electrical Systems*, vol. 7, no. 2, pp. 565–572, 2014, ISSN: 19464622. DOI: 10.4271/2014-01-0860.

[7] C. Chatzikomis *et al.*, "An energy-efficient torque-vectoring algorithm for electric vehicles with multiple motors," *Mechanical Systems and Signal Processing*, vol. 128, pp. 655–673, Aug. 2019, ISSN: 10961216. DOI: 10.1016/j.ymssp.2019.03.012.

[8] G. De Filippis *et al.*, "On the Energy Efficiency of Electric Vehicles with Multiple Motors," in *2016 IEEE Vehicle Power and Propulsion Conference, VPPC 2016 - Proceedings*, Institute of Electrical and Electronics Engineers Inc., Dec. 2016, ISBN: 9781509035281. DOI: 10.1109/VPPC.2016.7791737.

[9] J. M. Snider, "Automatic Steering Methods for Autonomous Automobile Path Tracking," Tech. Rep., 2009.

[10] C. C. MacAdam, "Application of an Optimal Preview Control for Simulation of Closed-Loop Automobile Driving," *IEEE Transactions on Systems, Man and Cybernetics*, vol. 11, no. 6, pp. 393–399, 1981, ISSN: 21682909. DOI: 10.1109/TSMC.1981.4308705.

[11] S. Dominguez-Quijada *et al.*, "Comparison of lateral controllers for autonomous vehicle : experimental results," Tech. Rep., 2016, p. 2 440 161. DOI: 10.0/Linux-x86{_}64. [Online]. Available: https://hal.inria.fr/hal-02440161.

[12] A. Sorniotti, P. Barber, and S. De Pinto, "Chapter 5 - Path Tracking for Automated Driving: A Tutorial on Control System Formulations and Ongoing Research," in *Automated Driving - Safer and More Efficient Future Driving*, 2017, pp. 71–140.

[13] M. Jonasson and M. Thor, "Steering Redundancy for Self-Driving Vehicles using Differential Braking," Tech. Rep., 2017.

[14] A. D. Dominguez-Garcia, J. G. Kassakian, and J. E. Schindall, "A Backup System for Automotive Steer-by-Wire, Actuated by Selective Braking," Tech. Rep., 2004.

[15] D. Zhang *et al.*, "Reduction of Steering Effort in the Event of EPAS Failure using Differential Braking Assisted Steering," *SAE International Journal of Transportation Safety*, vol. 5, no. 2, pp. 227–233, 2017, ISSN: 23275634. DOI: 10.4271/2017-01-1489.

[16] A. Mangia, B. Lenzo, and E. Sabbioni, "An integrated torque-vectoring control framework for electric vehicles featuring multiple handling and energy-efficiency modes selectable by the driver," *Meccanica*, vol. 56, no. 5, pp. 991–1010, May 2021, ISSN: 15729648. DOI: 10.1007/s11012-021-01317-3.

[17] Y. Ren, L. Zheng, and A. Khajepour, "Integrated model predictive and torque vectoring control for path tracking of 4-wheel-driven autonomous vehicles," *IET Intelligent Transport Systems*, vol. 13, no. 1, pp. 98–107, Jan. 2019, ISSN: 1751956X. DOI: 10.1049/iet-its.2018.5095.

[18] T. Kobayashi *et al.*, "Efficient direct yaw moment control: tyre slip power loss minimisation for four-independent wheel drive vehicle," *Vehicle System Dynamics*, vol. 56, no. 5, pp. 719–733, May 2018, ISSN: 17445159. DOI: 10.1080/00423114.2017.1330483.

[19] P. Gruber *et al.*, "Energy efficient torque vectoring control," Tech. Rep.

[20] Y. Q. Zhao *et al.*, "Estimation of Road Friction Coefficient in Different Road Conditions Based on Vehicle Braking Dynamics," *Chinese Journal of Mechanical Engineering (English Edition)*, vol. 30, no. 4, pp. 982–990, Jul. 2017, ISSN: 21928258. DOI: 10.1007/s10033-017-0143-z.

[21] N. Carey and C. Steitz, *EU proposes effective ban for new fossil-fuel cars from 2035*, Jul. 2021. [Online]. Available: https://www.reuters.com/business/retail-consumer/eu-proposes-effective-ban-new-fossil-fuel-car-sales-2035-2021-07-14/.

[22] "GLOBAL STATUS REPORT ON ROAD SAFETY 2018," Tech. Rep.

[23] F. Knobloch *et al.*, "Net emission reductions from electric cars and heat pumps in 59 world regions over time," *Nature Sustainability*, vol. 3, no. 6, pp. 437–447, Jun. 2020, ISSN: 23989629. DOI: 10.1038/s41893-020-0488-7.

[24] J. Torinsson, "Thesis for the degree of Licentiate of Engineering Power loss minimization in electric cars by wheel force allocation," Tech. Rep.

[25] Y. Chen and J. Wang, "Adaptive energy-efficient control allocation for planar motion control of over-actuated electric ground vehicles," *IEEE Transactions*

on Control Systems Technology, vol. 22, no. 4, pp. 1362–1373, 2014, ISSN: 10636536. DOI: 10.1109/TCST.2013.2287560.

[26] "Model Predictive Control for Autonomous Driving of a Truck MIA ISAKSSON PALMQVIST KTH ROYAL INSTITUTE OF TECHNOLOGY SCHOOL OF ELECTRICAL ENGINEERING Acknowledgement," Tech. Rep.

[27] K. Seshadri Chari, "Dynamic Modelling and Optimal Control of Autonomous Heavyduty Vehicles KTH Thesis Report," Tech. Rep.

[28] C. B. Ieee and S. Member, "The Dark Side of Loop Control Theory," Tech. Rep.

[29] B. Jacobson, "VEHICLE DYNAMICS COMPENDIUM rear coupling on unit front coupling on unit unit Control algorithm," Tech. Rep. [Online]. Available: www.chalmers.se.

[30] "Agreement Concerning the Adoption of Harmonized Technical United Nations Regulations for Wheeled Vehicles, Equipment and Parts which can be Fitted and/or be Used on Wheeled Vehicles and the Conditions for Reciprocal Recognition of Approvals Granted on the Basis of these United Nations Regulations* Uniform provisions concerning the approval of vehicles with regard to Automated Lane Keeping Systems," Tech. Rep.

[31] "Agreement Concerning the Adoption of Harmonized Technical United Nations Regulations for Wheeled Vehicles, Equipment and Parts which can be Fitted and/or be Used on Wheeled Vehicles and the Conditions for Reciprocal Recognition of Approvals Granted on the Basis of these United Nations Regulations*," Tech. Rep.

[32] J. Eriksson and L. Svensson, "Tuning for Ride Quality in Autonomous Vehicle Application to Linear Quadratic Path Planning Algorithm," Tech. Rep., 2015. [Online]. Available: http://www.teknat.uu.se/student.

[33] I. H. Wyllie and M. J. Griffin, "Discomfort from sinusoidal oscillation in the roll and lateral axes at frequencies between 0.2 and 1.6Hz," *The Journal of the Acoustical Society of America*, vol. 121, no. 5, pp. 2644–2654, May 2007, ISSN: 0001-4966. DOI: 10.1121/1.2715654.

[34] J. Xu *et al.*, "An experimental study on lateral acceleration of cars in different environments in sichuan, southwest China," *Discrete Dynamics in Nature and Society*, vol. 2015, 2015, ISSN: 1607887X. DOI: 10.1155/2015/494130.

[35] A. D. Dominguez-Garcia, J. G. Kassakian, and J. E. Schindall, "A Backup System for Automotive Steer-by-Wire, Actuated by Selective Braking," Tech. Rep., 2004.

[36] J. Torinsson *et al.*, "Energy reduction by power loss minimisation through wheel torque allocation in electric vehicles: a simulation-based approach," *Vehicle System Dynamics*, vol. 60, no. 5, pp. 1488–1511, 2022, ISSN: 17445159. DOI: 10.1080/00423114.2020.1858121.

A

Appendix A

A.1 Identifying position of point relative to line

The direction of an arbitrary line AB is defined as

$$\vec{AB} = (x_2, y_2) - (x_1, y_1) = (x_2 - x_1, y_2 - y_1)$$

$$A = (x_1, y_1)$$

$$B = (x_2, y_2)$$

The normal line $\vec{n}$ to $\vec{AB}$ will then be defined as

$$\vec{n} = (y_2 - y_1, -(x_2 - x_1))$$

It can be verified that $\vec{n}$ is normal to $\vec{AB}$ by ensuring that the vectors' dot product is equal to 0.

$$\vec{n} \cdot \vec{AB} = (y_2 - y_1, -(x_2 - x_1)) \cdot (x_2 - x_1, y_2 - y_1) =$$
$$= (y_2x_2 - y_2x_1 - y_1x_2 + y_1x_1) + (-x_2y_2 + x_2y_1 + x_1y_2 - x_1y_1) = 0$$

Now imagine a point Z on any side of the line $\vec{AB}$. One possible vector intersecting the line $\vec{AB}$ and the point Z is V = AZ.

$$\vec{AZ} = \vec{V} = (x - x_1, y - y_1)$$

$$Z = (x, y)$$

Note that the vector V can be written as a sum of two components, namely the vector $V^{||}$ parallel to the line $\vec{AB}$ and the vector $V^{\perp}$ perpendicular to the line $\vec{AB}$ as

$$V = V^{||} + V^{\perp}$$

The objective is to derive an expression that recognises which side of a line an arbitrary point is and be consistent in the way that the expression will provide a unique value for points on the right side of the line and another unique value for points on the left side of the line. With that being said, the expression will be given by

$$V \cdot \vec{n} = (V^{||} + V^{\perp}) \cdot \vec{n} = V^{\perp} \cdot \vec{n}$$

The term $V^{||} \cdot \vec{n}$ is equal to 0 since the lines are perpendicular. The expression given by $V^{\perp} \cdot \vec{n}$ however indicates if the direction of $\vec{n}$ and $V^{\perp}$ are equal. If they are, the expression will be equal to a positive value. Arithmetically, this is written as

$$V \cdot \vec{n} = V^{\perp} \cdot \vec{n} = (x - x_1, y - y_1) \cdot (y_2 - y_1, -(x_2 - x_1)) = (x - x_1) \cdot (y_2 - y_1) - (y - y_1) \cdot (x_2 - x_1)$$

Regarding relevance, point Z could be considered the current vehicle position. That would, however, insinuate that the product $V \cdot \vec{n}$ as defined above would change sign the instant the vehicle crossed the hypothetical reference path $\vec{AB}$. As a result of inertia, steering capability and several other phenomenons and factors, the vehicle would start to oscillate if the controller was absent any predictive behaviour. Solving this without the need to alter the controller, Z is instead set as the preview point of the vehicle in the formula given by $V \cdot \vec{n}$ in order for the vehicle to steer appropriately before it crosses the path. This slight change improves the smoothness and precision of the controller alike.

B

Appendix B

B.1 Transformation matrix and polynomial fitting

A discretised curve consisting of an arbitrary number of points can be rotated or transformed in euclidean space using a transformation matrix, defined as

$$\mathbf{R} = \begin{bmatrix} \cos(\theta) & -\sin(\theta) \\ \sin(\theta) & \cos(\theta) \end{bmatrix} \tag{B.1}$$

whereas θ is the angle of rotation. Now imagine a discretised curve C with points P_x

$$\vec{C} = [P_1\ P_2\ P_3\ ...\ P_n] \tag{B.2}$$

that needs to be rotated θ degrees. The rotated curve $\vec{C}_{rot}$ is obtained by multiplying the original curve C by the rotational matrix $\mathbf{R}$

$$C_{rot} = C \cdot \mathbf{R} \tag{B.3}$$

This is illustrated in Figure B.1.

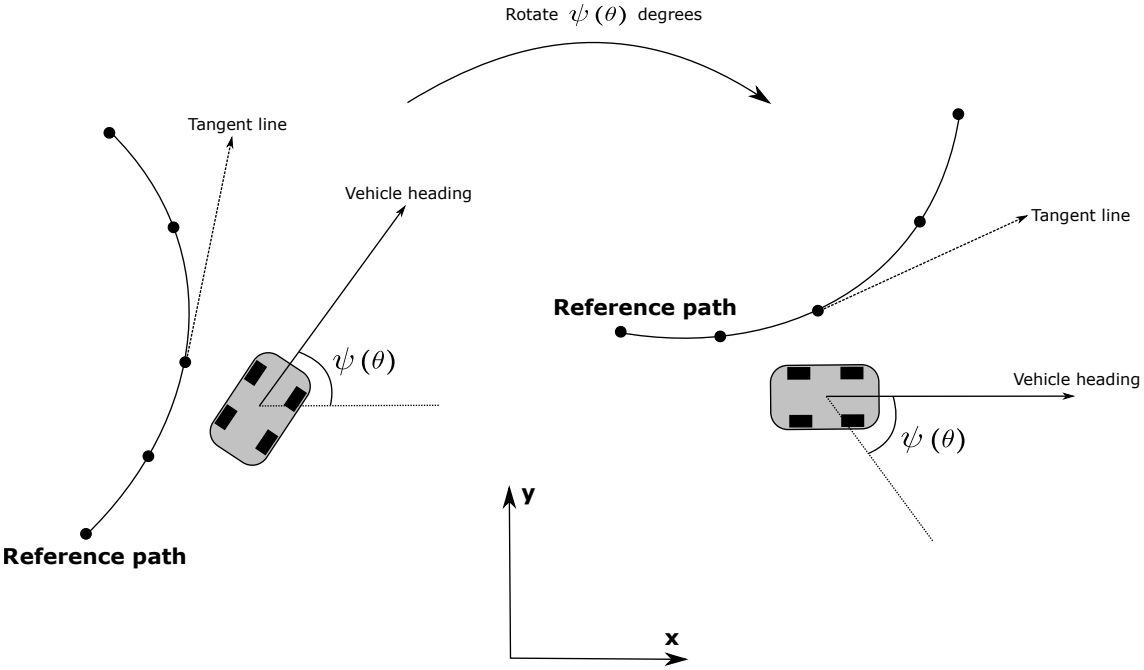

Figure B.1: Rotational transformation

Using the curve fitting toolbox in Matlab, the curve C_{rot} can be expressed by a polynomial expression, which can be redefined with more points to increase its resemblance to a continuous curve. If the point at which the tangent line is to be acquired is placed at index n, then the tangent line is defined by

$$L_{tangent} = \overrightarrow{P_n P}_{n+1} \tag{B.4}$$

This is illustrated in Figure B.2.

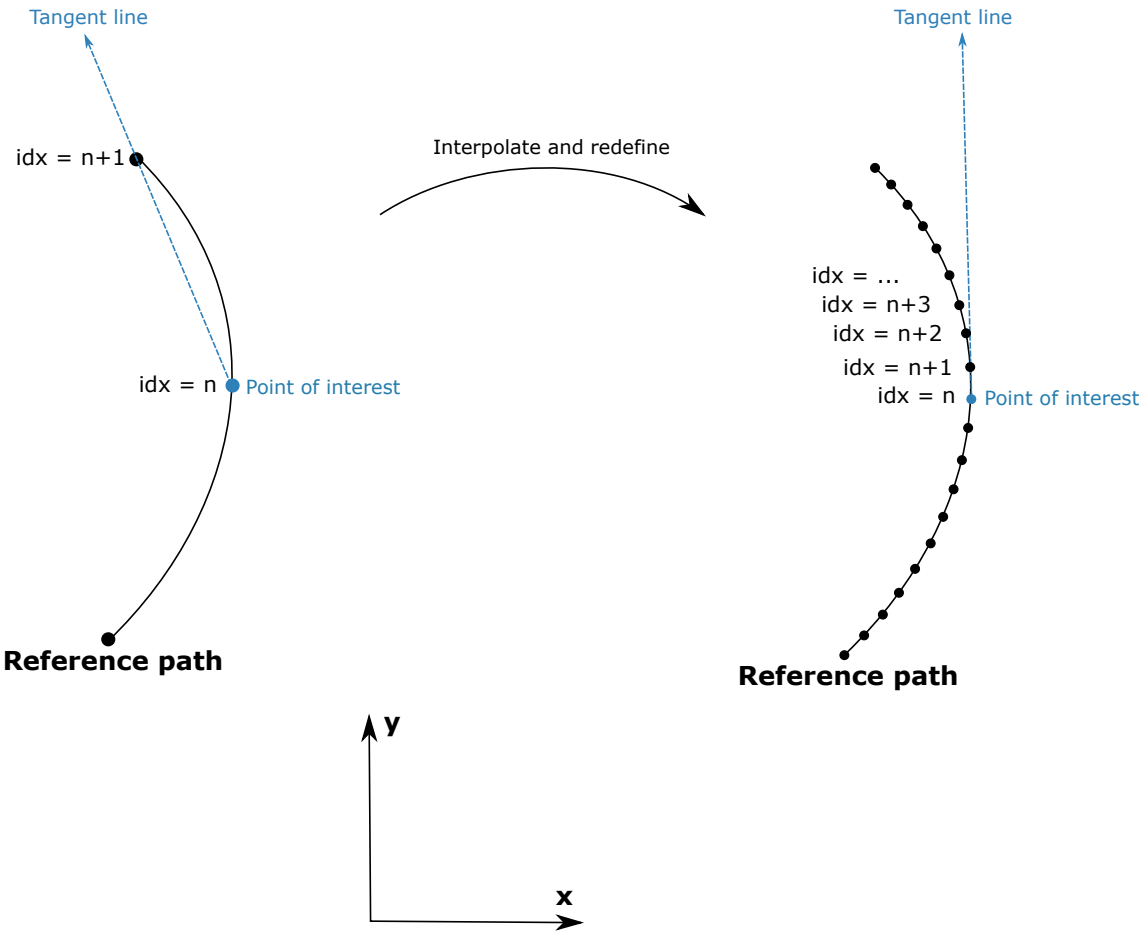

Figure B.2: Redefined fitted curve

The tangent line $L_{tangent}$ approaches the theoretically precise value as the number of points in C_{rot} approaches infinity. However, a sufficiently high amount of points will suffice in terms of precision.

Note that the transformation is conducted to avoid outputs with the value of infinity for when the polynomial fitting is to be applied to refine the curve. If the curve is rotated ψ degrees, then the relative heading is directed along the longitudinal axis in the global coordinate system. Figure B.1 visualises this operation. This simplifies the calculations as the angle between a horizontal line $L_{horizontal}$, which represents the relative heading after the transformation and the tangent line $L_{tangent}$ is easily acquired.

C

Appendix C

C.1 Thresholds and grading results

Tables C.1 - C.5 shows the **grading thresholds** for:

- RMSE of the precision $P_{RMSE,precision}$
- Maximum lateral deviation $P_{MAX,precision}$
- RMSE of the lateral jerk $P_{RMSE,jerk}$
- Maximum lateral jerk $P_{MAX,jerk}$
- Energy spectral density P_{ESD} (Area)

$P_{RMSE,precision}$ (Grade)	
$= 5$	if $RMSE_{precision} \leq 0.100$ m
$= 4$	if $0.100 \text{ m} < RMSE_{precision} \leq 0.150$ m
$= 3$	if $0.150 \text{ m} < RMSE_{precision} \leq 0.200$ m
$= 2$	if $0.200 \text{ m} < RMSE_{precision} \leq 0.300$ m
$= 1$	if $0.300 \text{ m} < RMSE_{precision}$

Table C.1: Grading thresholds for RMSE of the precision $P_{RMSE,precision}$

$P_{MAX,precision}$ (Grade)	
$= 5$	if $MAX_{precision} \leq 0.100$ m
$= 4$	if $0.100 \text{ m} < MAX_{precision} \leq 0.200$ m
$= 3$	if $0.200 \text{ m} < MAX_{precision} \leq 0.300$ m
$= 2$	if $0.300 \text{ m} < MAX_{precision} \leq 0.375$ m
$= 1$	if $0.375 \text{ m} < MAX_{precision}$

Table C.2: Grading thresholds for Maximum lateral deviation $P_{MAX,precision}$

$P_{RMSE,jerk}$ (Grade)	
$= 5$	if $RMSE_{jerk} \leq 0.800\ m/s^3$
$= 4$	if $0.800\ m/s^3 < RMSE_{jerk} \leq 1.200\ m/s^3$
$= 3$	if $1.200\ m/s^3 < RMSE_{jerk} \leq 1.600\ m/s^3$
$= 2$	if $1.600\ m/s^3 < RMSE_{jerk} \leq 2.000\ m/s^3$
$= 1$	if $2.000\ m/s^3 < RMSE_{jerk}$

Table C.3: Grading thresholds for RMSE of the lateral jerk $P_{RMSE,jerk}$

$P_{MAX,jerk}$ (Grade)	
$= 5$	if $MAX_{jerk} \leq 2.000\ m/s^3$
$= 4$	if $2.000\ m/s^3 < MAX_{jerk} \leq 3.000\ m/s^3$
$= 3$	if $3.000\ m/s^3 < MAX_{jerk} \leq 4.000\ m/s^3$
$= 2$	if $4.000\ m/s^3 < MAX_{jerk} \leq 5.000\ m/s^3$
$= 1$	if $5.000\ m/s^3 < MAX_{jerk}$

Table C.4: Grading thresholds for Maximum lateral jerk $P_{MAX,jerk}$

P_{ESD} (Grade)	
$= 5$	if Area $\leq 0.030\ m/s^2$
$= 4$	if $0.030\ m/s^2 <$ Area $\leq 0.050\ m/s^2$
$= 3$	if $0.050\ m/s^2 <$ Area $\leq 0.070\ m/s^2$
$= 2$	if $0.070\ m/s^2 <$ Area $\leq 0.090\ m/s^2$
$= 1$	if $0.090\ m/s^2 <$ Area

Table C.5: Grading thresholds for Energy spectral density (Area)

Tables C.6 - C.11 show the **grading results** for all test cases regarding:

- Precision $P_{precision}$
- Lateral jerk P_{jerk}
- Energy spectral density P_{ESD} (Area)

$P_{precision}$			P_{jerk}			P_{ESD}		
$\mathbf{T_p}$	**PPC**	**SC**	$\mathbf{T_p}$	**PPC**	**SC**	$\mathbf{T_p}$	**PPC**	**SC**
1	4.6	5.0	**1**	5.0	3.8	**1**	5	3
0.8	4.8	5.0	**0.8**	5.0	3.8	**0.8**	5	3
0.6	5.0	5.0	**0.6**	4.8	3.6	**0.6**	4	3
0.6 ($\mathbf{K_u}$)	5.0	5.0	**0.6 ($\mathbf{K_u}$)**	4.8	3.6	**0.6 ($\mathbf{K_u}$)**	4	3

Table C.6: Test Case 2 grading: 90° turn, $R = 50\ m$, $v = 36\ km/h$, $ay = 2\ m/s^2$, simulation results

$P_{precision}$			P_{jerk}			P_{ESD}		
$\mathbf{T_p}$	**PPC**	**SC**	$\mathbf{T_p}$	**PPC**	**SC**	$\mathbf{T_p}$	**PPC**	**SC**
1	1.8	3.8	**1**	4.0	1.0	**1**	3	1
0.8	2.6	3.8	**0.8**	3.8	1.0	**0.8**	2	1
0.6	3.8	4.8	**0.6**	2.6	1.0	**0.6**	1	1
0.6 ($\mathbf{K_u}$)	4.8	5.0	**0.6 ($\mathbf{K_u}$)**	2.6	1.0	**0.6 ($\mathbf{K_u}$)**	1	1

Table C.7: Test Case 2 grading: 90° turn, $R = 50\ m$, $v = 51\ km/h$, $ay = 4\ m/s^2$, simulation results

$P_{precision}$			P_{jerk}			P_{ESD}		
$\mathbf{T_p}$	**PPC**	**SC**	$\mathbf{T_p}$	**PPC**	**SC**	$\mathbf{T_p}$	**PPC**	**SC**
1	1.0	2.0	**1**	5.0	3.6	**1**	5	3
0.8	1.8	3.0	**0.8**	5.0	3.6	**0.8**	5	3
0.6	3.0	4.0	**0.6**	4.8	3.4	**0.6**	4	3
0.6 ($\mathbf{K_u}$)	5.0	4.0	**0.6 ($\mathbf{K_u}$)**	4.8	2.8	**0.6 ($\mathbf{K_u}$)**	4	3

Table C.8: Test Case 2 grading: 90° turn, $R = 312.5m$, $v = 90\ km/h$, $ay = 2\ m/s^2$, simulation results

$P_{precision}$			P_{jerk}			P_{ESD}		
$\mathbf{T_p}$	**PPC**	**SC**	$\mathbf{T_p}$	**PPC**	**SC**	$\mathbf{T_p}$	**PPC**	**SC**
1	1.0	1.0	**1**	4.0	1.0	**1**	4	1
0.8	1.0	1.0	**0.8**	3.8	1.0	**0.8**	3	1
0.6	1.0	1.0	**0.6**	2.6	1.0	**0.6**	2	1
0.6 ($\mathbf{K_u}$)	4.8	1.8	**0.6 ($\mathbf{K_u}$)**	2.6	1.0	**0.6 ($\mathbf{K_u}$)**	1	1

Table C.9: Test Case 2 grading: 90° turn, $R = 312.5m$, $v = 128\ km/h$, $ay = 4m/s^2$, simulation results

$P_{precision}$			P_{jerk}			P_{ESD}		
$\mathbf{T_p}$	**PPC**	**SC**	$\mathbf{T_p}$	**PPC**	**SC**	$\mathbf{T_p}$	**PPC**	**SC**
1	1.0	1.8	**1**	1.8	1.8	**1**	1	1
0.8	1.8	1.8	**0.8**	1.8	1.8	**0.8**	1	1
0.6	2.6	3.6	**0.6**	1.8	1.8	**0.6**	1	1
0.6 ($\mathbf{K_u}$)	4.8	4.8	**0.6 ($\mathbf{K_u}$)**	1.8	1.8	**0.6 ($\mathbf{K_u}$)**	1	1

Table C.10: Test case 3 grading: Simulation results from Handling Track 1 at 50 km/h

$P_{precision}$			P_{jerk}			P_{ESD}		
$\mathbf{T_p}$	**PPC**	**SC**	$\mathbf{T_p}$	**PPC**	**SC**	$\mathbf{T_p}$	**PPC**	**SC**
1.0 ($\mathbf{K_u}$)	1.8	1.0	**1.0 ($\mathbf{K_u}$)**	2.8	1.8	**1.0 ($\mathbf{K_u}$)**	4	4
0.8 ($\mathbf{K_u}$)	2.6	1.0	**0.8 ($\mathbf{K_u}$)**	2.8	1.0	**0.8 ($\mathbf{K_u}$)**	4	2
0.6 ($\mathbf{K_u}$)	3.6	1.0	**0.6 ($\mathbf{K_u}$)**	1.8	1.0	**0.6 ($\mathbf{K_u}$)**	4	1

Table C.11: Test case 3 grading: Test vehicle results from Handling Track 1 at 50 km/h

D

Appendix D

D.1 Comfort evaluation figures

Figures D.2 - D.3 illustrates the evaluated quantities of the PPC and SC in test case 2 at a 50 m radius 90° turn with look-ahead time $T_p = 1$.

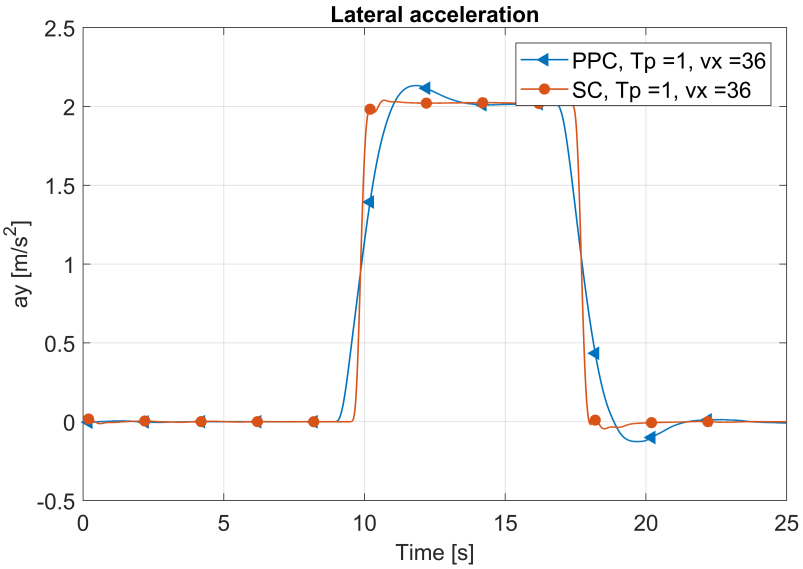

Figure D.1: Radius 50 m, lateral acceleration at 36 km/h

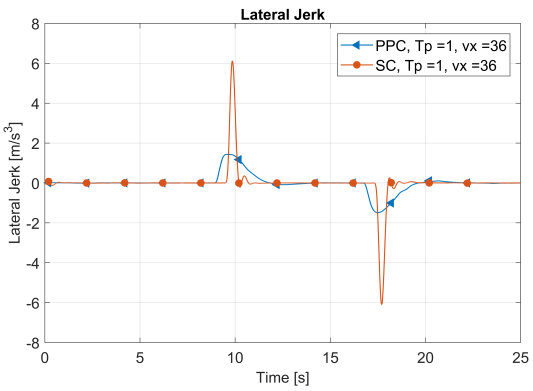

Figure D.2: Radius 50 m, lateral jerk at 36 km/h

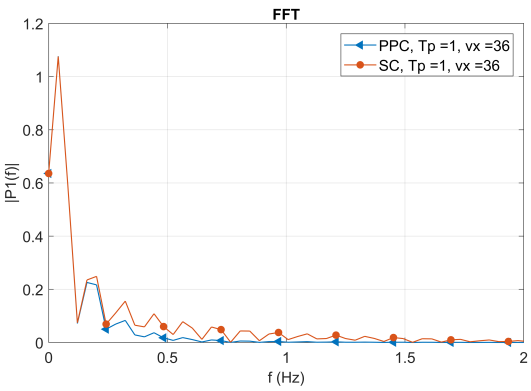

Figure D.3: Radius 50 m, Fourier transform at 36 km/h

E

Appendix E

E.1 Steering capability comparison

The difference between the contribution from the chassis yaw moment and the scrub radius effect on the steering capability is presented in Figure E.1 and E.2 for the simulation results. Note that Figure E.1 showcases the steering capability with both yaw moment and scrub radius contributions, i.e. hands-off the steering wheel. In contrast, Figure E.2 display the steering capability with only yaw moment contribution, i.e. steering wheel locked to zero degrees (hand-on steering wheel). Consequently, the difference between the figures is the contribution from the scrub radius effect.

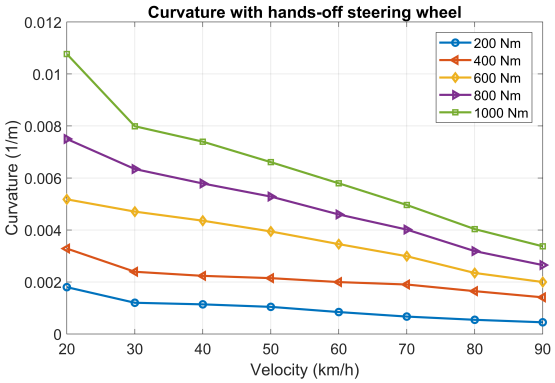

Figure E.1: SbTV, capability with hands-off the steering wheel

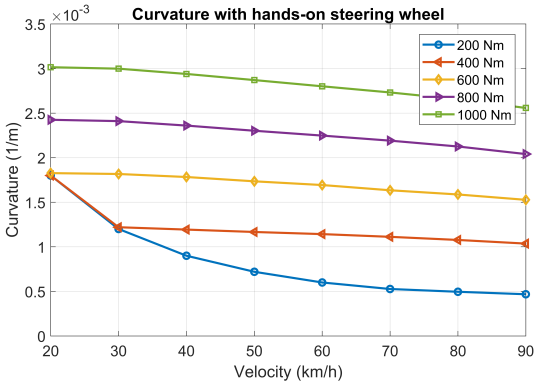

Figure E.2: SbTV, capability with hands-on the steering wheel

The difference between the yaw moment and scrub radius contribution for each specific differential torque is showcased in Figure E.3 to Figure E.7. The figures show that the scrub radius effect contribution on the steering capability is more prominent at lower velocities and higher differential torque on the front axle.

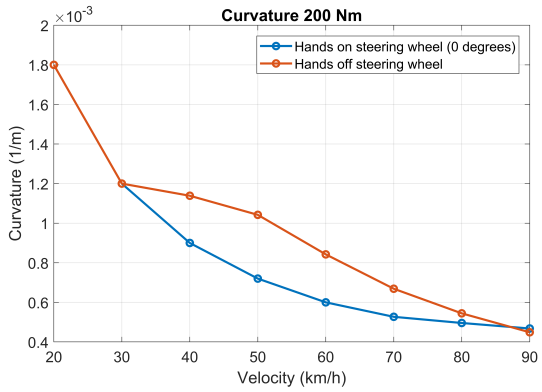

Figure E.3: SbTV, capability 200 Nm

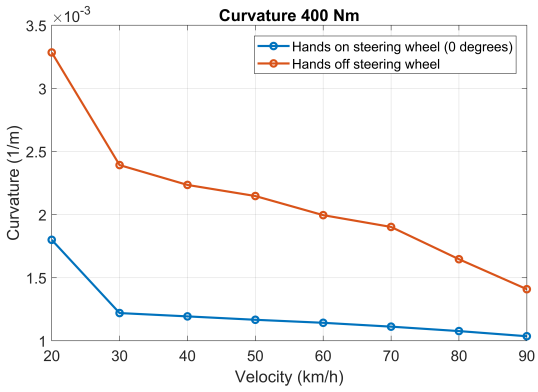

Figure E.4: SbTV, capability 400 Nm

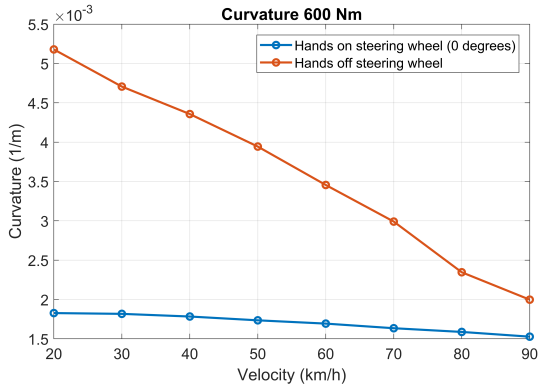

Figure E.5: SbTV, capability 600 Nm

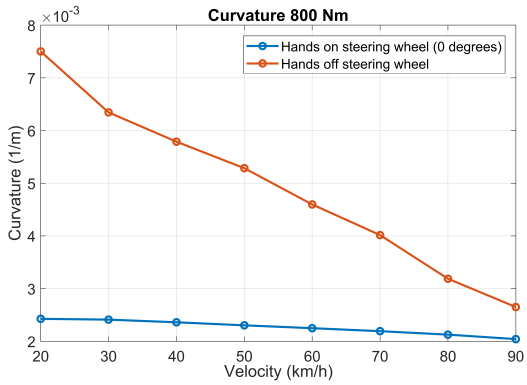

Figure E.6: SbTV, capability 800 Nm

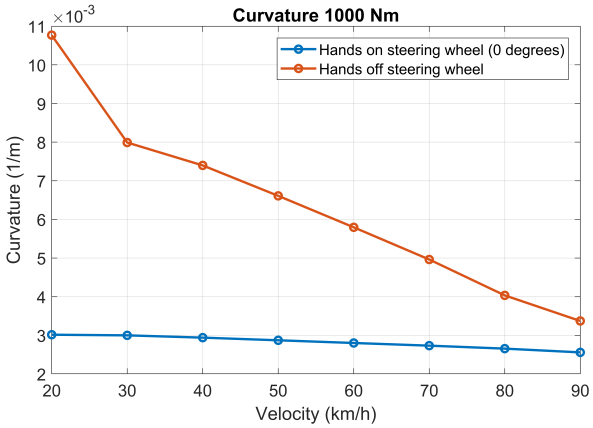

Figure E.7: SbTV, capability 1000 Nm

F

Appendix F

F.1 Energy consumption with FWD and RWD

This appendix presents the vehicle's energy consumption for one lap at Handling Track 1 for FWD and RWD, i.e. 100-0 and 0-100 front/rear torque distributions. The results compare the vehicle's energy consumption between the rule-based optimisation strategy and applying no TV. Note that the total energy consumption is lower than when AWD is used since the front, or rear motors are decoupled when using RWD or FWD.

EETV: Rule Based + IPG Driver - Energy Consumption [kJ]			
Comparison	**No TV**	**With TV**	**Difference**
Total Consumption	416.96 [kJ]	416.21 [kJ]	-0.18 [%]
EPAS Consumption	0.69 [kJ]	0.58 [kJ]	-15.64 [%]
Lateral Deviation (RMSE)	0.170 [m]	0.166 [m]	-0.004 [m]
Lateral Deviation (Max)	0.517 [m]	0.499 [m]	-0.018 [m]

Table F.1: Handling Track 1 - Rule Based Torque Distribution, Energy Consumption with IPG Driver for a 100-0 front/rear distribution

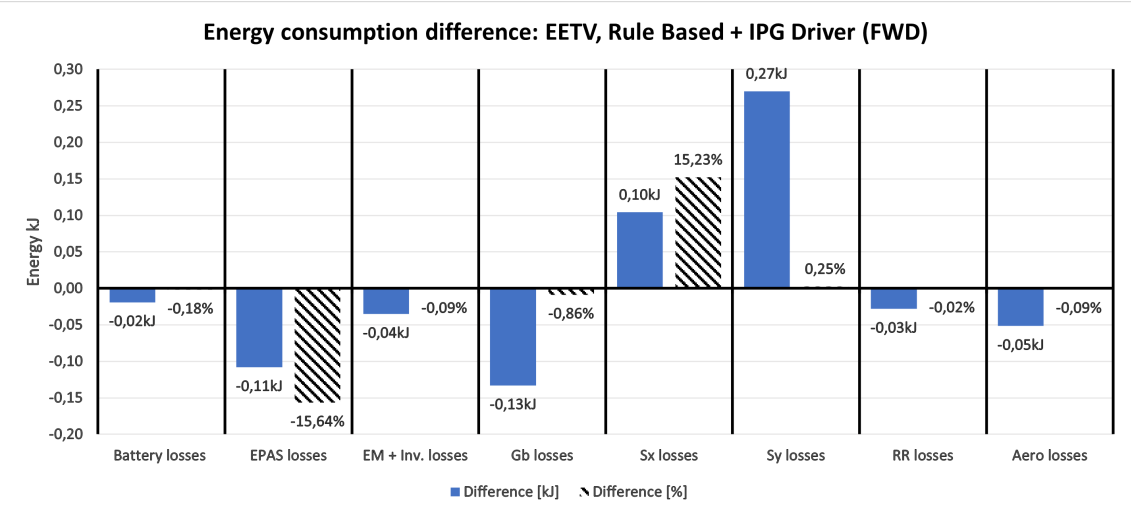

Figure F.1: Difference in energy losses without EETV + IPG Driver compared to with Rule Based EETV + IPG Driver for a 100-0 front/rear distribution

EETV: Rule Based + IPG Driver - Energy Consumption [kJ]			
Comparison	**No TV**	**With TV**	**Difference**
Total Consumption	416.34 [kJ]	414.79 [kJ]	-0.37 [%]
EPAS Consumption	0.70 [kJ]	0.67 [kJ]	-4.15 [%]
Lateral Deviation (RMSE)	0.170 [m]	0.166 [m]	-0.004 [m]
Lateral Deviation (Max)	0.516 [m]	0.498 [m]	-0.018 [m]

Table F.2: Handling Track 1 - Rule Based Torque Distribution, Energy Consumption with IPG Driver for a 0-100 front/rear distribution

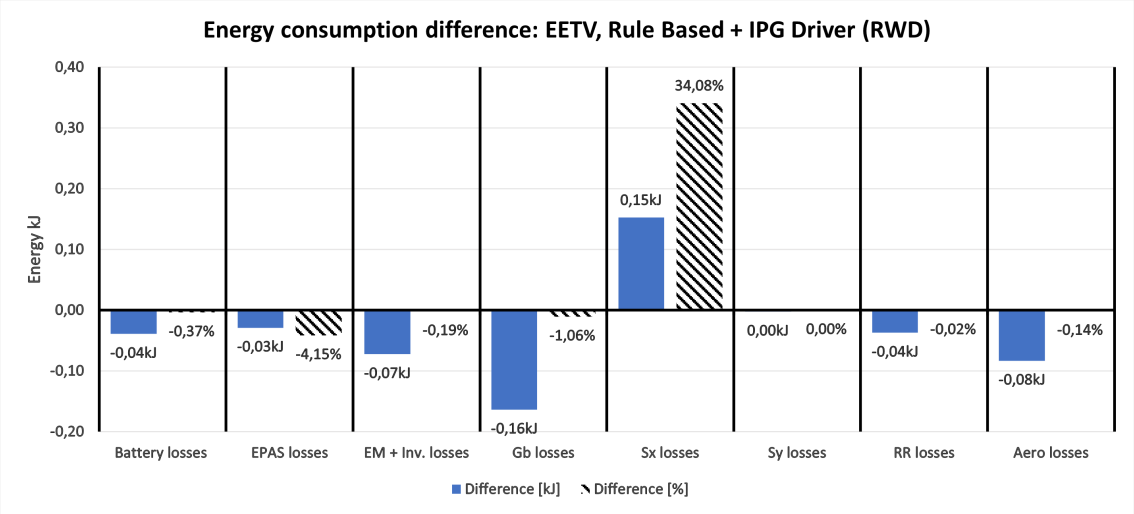

Figure F.2: Difference in energy losses without EETV + IPG Driver compared to with Rule Based EETV + IPG Driver for a 0-100 front/rear distribution

EETV: Rule Based + IPG Driver - Energy Consumption [kJ]			
Comparison	**No TV**	**With TV**	**Difference**
Total Consumption	420.85 [kJ]	419.96 [kJ]	-0.21 [%]
EPAS Consumption	0.76 [kJ]	0.64 [kJ]	-16.14 [%]
Lateral Deviation (RMSE)	0.061 [m]	0.059 [m]	-0.002 [m]
Lateral Deviation (Max)	0.153 [m]	0.150 [m]	-0.003 [m]

Table F.3: Handling Track 1 - Rule Based Torque Distribution, Energy Consumption with PPC ($T_p = 0.6$) for a 100-0 front/rear distribution

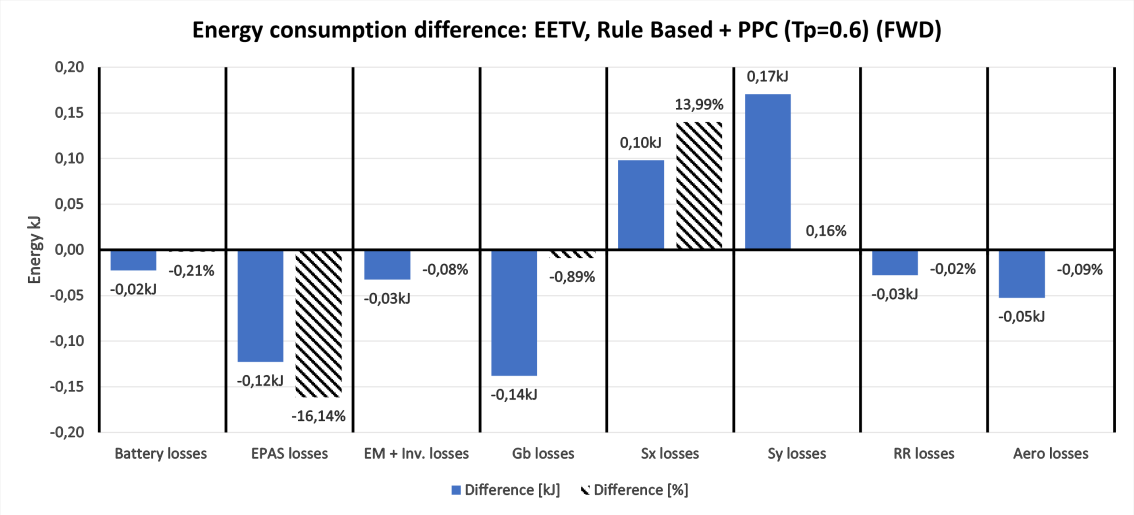

Figure F.3: Difference in energy losses without EETV + PPC ($T_p = 0.6$) compared to with Rule Based EETV + PPC ($T_p = 0.6$) for a 100-0 front/rear distribution

EETV: Rule Based + IPG Driver - Energy Consumption [kJ]			
Comparison	**No TV**	**With TV**	**Difference**
Total Consumption	420.24 [kJ]	418.59 [kJ]	-0.39 [%]
EPAS Consumption	0.77 [kJ]	0.73 [kJ]	-4.89 [%]
Lateral Deviation (RMSE)	0.062 [m]	0.060 [m]	-0.002 [m]
Lateral Deviation (Max)	0.155 [m]	0.153 [m]	-0.002 [m]

Table F.4: Handling Track 1 - Rule Based Torque Distribution, Energy Consumption with PPC ($T_p = 0.6$) for a 0-100 front/rear distribution

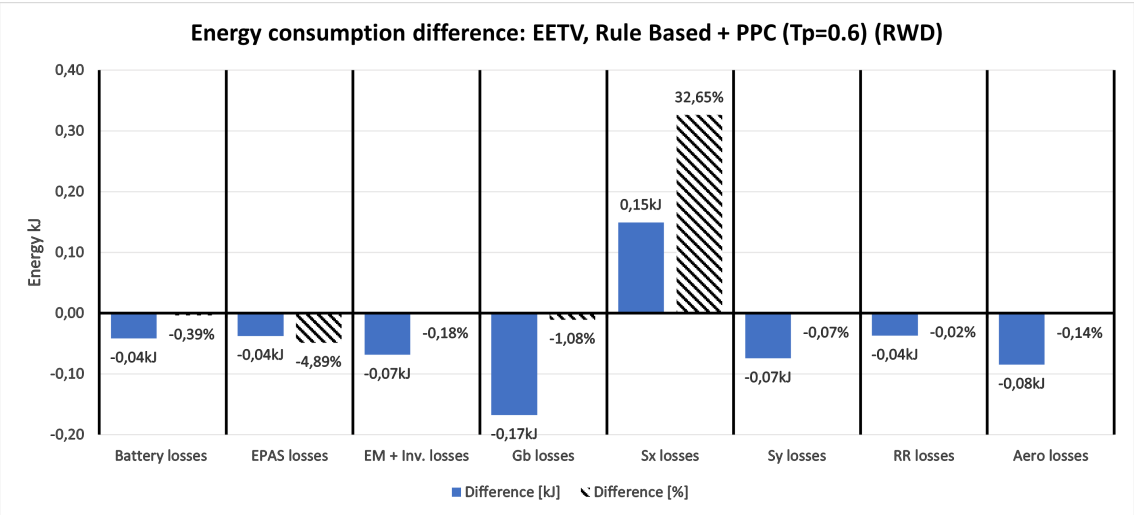

Figure F.4: Difference in energy losses without EETV + PPC ($T_p = 0.6$) compared to with Rule Based EETV + PPC ($T_p = 0.6$) for a 0-100 front/rear distribution

EETV: Rule Based + IPG Driver - Energy Consumption [kJ]			
Comparison	**No TV**	**With TV**	**Difference**
Total Consumption	420.85 [kJ]	416.37 [kJ]	-1.06 [%]
EPAS Consumption	0.76 [kJ]	0.61 [kJ]	-19.36 [%]
Lateral Deviation (RMSE)	0.061 [m]	0.168 [m]	+0.107 [m]
Lateral Deviation (Max)	0.153 [m]	0.616 [m]	+0.463 [m]

Table F.5: Handling Track 1 - Rule Based Torque Distribution, Energy Consumption with PPC ($T_p = 1.0$) for a 100-0 front/rear distribution

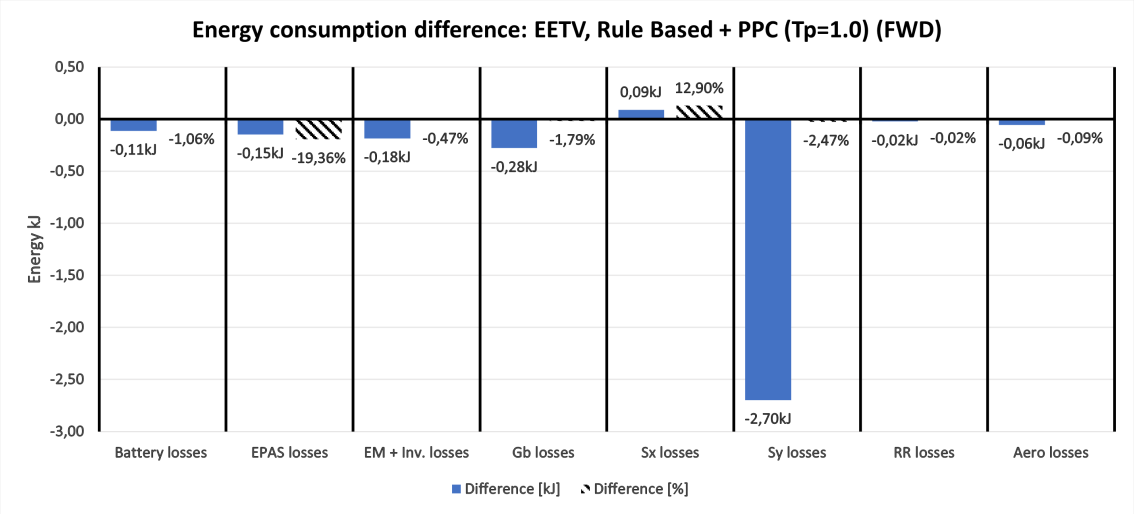

Figure F.5: Difference in energy losses without EETV + PPC ($T_p = 1.0$) compared to with Rule Based EETV + PPC ($T_p = 1.0$) for a 100-0 front/rear distribution

EETV: Rule Based + IPG Driver - Energy Consumption [kJ]			
Comparison	**No TV**	**With TV**	**Difference**
Total Consumption	420.24 [kJ]	415.03 [kJ]	-1.24 [%]
EPAS Consumption	0.77 [kJ]	0.70 [kJ]	-8.33 [%]
Lateral Deviation (RMSE)	0.062 [m]	0.167 [m]	+0.105 [m]
Lateral Deviation (Max)	0.155 [m]	0.610 [m]	+0.455 [m]

Table F.6: Handling Track 1 - Rule Based Torque Distribution, Energy Consumption with PPC ($T_p = 1.0$) for a 0-100 front/rear distribution

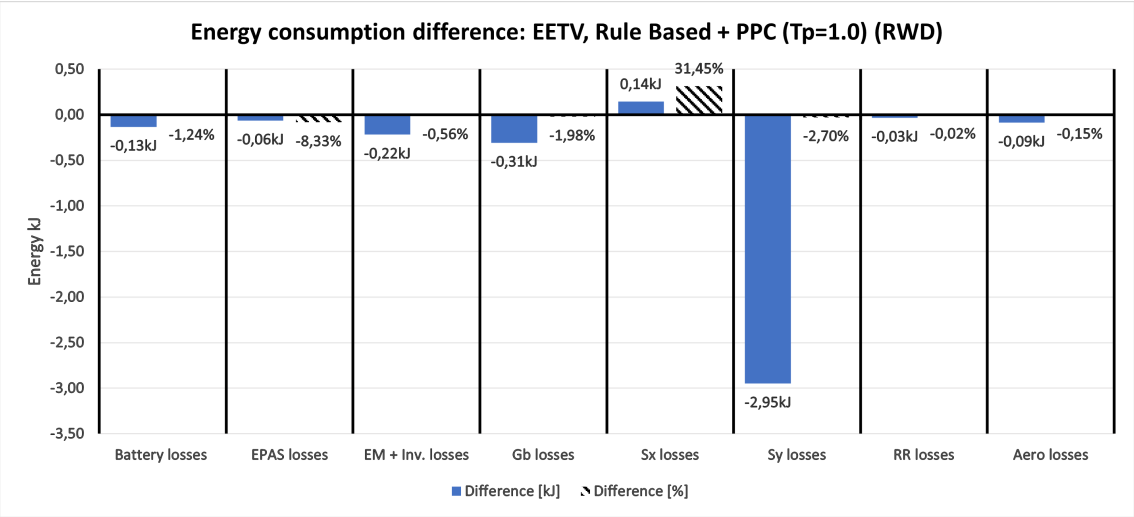

Figure F.6: Difference in energy losses without EETV + PPC ($T_p = 1.0$) compared to with Rule Based EETV + PPC ($T_p = 1.0$) for a 0-100 front/rear distribution

DEPARTMENT OF MECHANICS AND MARITIME SCIENCES
CHALMERS UNIVERSITY OF TECHNOLOGY
Gothenburg, Sweden
www.chalmers.se

CHALMERS
UNIVERSITY OF TECHNOLOGY